

Solar-assisted ground-source heat pump solutions for Dutch terraced houses

Investigation and modelling of SAGSHP technology as an alternative to gas heating system

Daniele Tarantini

Solar-assisted ground-source heat pump solutions for Dutch terraced houses

Investigation and modelling of SAGSHP technology as an alternative to gas heating system

by

Daniele Tarantini

to obtain the degree of Master of Science
at the Delft University of Technology,
to be defended the 30th of March at 11.30 a.m.

Student number: 4744578
Supervisor: C.A. Infante Ferreira
Thesis committee: Thijs Vlugt
Ivo Pothof
Diego Pineda Quijano

An electronic version of this thesis is available at <http://repository.tudelft.nl/>.

Abstract

In the last decades, the excessive increase in average global temperature related to a massive rise in greenhouse gas emissions showed the world how the fossil fuel society we live in today is drastically modifying and destroying the world we live in and is turning it in an un-habitable planet. Scientist all over the world made it clear that if we stay on the current patterns and we don't reduce drastically our greenhouse gas emissions, we are gonna end up with the extinction of the human species.

The urgency of the problem seems to be clear to most people, what we need now are immediate actions to drastically reduce our greenhouse gas emissions.

Among all different sectors, the residential sector is one of the biggest contributors to greenhouse gases (GHG) emissions and most of the energy is used for space heating (SH) and electrical appliances. In the specific case of the Netherlands, most energy provided to the residential sector is produced by means of natural gas, and the goal of the country is to replace natural gas with net-zero CO_2 solutions.

In this thesis work, a solar-assisted ground-source heat pump (SAGSHP) system for space heating for a typical Dutch terraced house is thoroughly investigated. In particular a 115 m^2 house with 3 people living in it.

The main different components of the system are investigate by looking at the state-of-the-art technology to understand what are the different system components that would be more convenient to use in the Netherlands in terms of efficiency, costs, etc.

After the different system components have been selected and a general layout of the system is determined, the different components are designed and modelled using Matlab or Simulink environment.

Finally, the whole system is assembled together and simulated in a Simulink environment. The simulation runs over a period of one year using a simulation time step of 6 minutes (0.1 hours). In particular two different cases have been used for the simulation. The base case used is an year where the ambient conditions used (ambient temperature and irradiance intensity) are values averaged over a period of twenty years (1991-2020). The second case is the simulation of a very cold year to see how the system performs in extreme cases. The simulated year is the year 2010.

The obtained results are presented and discussed to draw conclusions and future work recommendations.

The final goal of this work is to understand the competitiveness of the system with respect to a traditional gas boiler in terms of CO_2 emission reduction, performance and costs.

From this work it was possible to conclude that the chosen SAGSHP system performs slightly better in colder climates where a higher heat load requirement is needed. From the base case study used in this work, it was concluded that the modelled SAGSHP system can achieve a system seasonal coefficient of performance (SSCOP) of about 3.8 and it can significantly reduce the amount of CO_2 emissions generated, up to about 2.8 ton of CO_2 every year. From an economical point of view, the system levelized cost of energy (LCOE) is still higher than the LCOE of a traditional gas boiler system due to the high initial investment associated with SAGSHP systems.

Acknowledgments

I would like to thank everyone I met in these years and who made this study experience full of nice and interesting moments, everyone who made me laugh and helped me remember not to take life too seriously.

In particular, I would like to thank my lovely house mates, Andrea and Camilla, my friends Piero, Joost, Vezz and everyone else I shared something with during these years in Delft.

Everyone I met taught me something that I will bring with me in my life and they somehow helped shaping the person I am today and for that I am grateful.

Finally, I would like to thank my family for the continuous support they gave me throughout these years, always helping me take the right decisions and supporting me unconditionally.

*Daniele Tarantini
Delft, March 2021*

Contents

1	Introduction	1
1.1	Thesis objectives	2
1.2	Research questions	2
2	Literature study	3
2.1	Heat Pumps	3
2.2	Solar-Assisted Ground-Source Heat Pumps (SAGSHP)	9
2.2.1	System's components	9
2.2.2	Operating modes	15
2.3	Selection of SAGSHP components for utilisation in Dutch terraced house	15
2.4	Systems model	16
2.4.1	Single U-tube BHE model	16
2.4.2	Heat Pump model	21
3	Components - Design, Model and Validation	23
3.1	Heat Pump	23
3.1.1	HP design	23
3.1.2	HP model	29
3.2	Borehole Heat Exchanger	35
3.2.1	BHE design	35
3.2.2	BHE model	36
3.3	Evacuated Tube Collectors	39
3.3.1	ETC design	39
3.3.2	ETC model	39
3.4	DHW storage tank	40
3.4.1	DHW storage tank design	40
3.4.2	DHW storage tank model	40
3.4.3	DHW consumption hourly profile	42
3.5	House model	43
3.6	Other system components	43
4	Overall system - Design and Model	45
4.1	Design and Layout	45
4.2	Control strategy	47
4.3	Model implementation	47
5	Results and Discussion	51
5.1	Results for averaged values between 1991 and 2020	52
5.2	Results for year 2010	64
6	Conclusions and future recommendations	75
	Bibliography	79

1

Introduction

In the last few years, more than 170 countries signed the Paris agreement to keep a global temperature rise well below 2°C above pre-industrial levels by reducing carbon emissions [1, 2].

In December 2019, the European Commission presented the European Green Deal, a document that provides a roadmap with actions to boost the economy through green technology, creating sustainable industry and transport and cutting pollution. This would make the European Union the first carbon neutral continent with the final goal of having zero net-emissions by 2050 [3].

This means that for all sectors involved with greenhouse gases (GHG) emissions, alternatives that have zero carbon footprint need to replace the current technologies that can no longer be used if we want to achieve such targets.

Among all different sectors, the residential sector is one of the biggest contributors to GHG emissions and most of the energy is used for space heating (SH) and electrical appliances. The heating, ventilation and air conditioning (HVAC) systems account for about one third of global GHG emissions [4]. Of the total final energy use in EU households, 79% is used for space heating and hot water consumption [5].

Moreover, the rapid increase of urban population (projected to be 66% of the global population by 2050) will increase the energy demand of residential buildings even more [6].

If we look into the specific case of the Netherlands, the Energy Report published in 2016 by the Ministry of Economic Affairs of the Netherlands stated that in 2012, just for space heating of homes, buildings and greenhouses, about 45 million tonnes of CO_2 were emitted in the atmosphere. In 2016, 790 petajoule (PJ) of energy mainly obtained from natural gas were used to produce low-temperature heat for space heating. To meet the EU obligation to create an energy-neutral built environment by 2050, the Netherlands aims at drastically reducing the utilisation of natural gas for space heating so that by 2050 the provision of low-temperature heating can have zero CO_2 emissions on balance [7].

In the National Climate Agreement of the Netherlands, presented to the House of Representatives in June 2019, it is stated that the objective for what concerns the built environment is to ensure a reduction of 3.4 Mt of carbon dioxide by 2030 compared to the reference scenario. In order to achieve this, it is reported that roughly 1.5 million existing homes will have to be made more sustainable by 2030. To achieve this objective, we need to move towards a system where the application of circular heating is maximized, a system where we upgrade the waste heat instead of emitting it into the environment. The report states that until 2030, innovation must focus on the completion of technologies for temperatures up to about 300°C, such as heat pumps, while the shift in the highest temperature range will be achieved after 2030. In this scenario, a substantial scaling up of the supply of sustainable heating is required and here the innovation and cost reduction of new and existing technologies play a crucial role [8].

The reduction of natural gas consumption will be achieved thanks to a switch to alternative heat sources such as geothermal energy, electric heat pumps, residual heat, biomass combined heat and power and others. The local availability of heat sources together with building density will be the two main factors that will dictate which technology will be used. In areas with high building density, heat will be produced from various sources. In areas with lower building density, electric heat pumps will be the best option to replace natural gas. In some neighbourhoods, green gas will slowly replace natural gas [9].

In this work, we will focus on electric heat pump and in particular on solar-assisted ground-source heat pump (SAGSHP) technology.

1.1. Thesis objectives

SAGSHP is a relatively new technology that has been investigated recently by many researchers as an alternative to traditional gas boiler heaters for domestic applications. Different combinations of heat pump, solar collectors and borehole heat exchangers can be used in a SAGSHP system and different combinations can have different benefits and drawbacks. The objective of this thesis is to select appropriate system's components and design and model a solar-assisted ground-source heat pump system to provide space heating and domestic hot water for a typical Dutch terraced house. The goal is to try and find a solution that provides high performances together with being as sustainable as possible and model the system to see how this would perform and if it can be an interesting alternative to traditional gas boiler heating systems.

1.2. Research questions

The thesis work has been trying to answer the following questions:

1. What are the different technologies that were used for SAGSHPs in the past?
2. What is the best combination of technologies to be used in the specific case of Dutch terraced houses?
3. What models can be used to model the different components?
4. How can each component be designed and modelled?
5. How can the whole system be designed and modelled?
6. Can the system achieve a SCOP larger than 8?
7. Is this system economically competitive compared to a traditional gas heating system?
8. What is the advantage of this system compared to a gas heating system in terms of CO_2 emission reduction?

The thesis outline has been developed trying to find an answer to the research questions presented above in the order these are presented. This made it possible to gradually move towards the final objectives of the thesis. The different chapters presented below have been written following these research questions. Each chapter tries to answer one or more research questions.

2

Literature study

The goal of this section is to gain a better understanding of the basic working principles of solar assisted ground source heat pump technology and of its main components.

In this chapter we try to find an answer to research questions no. 1, 2 and 3 provided in section 1.2 by looking at the different technologies that have been used in the past for SAGSHP systems, by understanding what is the best combination of technologies for the specific case of Dutch terraced houses and by investigating the models that can be used to model the heat pump system and the BHE.

This section focuses on the literature study. It starts with a very generic explanation about heat pump systems in general, all possible kinds of source and different thermodynamic cycles that are used nowadays. Then the focus will shift towards the specific topic of ground source heat pumps, where the advantages of SAGSHP systems will be presented. Once the advantages of SAGSHP systems have been explained and the reasons for choosing this technology are clear, every different main components used in this kind of system will be analysed in detail. The different available technologies with respective advantages and disadvantages will be presented in order to choose the appropriate combination for the specific case of Dutch terraced houses. This choice is mainly based on the following criteria:

- maximize system performance,
- minimize environmental impact and resources depletion associated with production and utilisation of the different technologies,
- minimize the system's cost.

Once the optimal system layout is defined, the final section is dedicated to studying and introducing the mathematical models used for modelling the different system components.

2.1. Heat Pumps

The European Directive on the energy performance of buildings defines a heat pump as "a machine, a device or an installation that transfers heat from natural surroundings (e.g air or water) to buildings or industrial applications by reversing the natural flow of heat such that it flows from a lower to a higher temperature" [10].

The flow of heat from a source with low temperature to a sink with high temperature is achieved by consuming drive energy and is based on a reverse Carnot cycle [11] as shown in Figure 2.1.

Classification There are different types of heat pumps and these can be classified based on several characteristic features.

A first classification is based on the type of thermodynamic cycle. Here we can distinguish between vapour compression and absorption heat pumps.

In vapour compression heat pumps, the thermodynamic cycle is a traditional inverse cycle, where the compressor is driven either by an engine or by an electric motor. For the case of absorption heat pumps, no mechanical compressor is used. What is used is a mixture of two fluids that have a different vapour pressure so that the more volatile one

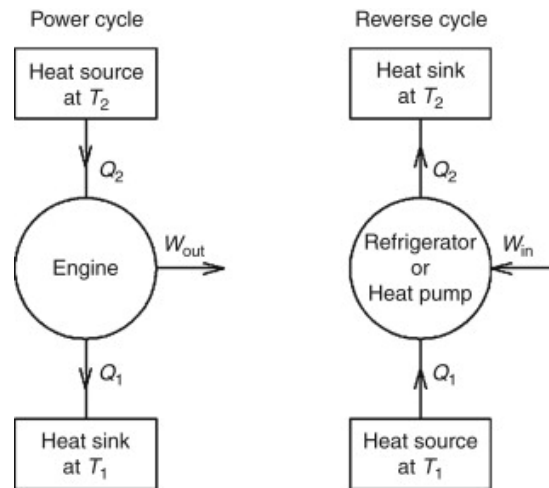


Figure 2.1: Operating principles of heat engines and heat pumps [12]

evaporates and then recombines with the other fluid [13]. Even though absorption heat pumps have some advantages over vapour compression systems, such as a reduced dependency on electricity and more environment friendly working fluids, this technology still needs improvements to achieve large scale commercialization [14].

For this reason, we are going to focus on vapour compression systems only, which are a more mature technology.

Another classification of heat pumps is based on the type of heat source used by the system [13].

The different kinds of heat sources that can be used in heat pump systems are:

- a gas

This can be either the outdoor air or warm air from ventilation or hot gases from industrial processes.

- a liquid

It can be either surface water (such as rivers, lakes or the sea) or ground water or discharged water (from domestic applications or the water recirculated from cooling towers).

- the ground

[11]

The utilisation of heat pumps for heating/cooling purposes is increasing throughout the world and this is happening for different reasons.

First of all, compared to traditional heating systems, such as electric heater and gas boiler, heat pumps can produce much more useful energy using the same input power. This makes such technology more sustainable than traditional alternatives.

Another advantage of heat pump technology is that it allows to use renewable heat (such as aero-thermal or hydrothermal heat) to generate heat for buildings or industrial applications. Additionally, these systems are becoming more and more efficient as well as cheaper, which makes them competitive also from the economical point of view [15].

Working Principle The basic operation of a heat pump system consists in the absorption of heat from a low temperature renewable energy source in order to produce higher temperature heat that can be then used for space heating and domestic hot water (DHW) supply. They can be used both in heating mode or cooling mode by reversing the refrigerant flow accordingly [16]. There are several different heat pump cycles that have been developed and investigated for improving performances depending on the application and on the operating conditions. The most simple cycle consists of a single stage compressor, a condenser, an expansion valve and an evaporator [17]. Since more complex systems introduce additional technical challenges and costs, in this work we are going to focus on simple cycles.

For residential use, the simplest configuration of a heat pump consists of an outdoor unit and an indoor unit. The outdoor unit contains the compressor and a heat exchanger which works as a condenser during summer and as an evaporator in winter. On the other hand, the indoor unit consists of an expansion valve and another heat exchanger which is complementary to the other one, hence working as an evaporator in summer and as a condenser in winter [13].

The simplest refrigeration cycle consists of four different stages; an illustration of the four-stage heat pump system

is shown in Figure 2.2 while in Figure 2.3(a) and Figure 2.3(b) is shown the $P-h$ and $T-S$ diagram, respectively, for the ideal vapour-compression refrigeration cycle. Here below each of the different stages is described:

- (1→2) **COMPRESSOR** The refrigerant enters the compressor in gaseous state as saturated vapour and after undergoing an adiabatic irreversible compression, it exits in a superheated state;
- (2→3) **CONDENSER** The superheated gas goes through the condenser where the refrigerant gas is condensed into liquid as a result of heat rejection to the surroundings;
- (3→4) **EXPANSION VALVE** The liquid refrigerant goes through the expansion valve where it expands and it becomes a mixture of liquid and gas at lower pressure and lower temperature;
- (4→1) **EVAPORATOR** The mixture of liquid and gas goes through the evaporator, where it is completely vaporized by absorbing heat from the low temperature heat source.

[15]

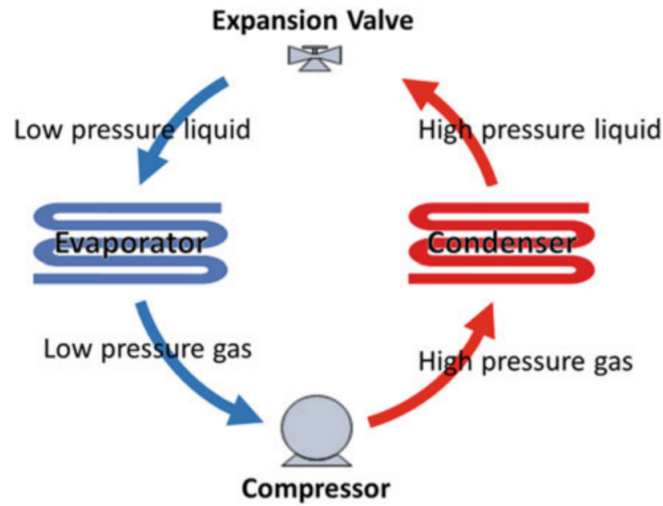


Figure 2.2: Four-stage refrigerant cycle [15]

The heat exchanged with the indoor environment is considered as the useful effect. This means, in winter the useful effect is the heat provided to the indoor environment while in summer it is the heat removed from the indoor environment [13].

The efficiency of a heat pump can be measured using an index called coefficient of performance (COP) which is calculated as the ratio of the heat exchanged with the indoor environment and the energy input provided to run the compressor [19].

$$COP_{heat} = \frac{Q_H}{W} \quad (2.1)$$

and

$$COP_{cool} = \frac{Q_C}{W} \quad (2.2)$$

Where COP_{heat} and COP_{cool} refer to the heating and cooling mode, respectively. Q_H is the heat exchanged with the hot heat sink (in heating mode is the heat provided to the indoor environment) and Q_C is the heat exchanged with the cold heat source (in cooling mode is the heat removed from the indoor environment). W is the energy input used by the compressor. It needs to be stated that all of these quantities are referring to the absolute value of the work and

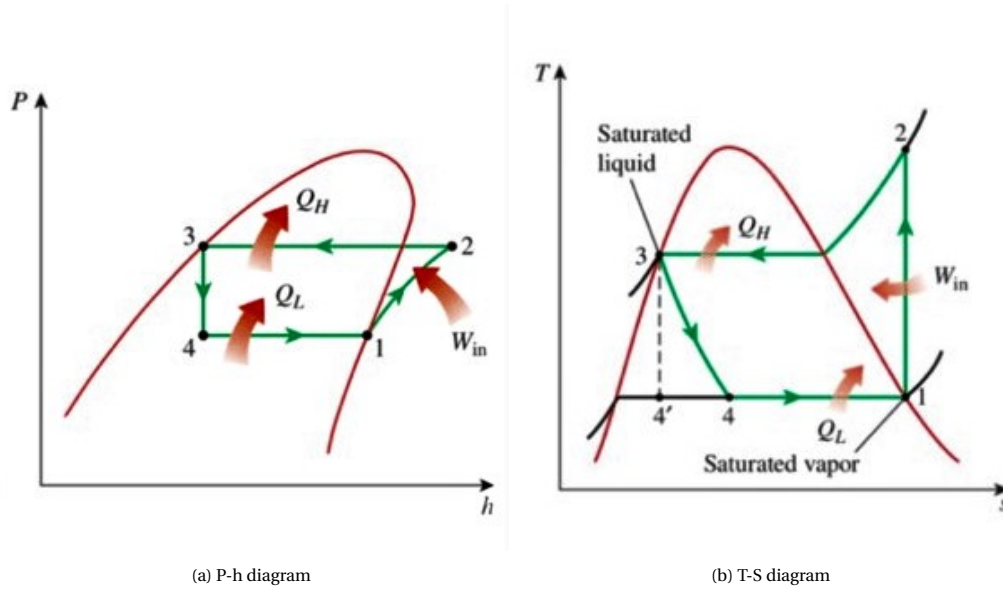


Figure 2.3: Ideal vapour-compression cycle [18]

heat and that the heat is considered positive when it is supplied by the cycle while the work supplied to the cycle is negative.

By the first law of thermodynamics we know that $W = Q_H - Q_C$, which substituted in the equations above gives

$$COP_{heat} = \frac{Q_H}{Q_H - Q_C} \quad (2.3)$$

and

$$COP_{cool} = \frac{Q_C}{Q_H - Q_C} \quad (2.4)$$

The second principle of thermodynamics states that the following holds

$$-\frac{Q_H}{T_H} + \frac{Q_C}{T_C} + S = 0 \quad (2.5)$$

Where T_H and T_C are the temperatures of hot heat sink and cold heat source, respectively, and S is the amount of produced entropy due to internal and external irreversibilities.

Rearranging Equation 2.5 we get

$$\frac{Q_C}{Q_H} = \frac{T_C}{T_H} - \frac{ST_C}{Q_H} = \frac{T_C}{T_H} \left(1 - \frac{T_H S}{Q_H}\right) \quad (2.6)$$

and

$$\frac{Q_H}{Q_C} = \frac{T_H}{T_C} + \frac{ST_H}{Q_C} = \frac{T_H}{T_C} \left(1 + \frac{T_C S}{Q_C}\right) \quad (2.7)$$

Rearranging Equation 2.3 and 2.4 and substituting the values obtained in Equation 2.6 and 2.7 we obtain the following values for the real efficiency of heat pump systems

$$COP_{heat} = \frac{1}{1 - \frac{Q_C}{Q_H}} = \frac{1}{1 - \frac{T_C}{T_H} \left(1 - \frac{T_H S}{Q_H}\right)} \quad (2.8)$$

and

$$COP_{cool} = \frac{1}{\frac{Q_H}{Q_C} - 1} = \frac{1}{\frac{T_H}{T_C} \left(1 + \frac{T_C S}{Q_C}\right) - 1} \quad (2.9)$$

The maximum theoretical efficiency that a heat pump can achieve is given by the ideal Carnot cycle, where $S = 0$. Substituting $S = 0$ in Equation 2.8 and 2.9 we get that the maximum theoretical efficiency of heat pumps in heating and cooling mode is given by

$$COP_{heat} = \frac{T_H}{T_H - T_C} \quad (2.10)$$

and

$$COP_{cool} = \frac{T_C}{T_H - T_C} \quad (2.11)$$

Therefore, from this formula we can state that the maximum theoretical efficiency of a heat pump is affected by the temperature difference between hot and cold source both in heating and cooling mode [13].

The heat source is not only affecting the coefficient of performance of the system but it has also an impact on the system's volume. Increasing the evaporation temperature will decrease the heat-exchanger volume which has a significant impact on the initial cost of the system [17].

Other factors that influence the COP of a heat pump are the working medium which is used as well as the components of the system [15].

The seasonal performance factor (SPF) is also used to characterize the performance of an heat pump system. The SPF of an heat pump system is defined as the ratio of the useful energy output delivered by the system to the input energy required by the system. This factor depends on all the energy-consuming units present in the system and not only on the heat pump [20].

Ground source heat pumps (GSHP) In general, air source heat pumps are the most widespread technology in sustainable buildings and industrial application [15].

However, in terms of performances, ground source heat pumps are the most competitive system [21]. This type of heat pump absorbs heat from the ground by means of a ground heat exchanger. The pipes of the exchanger can be installed either horizontally at a depth of 1-1.5 m underneath the surface or inside vertical boreholes that can have a length of up to 200 m [22]. It is the more stable temperature of the ground, both during the day and throughout the year, that makes this technology more performing than air source heat pumps [16]. Moreover, this systems have the lowest CO_2 emissions which means the lowest environmental impact and they use less energy compared to traditional systems in different climates [22].

Ground source heat pumps are a very valuable alternative to air source heat pumps, especially in cold climates. This is because air source heat pumps can have performance degradation due to frosting of the evaporator during the heating periods, while with ground source heat pumps this risk is very low if the heat pump is properly designed [23]. Additionally, in cold climates, the efficiency of air source heat pumps drops dramatically due to the very large temperature difference between the two reservoirs, which has a negative effect on the performances of the system, as shown by Equation 2.10 and 2.11. This is not the case for ground source heat pumps, where the temperature difference between the two reservoirs is reduced thanks to the insulating properties of the soil [13, 15].

For the aforementioned reasons, for the case of Dutch terraced houses the utilisation of ground source heat pumps seems to be the best choice to maximize the performances of the system.

For what concerns the ground heat exchanger configuration, even though horizontal heat exchangers have lower installation costs, the vertical ground heat exchanger is chosen in order to maximize systems performances. This is the case since soil temperature is more stable at deep depth as shown in Figure 2.4. This makes the borehole heat exchanger (BHE) less influenced by ambient temperature variations and hence more efficient and requiring less pumping energy [24, 25].

Refrigerants Another important factor that influences the performances of heat pump systems as well as their environmental impact is the choice of the refrigerant that will be used in the vapour compression cycle of the heat pump. There are several different kinds of refrigerants and the choice of these needs to be done properly to maximize the performances of the system while minimizing its environmental impact.

Thanks to their good thermodynamic and thermo-physical properties, the most used refrigerants for vapour-compression-based systems in the last century have been the halogenated refrigerants. The most used of these refrigerants are chemical compounds derived from hydrocarbons (HCs), either methane or ethane, where the atoms of

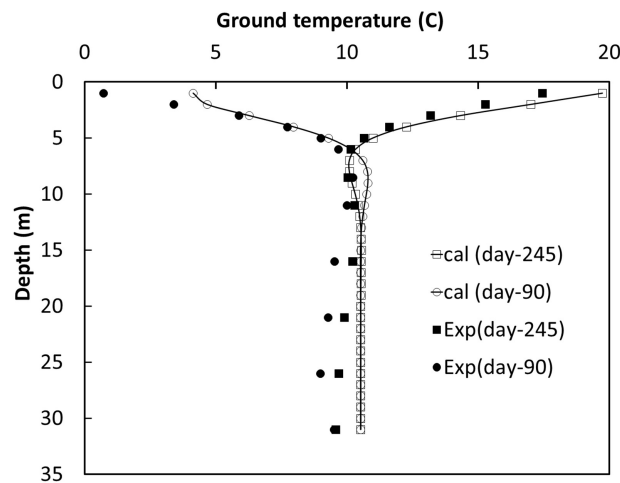


Figure 2.4: Experimental (Exp) measure and calculated (cal) ground temperature at different depth at Varennes for April 10th and September 2nd, 2014. [24]

hydrogen are substituted by either chlorine or fluorine. These refrigerants have, however, very poor environmental properties since they have a very high ozone depletion potential (ODP) as well as a very high global warming potential (GWP). Basic refrigerants have then been substituted by chlorofluorocarbons (CFCs) and hydro-chlorofluorocarbons (HCFCs). However, these refrigerants are still harmful to the environment and for this reason their use has been banned in 1989 according to the Montreal Protocol [26].

Hydrofluorocarbons (HFCs) were used as alternative to the CFCs and HCFCs. These refrigerants don't deplete the ozone layer and share many of the positive properties of the CFCs and HCFCs. However, they still have high GWP which makes them not very environment-friendly [27].

In 1997, thanks to the Kyoto Protocol, the utilization of halogenated refrigerants (hydrofluorocarbons - HFC) has been limited because of their high GWP [28]. The EU Regulation No 517/2014 imposes the drastic reduction of HFC refrigerants as well as of all other refrigerants with a high GWP in the coming future. [29, 30].

The other alternatives are natural hydrocarbons (HCs), HC-based mixtures, HFC-based mixtures, hydrofluoroolefins (HFO) and inorganic refrigerants [26].

HCs and HC-based mixtures have good thermodynamic properties and have a lower GWP compared to HFCs which makes these refrigerants environment-friendly. However, because of their high flammability, the use of these refrigerants is limited in large capacity systems [26, 27, 31].

HFO refrigerants are unsaturated organic compounds composed of hydrogen, fluorine and carbon. Differently from the other halogenated hydrocarbons such as CFCs, HCFCs and HFCs, HFOs have short atmospheric lifetime and are chlorine free, which is the reason why they have zero ODP and extremely low GWP. Only a few HFO refrigerants do not have the problem of being flammable and are suitable as refrigerants, having appropriate thermodynamic properties [32].

Inorganic refrigerants, such as NH_3 and CO_2 , are environment-friendly alternatives. However, the utilisation of these refrigerants may reduce the system's performances [26].

Table 2.1 reports the main characteristics of the most known types of refrigerants together with the restrictions imposed by the different regulations on refrigerants. The toxicity level is indicated with the letters A and B, which stand for low and high toxicity, respectively. The number after the letter refers to the level of flammability of the refrigerants. The number 1 indicates no flame propagation and 3 high flammability. In the specific case of HFOs, the index 2L indicates a mildly flammable refrigerant with a flammability in between the level 1 and 2.

The substitution of halogenated refrigerants with low GWP refrigerants requires a redesign of the components of the heat pump to improve the performances at various operating conditions [28]. The development of systems that use different and more environment-friendly refrigerants is therefore of fundamental importance in the near future.

For this reason, for the development of heat pump systems it is best to use refrigerants that have zero ODP and low GWP values that are allowed by the EU regulation No 517/2014. However, if the utilisation of refrigerants with zero ODP and low GWP reduce the overall efficiency of the system, the net global warming impact of the system is likely to increase. For this reason, it is fundamental to find a fluid that together with accomplishing the GWP limitations can also ensure a low energy consumption in vapour compression systems [29]. In this work, even if it may lower the performance of the heat pump we are going to use refrigerants with zero ODP, low GWP and low flammability of toxicity. From table 2.1 we can see that the refrigerants that satisfy this requirement are HFOs and inorganic refrigerants.

Table 2.1: Comparison of different refrigerants [30, 33]

	ODP	GWP	Flammability and Toxicity	Restrictions
CFC	High	High	A1	Banned
HCFC	Medium	Medium-High	A1/A2	Banned
HFC	Zero	Medium-High	A1	Phasing out (80% reduction by 2030)
HC	Zero	Low	A3	None
HFO	Zero	Low	A2L	None
Inorganic	Zero	Low	A1/B2	None

2.2. Solar-Assisted Ground-Source Heat Pumps (SAGSHP)

In cold climates, where the thermal load profile of buildings is not balanced between heating and cooling, the heat pump mainly works in heating mode and this implies that it extracts continuously heat from the ground. This causes the ground temperature to decrease gradually during the years reducing the performances of the heat pump [34]. The integration of solar thermal collectors (STC) with GSHP can improve the system's performance by stabilizing or gradually increasing the mean ground temperature. Additionally, the recharging of the ground throughout the summer solves the overheating problem of solar collectors which is typical of systems with low cooling demand [35]. It has been found that, for a period of ten years, the seasonal efficiency of the system was stable thanks to the integration of solar thermal collectors with geothermal systems [34]. The utilization of solar thermal collectors in combination with GSHP in cold climates has been proved to reduce the length of the geothermal heat exchangers and therefore lowering significantly the initial investment costs [36].

In cold climates, a further reduction in electricity consumption can be achieved by means of free ground cooling (FGC). This mechanism directly cools the building in summer using the soil as the cold thermal source. Here the fluid flows only through the heat exchanger while the heat pump is bypassed. FGC is not always applicable and its applicability depends on the temperature of the working fluid entering the indoor ambient. The higher this temperature the better the performances of FGC. When applicable, this mechanism allows to cool the indoor environment using very little electricity since the heat pump is not used [16].

2.2.1. System's components

The main components of a SAGSHP system are:

- Heat pump
- Solar thermal collectors
- Borehole heat exchanger

For each of these components, several technologies are currently available. While the different heat pump technologies have been discussed above, for solar thermal collectors and borehole heat exchangers it is worth to spend some time looking into which are the different options and find the best solutions for the specific case of Dutch terraced houses.

Solar thermal Collectors (STCs) For solar hot water and space heating, the solar collector types that are proposed are flat plate collectors (FPCs), evacuated tube collectors (ETCs) and compound parabolic collectors (CPCs) [37]. However, in this work we will focus on the first two types of collectors (FPC and ETC) since these are the kind of solar thermal collectors which are used the most for SH and DHW applications [38]. CPCs will not be taken into consideration because these type of collectors are more convenient compared to FPCs and ETCs only in the case of higher temperatures. Additionally, the high maintenance cost of CPCs makes these collectors less attractive compared to the other

types.

Flat-plate and evacuated tube collectors are non-concentrating collectors. These type of solar collectors are the most used and most economic ones. They have the same area both for intercepting and for absorbing radiation and they exploit both beam and diffuse radiation. No sun tracking technology is needed [39].

Flat-plate collectors are the most common solar collectors. The working principle is that the solar radiation heats up the absorber sheet, a dark flat surface which converts the solar radiation into heat energy. The heat absorbed by the absorber sheet is then transferred to the working fluid which flows through pipes that are attached to the absorber sheet. A schematic of the components of a FPC is shown in Figure 2.5. These collectors have a simple design which favours cheap manufacturing hence low initial costs. Moreover, these collectors are usually permanently fixed, hence they don't need any sophisticated positioning or mounting system [40]. This kind of solar collectors are low-temperature devices ($< 100\text{ }^{\circ}\text{C}$) and are used for situations where the fluid temperature needs to be heated to temperatures not higher than $80\text{ }^{\circ}\text{C}$ [41].

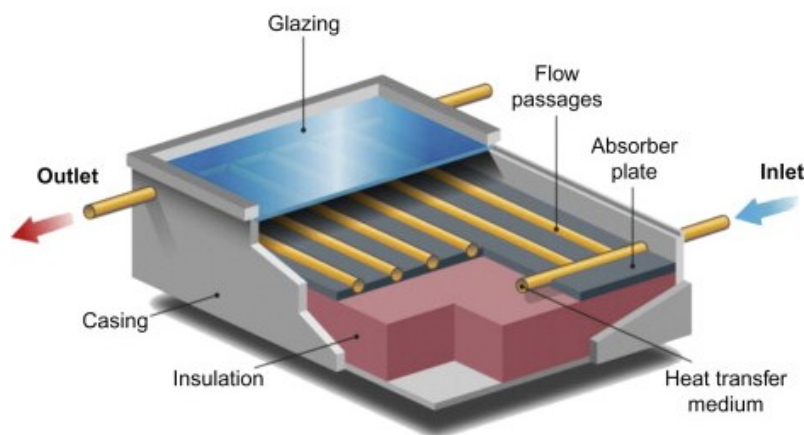


Figure 2.5: Components of a flat plate collector, Illustration by Alfred Hicks/NREL [41]

The typical evacuated tube collectors are water-in glass, U-type and heat pipe collectors. They are all characterized by the presence of vacuum between the absorber sheet and the transparent cover in order to reduce heat losses due to convection and conduction [37].

Here we are going to focus only on heat pipe solar collectors.

These collectors are made up of parallel rows of twin glass tubes, inside the inner glass tube there is a metal heat pipe attached to the absorber sheet. A schematic of a typical heat pipe ETC is shown in Figure 2.6. The working principle of these collectors is based on the evaporation of the heat transfer fluid inside the heat pipe which then rises to a condenser placed at the top of the pipe. The water flowing through a manifold absorbs the heat and the condensed fluid falls back to the bottom of the pipe [42].

A schematic of this phenomenon is shown in Figure 2.7.

The main advantages of the utilisation of heat pipes in these kind of collectors is a low thermal resistance and a high heat removal from absorbing surface [43]. Moreover, the fact that the heat transfer is based on phase change process implies a high heat transfer coefficient [44]. With this type of collectors the working fluid can reach temperatures up to about $200\text{ }^{\circ}\text{C}$. In cold climates, ETCs generally are more efficient than FPCs since their efficiency is less affected by the outside temperature [41].

Compared to flat-plate collectors, this kind of collectors are used either to reach higher temperatures or to reduce the area of the solar field [45].

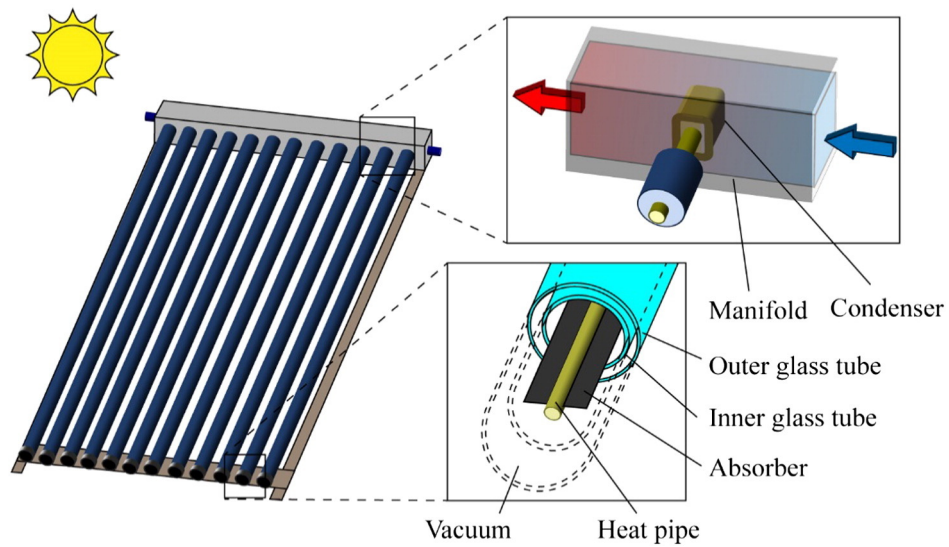


Figure 2.6: Evacuated tube solar collector [42]

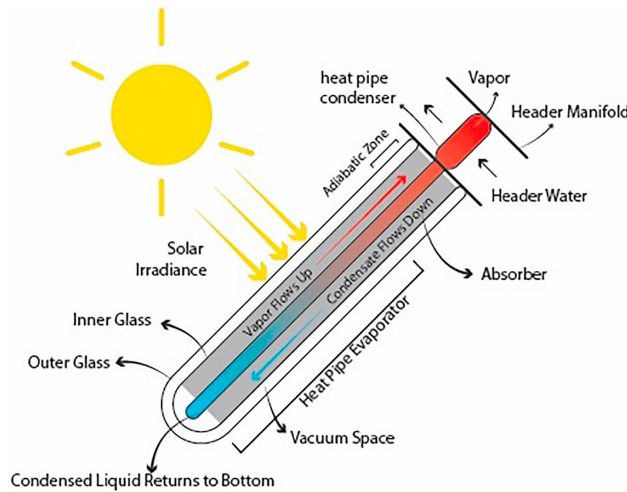


Figure 2.7: Working principle of evacuated tube solar collector [46]

In Table 2.2 a comparison of these different solar collector technologies is reported. The indications on efficiency and initial and maintenance cost for each technology are given relatively to the other technology considered.

Table 2.2: Comparison of solar thermal technologies

	FPC	ETC
T range (°C)	30-80	50-200
Efficiency (Low irradiance)	Lower	Higher
Efficiency (High irradiance)	Higher	Lower
Initial cost	Lower	Higher
Maintenance cost	Higher	Lower

Solar thermal collectors can be placed either in series or in parallel arrangements. While the parallel arrangement is preferred to minimize the pressure drop, it requires a more complicated control of the system to ensure the same flow rate of working fluid through each panel. A rule of thumb is to use a series arrangement when the design system flow rate is low and parallel branches of series collectors when the design system flow rate is high [16].

The performances of solar collectors used for DHW and SH are measured in terms of solar fraction (SF). This quantity measures the percentage of heating energy that is supplied by solar energy on an annual base and it can be used to compare the performances of different systems [41]. The value of SF can be calculated as shown by Equation 2.12

$$SF = \frac{Q_{sol}}{Q_{heat}} = \frac{Q_{sol}}{Q_{SH} + Q_{DHW}} \quad (2.12)$$

Where Q_{sol} is the solar energy supplied to the system, Q_{heat} is the overall energy supplied for heating, Q_{SH} is the portion of energy used for space heating and Q_{DHW} is the portion of energy used for DHW. All this quantities are measured in kWh [47].

Another parameter that is generally used to quantify the performances of solar collector systems for SH and DHW applications is the annual system efficiency η_{sol} which calculates the fraction of solar energy reaching the collectors that is supplied to the hot tank. The efficiency of a solar collector is calculated as shown by Equation 2.13

$$\eta_{coll} = \frac{Q_{sol}}{Q_{inc}} \quad (2.13)$$

Where Q_{inc} is the solar energy that reaches the collectors on an annual basis measured in $kWh/year$. The incident solar energy is calculated as

$$Q_{inc} = A_{coll} * Irr \quad (2.14)$$

Where A_{coll} is the area of solar collectors (m^2) and Irr is the annual solar irradiance measured in $kWh/(m^2 * year)$.

Among these two technologies, flat-plate collectors provide best performances for low temperature applications based on solar contribution [48].

However, in this work FPC technology will not be considered because of the drawbacks of such technology when used for applications in cold climates, where their technical and economical advantages are highly reduced. In particular, FPCs have lower efficiencies (below 40%) in cold climates because their efficiency is highly affected by outside temperature [49].

On the other hand, because of their very good antifreeze capabilities, ETCs may be an interesting alternative for the case of Dutch terraced houses [50].

[51] compared the performance of FPC and ETC for buildings in both hot and cold climates. The results showed that the yearly useful energy gain of ETC compared to FPC is 15 % higher in hot climates and 30 % higher in cold climates. They also performed an economical analysis which showed that FPC are preferred in hot climates while ETC in cold climates.

For these reasons, in this work ETCs will be considered as the solar collector technology utilised in the SAGSHP system for Dutch terraced houses.

Borehole Heat Exchangers (BHE) When used for thermal storage, BHEs constitute one of the main components of the systems and its configuration and dimension have high influence on both the performances and the initial cost of the system [16]. In general, BHEs have a depth in the range of 50 - 200 m [52]. The depth of the borehole has a big influence on the system's performance and cost. Increasing the BHE depth increases the total extracted heat as well as the temperature difference between inlet and outlet, hence improving the performance of the system but at the same time increasing its cost. An optimum depth can be found by a trade-off between performance and cost [53]. The storage surface of the system determines the heat losses while the volume defines the storage capacity. The volume of such system should be large enough since a good surface-to-volume ratio can limit the heat losses to the ground [54].

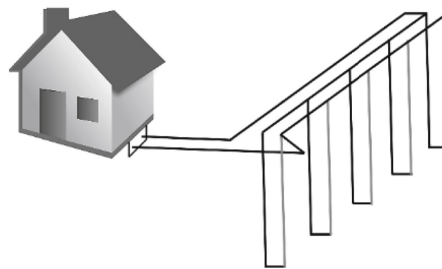


Figure 2.8: Borehole Heat Exchanger [53]

The pipes which are inserted in the ground are generally made of polymers (either polyethylene or polypropylene) and can have varying diameters depending on the specific application [52]. Other materials widely used for the pipes

of the heat exchanger are steel, copper and polyvinyl chloride (PVC) [54]. In general, it has been shown that the pipe material affects the rate of heat exchange less than 1% and it doesn't affect the system performance [53]. A pipe made of high-density polyethylene (HDPE) will be used in this study.

In order to reduce the thermal resistance and to ensure good contact between the pipes and the grout, the space between pipes and grout should be filled with an appropriate material that enhances the thermal connection to the soil [52].

The geometry of the BHEs is another important factor in determining the system's performances and costs. In Figure 2.9 and Figure 2.10 the main BHE geometries are shown. In the literature, the most used geometry is the U-tube. This includes single, double and triple U-tube configuration as well as multiple configurations [53]. Double U-tube BHEs have a higher specific thermal power and higher efficiencies than single U-tube exchangers [55, 56]. On the other hand, construction costs are almost one third higher for double U-tube configurations compared to single U-tube ones. [56]. Triple U-tube BHEs show the highest net output energy followed by double U-tube heat exchangers [57].

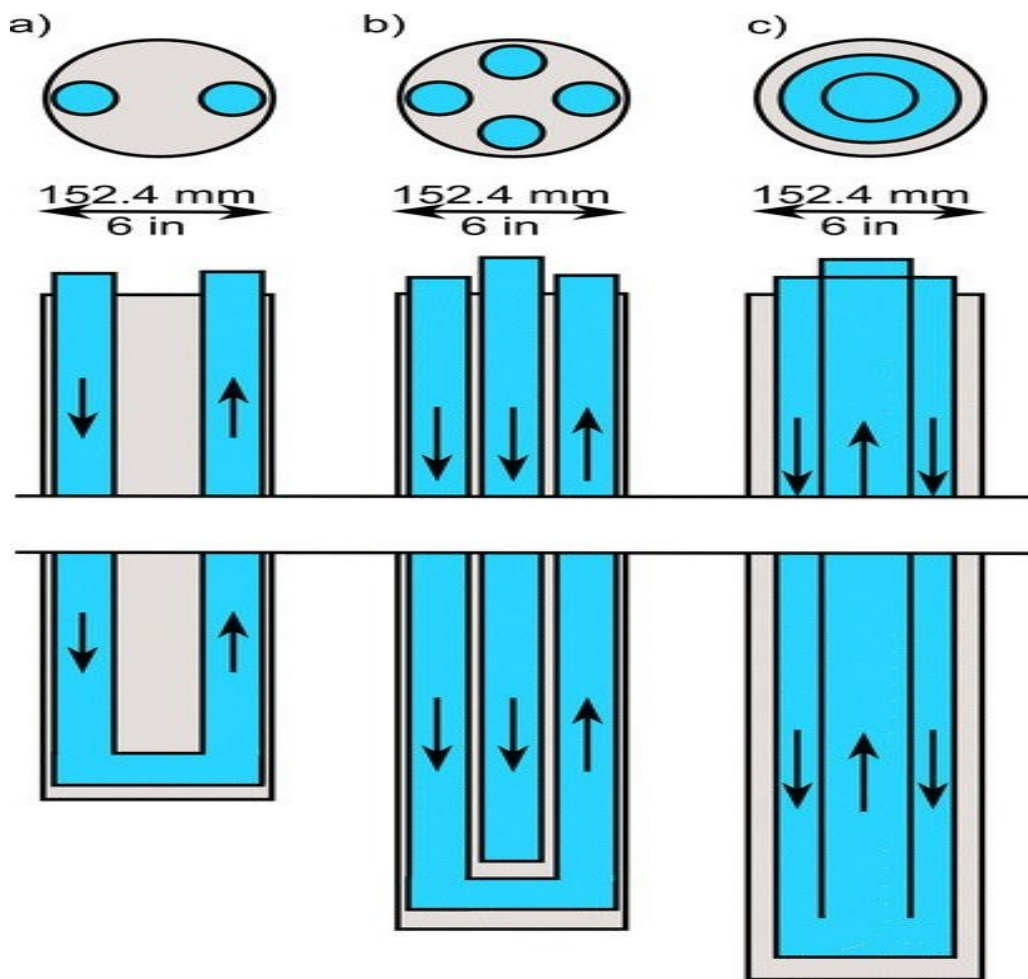


Figure 2.9: Schematic diagram of different types of BHEs (from left to right: single U-pipe, double U-pipe and coaxial) [58]

Alternatives to U-tube BHEs are coaxial, W-tube and helical BHEs.

Coaxial BHEs are the most competitive and interesting alternative to U-pipe BHEs since W-tube BHEs are not very widespread and helical BHEs have the drawback of having a very high pressure drop over the heat carrier fluid [57, 60]

Coaxial BHEs are generally the most advantageous exchangers in terms of performance [61]. It has been shown that the borehole thermal resistance of a coaxial BHE can be significantly lower than the thermal resistance of single U-pipe BHEs but higher than that of double U-pipe BHEs [58]. The larger the coaxial BHE the higher is its thermal resistance but at the same time also the storage capacity increases which allows for substantial reduction in the borehole length [?]. A borehole length reduction of up to 23% has been estimated when using coaxial BHEs instead of U-pipe BHEs. A further advantage of coaxial BHEs is a reduced pressure drop of the heat carrier fluid [58]. In particular, this

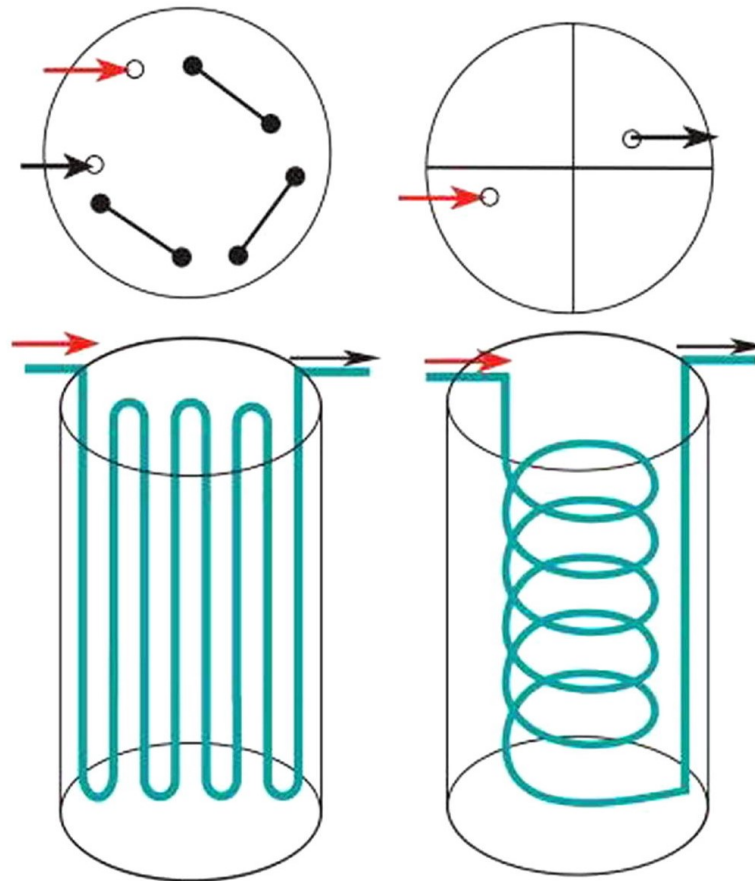


Figure 2.10: Schematic diagram of different types of BHEs (left double w-type, right helical type) [59]

reduced pressure drop is very useful when deeper boreholes are used.

The main drawback of this technology is the higher construction cost compared to U-tube BHEs [61].

Even though coaxial BHEs present several advantages compared to U-tube BHEs, in this work we will focus on single U-tube BHEs since this is the most widespread technology and coaxial BHEs are generally used for deep boreholes while in the case of SAGSHPs the borehole is generally not that deep to justify the utilisation of coaxial BHEs.

Eventually, the choice of the working fluid is another thing that has influence on the performance of the system. Desired properties of the working fluid are a high heat capacity as well as a not too high viscosity [62]. The most used working fluid is pure water, followed by glycol and gasoline. Water has significant advantages over other working fluid because of its availability and low cost [?]. A research done on water, glycol and gasoline as fluid carriers showed that more heat can be recovered and stored when using water compared to glycol and gasoline [62]. Because of its low cost, high availability and the other advantages mentioned above, in this work water will be considered as the working fluid. When water is used as fluid carrier, the addition of antifreeze solutions is needed only when the working fluid's temperature can fall below 0 °C [54].

2.2.2. Operating modes

A SAGSHP system can have different operating modes. The different modes are mainly defined by the way the solar heat absorbed by the solar collectors is used in the system. Different operating modes are preferred to maximize the effective use of the solar energy depending on borehole depths, STC typology and area of the solar collectors [47].

Recharging mode In the recharging mode, all the heat absorbed by solar collectors is used to recharge the BHE. In this operating mode, the solar system is connected only to the ground [63].

Limited recharging mode The recharging of the BHE is limited to the cold months of the year while the rest of the year the solar heat is used for DHW and SH through the hot tank [64]. [47] in his work used as recharging period the time from November to February while from March to October the solar collectors were connected only to the storage tank.

Temperature based recharging mode In this operating mode, the solar heat is used primarily for DHW and SH and only once the DHW and SH requirements are satisfied the solar heat is used for recharging the BHEs. This system allows to maximize the utilisation of solar energy and this makes it the most interesting operating mode [47]. The injection of solar heat in the ground is controlled by the temperature difference between the outlet temperature of the hot tank and the inlet temperature, which corresponds to the outlet temperature of the BHEs. Only when this difference is higher than a certain value then the system switches to ground charging [64].

[47] compares the performances of different SAGSHP systems (different borehole length and area of solar collectors) for a cold climate using the above mentioned operating mode for the same heating requirements. In this work, a single U-tube BHE was used. Part of the results of his work can be summarized in Table 2.3 where for each combination of borehole length and solar collector area, the collector types for which the temperature based recharging mode was preferred are reported.

Table 2.3: BHE length, solar field area and collector type for which the temperature based recharging mode is preferred to others [47].

	70.5 m	100.5 m	150.5 m
46.8 m ²	FPC	FPC/ETC	FPC/ETC
93.6 m ²	ETC	ETC	ETC

2.3. Selection of SAGSHP components for utilisation in Dutch terraced house

The different technologies used in SAGSHPs have been studied and compared in order to select the most suitable combination for Dutch terraced houses with the goal of maximizing system's performance and efficiency, minimizing environmental impact and resources depletion while still trying to maintain competitive costs. In most cases, as expected, a trade-off between these goals was found.

The following conclusions have been drawn from this initial investigation to answer the research question no. 2 "What is the best combination of technologies for a SAGSHP system to be used in the specific case of Dutch terraced houses?":

- Vapour-compression heat pumps are a better option than absorption heat pumps since absorption heat pumps still need improvements to achieve large scale commercialization;
- The refrigerant used in the heat pump will be selected among refrigerants that have a low GWP, zero ODP and low flammability. The chosen refrigerants are HFO and inorganic refrigerants since these can provide good performances and have a low GWP and zero ODP;
- Heat pipes ETC are preferred to FPC because of their higher efficiency in cold climates;
- Vertical BHE ensure a higher system's efficiency compared to horizontal BHE because of the underground soil temperature profile being more stable at larger depths;
- The single U-tube is the selected geometry for the system since it gives a good trade-off between performance and cost;
- Water has been selected as the BHE working fluid because of its high heat capacity, low cost and availability; it can be mixed with ethylene-glycol if risk of freezing can occur.
- A recharging mode has been chosen as the main operation mode in order to use the ETC heat output to recharge the BHE only.

2.4. Systems model

The different components of the SAGSHP system have different impacts on the systems behaviour. The level of detail of the model of each component will change depending on the impact of the component on the behaviour of the system.

In our case, we are mainly interested in the heat pump and the BHE which have the main influence on the system performance and which should be modelled accurately while the model for ETCs will have a lower accuracy since this component has a lower impact on the performance of the system. In the following section, we will focus on the heat pump and BHE models while the ETC model, together with the storage tank and the other additional components, will be presented directly in the section where the model implementation is discussed.

2.4.1. Single U-tube BHE model

There are several different analytical and numerical models that have been developed in the past years to model the thermal behaviour of BHEs. The analytical models that have been developed can be divided into two main groups: line source models and surface source models. Both these models have been used in different studies to perform long-term simulation and analysis of BHE. However, these analytical models are not able to simulate the BHE thermal behaviour in the case of quick variations of operational conditions. Therefore, in order to model the heat transfer mechanism occurring inside the single U-tube BHE when quick changes in operational conditions occur (such as on-off cycles of heat pump or flow rate and temperature variation), a numerical unsteady heat transfer model is required in order to be able to predict the short-term response of the system [65].

There are different heat transfer mechanisms which occur in a U-tube BHE. Convective heat transfer occurs between the working fluid and the U-pipe while conduction heat transfer occurs between the U-pipe and the grout and between the grout and the soil. The governing equations of the heat transfer process for each region of the BHE are obtained combining the energy balance relationships among the different heat exchange media and the thermal resistance model as suggested by [66]. Once the governing equations are obtained, these are solved using the Crank-Nicolson method, a fully implicit numerical method which combines high accuracy with stability.

The following simplifying assumptions have been made:

1. The heat transfer in vertical direction between different grid elements of the grout and ground domain is considered to be negligible compared to the heat transfer in the radial direction.
2. The ground is considered to be an homogeneous medium having homogeneous properties and underground water flow is not taken into account.
3. Both in the grout and in the ground domains, the only heat transfer mechanism considered is conduction.
4. Material properties of both ground, grout and U-pipe are independent of temperature. An average value is considered for the simulation.
5. Ground temperature at far boundary is not affected by the heat transfer in the BHE and remains constant.
6. The contact resistance between U-tube and grout and between borehole wall and ground is considered to be negligible.
7. The heat generated by the viscous friction is assumed to be negligible since it is much smaller than the heat exchange occurring between the different media.

Energy balance equations The derivation of the energy balance equations follows the procedure suggested by [66]. Here the control volume shown in Figure 2.11 is used to describe the heat transfer process occurring inside the BHE. In Figure 2.12 are shown the energy interactions occurring for a fluid element inside the U-tube both for an i th fluid element and for the first fluid element. Here, the inlet pipe is called tube-u and the outlet pipe is called tube-v.

The two-dimensional thermal resistance and capacity model which is combined with the energy balance equation is the model developed by [67]. This is shown in Figure 2.13.

The equation for the i^{th} fluid element inside the tube-u can then be obtained making an energy balance on the node inside the fluid as shown in Figure 2.12. The resulting equation is:

$$M_f c_{p_f} \frac{dT_{f_u}}{dt} = \dot{m}_f c_{p_f} T_{f_u, i-1} - \dot{m}_f c_{p_f} T_{f_u, i} - \frac{T_{f_u, i} - T_{f_v, i}}{R_{f_f} / \Delta z} - \frac{T_{f_u, i} - T_{g, i}}{R_{f_g} / \Delta z} \quad (2.15)$$

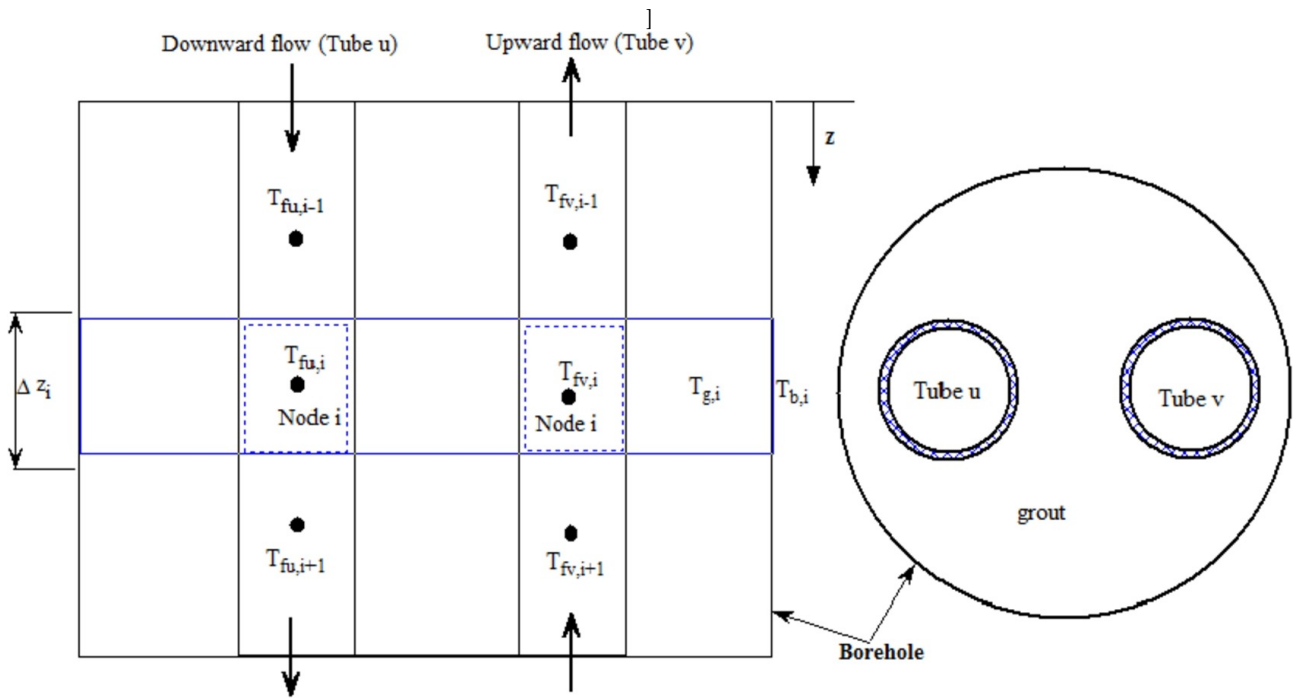


Figure 2.11: Schematic diagram of borehole and grid scheme inside the borehole [66]

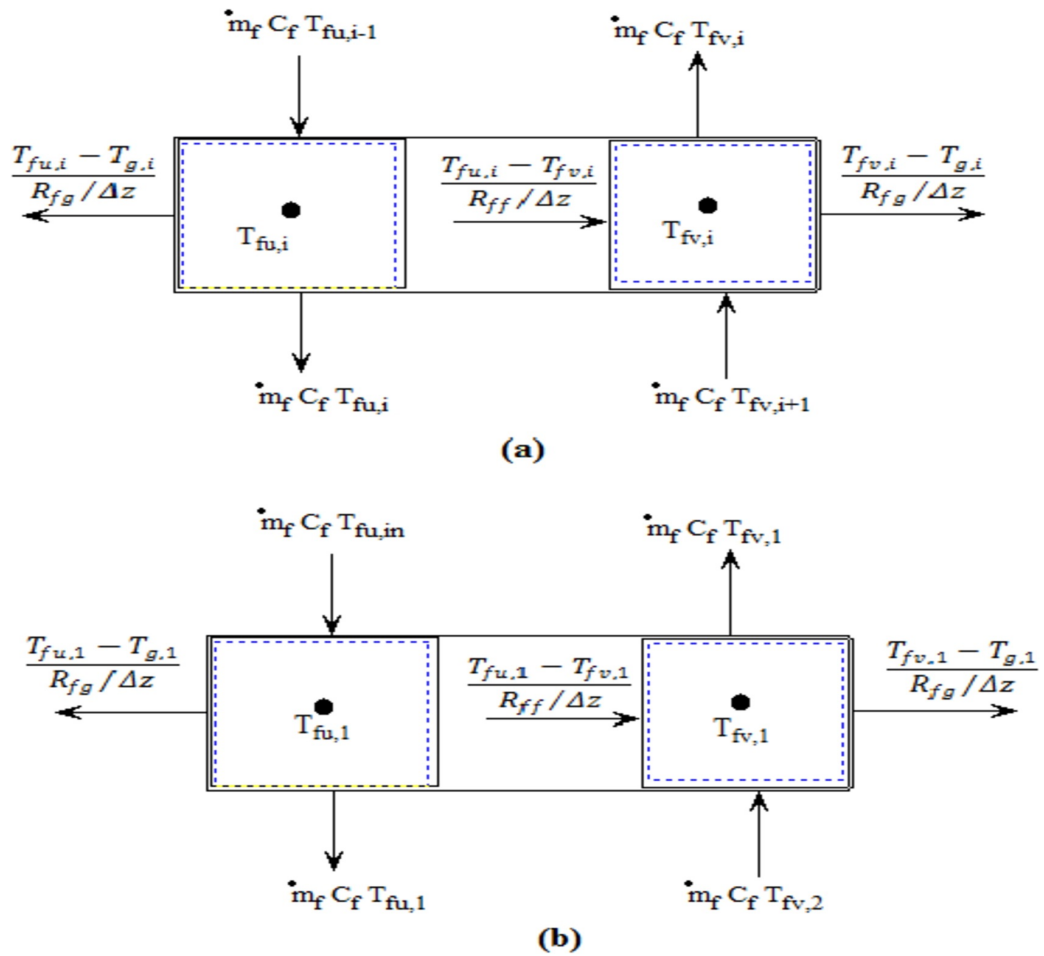


Figure 2.12: Energy interaction on node inside tube-u and tube-v: (a) *i*th fluid element and (b) the first fluid element [66]

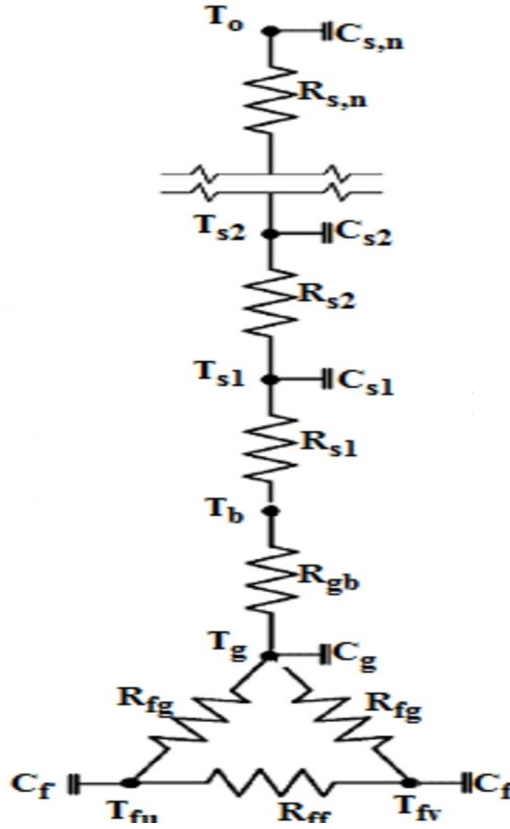


Figure 2.13: Thermal circuit inside and outside the borehole [66]

Following the same procedure, the equations for the i^{th} fluid element inside the tube-v and for the grout element inside the borehole are obtained as shown by Equation 2.16 and Equation 2.17, respectively

$$M_f c_{pf} \frac{dT_{fv}}{dt} = \dot{m}_f c_{pf} T_{fv,i+1} - \dot{m}_f c_{pf} T_{fv,i} + \frac{T_{fu,i} - T_{fv,i}}{R_{ff}/\Delta z} - \frac{T_{fv,i} - T_{g,i}}{R_{fg}/\Delta z} \quad (2.16)$$

$$M_g c_{pg} \frac{dT_{g,i}}{dt} = \frac{T_{fv,i} - T_{g,i}}{R_{fg}/\Delta z} + \frac{T_{fu,i} - T_{g,i}}{R_{fg}/\Delta z} - \frac{T_{g,i} - T_{b,i}}{R_{gb}/\Delta z} \quad (2.17)$$

Eventually, the energy balance equation for the k^{th} element outside the borehole is obtained as follows:

$$M_{s,k} c_{ps} \frac{dT_{s,k}}{dt} = \frac{T_{s,k-1} - T_{s,k}}{R_{s,k}/\Delta z} - \frac{T_{s,k} - T_{s,k+1}}{R_{s,k+1}/\Delta z} \quad (2.18)$$

where $k = 1, 2, 3, \dots, n$. For $k = 1$, $T_{s,0} = T_b$ and for $k = n$, $T_{s,n+1} = T_o$

In the above equations the subscripts f , g , b and s , refer respectively to the working fluid, the grout, the borehole wall and the soil. M is the mass of the discretized element [kg], c_p is the specific heat of the material [$J/(kg \text{ } ^\circ C)$], \dot{m}_f is the mass flow rate of the working fluid [kg/s], Δz is the length of the discretized element in the vertical direction [m], R_{ff} is the thermal resistance per unit length between the upward and downward flowing fluid, R_{fg} is the thermal resistance per unit length between the working fluid and the grout, R_{gb} is the thermal resistance per unit length between the grout and the borehole wall, $R_{s,1}$ is the thermal resistance per unit length between the borehole and the soil ($= R_{bs}$) and R_s is the thermal resistance per unit length between two adjacent soil elements. The unit of measurement of the thermal resistance per unit length is $(m^\circ C)/W$.

The thermal resistance per unit length between the upward and downward flowing fluid (R_{ff}) can be calculated using the following equation [68]:

$$R_{ff} = \frac{R_{11}R_{22} - R_{12}^2}{R_{12}} \quad (2.19)$$

where R_{12} is the thermal resistance between the centres of the two legs, R_{11} and R_{22} are the thermal resistances between the borehole wall and the circulating fluid inside a certain U-tube leg, respectively. In the case of symmetrically disposed U-tube legs, $R_{11} = R_{22}$ and hence Equation 2.19 can be rearranged as follows:

$$R_{ff} = \frac{R_{11}^2 - R_{12}^2}{R_{12}} \quad (2.20)$$

The two terms R_{11} and R_{12} are calculated using the following equations [68]:

$$R_{11} = \frac{1}{2\pi k_p} \ln\left(\frac{r_{po}}{r_{pi}}\right) + \frac{1}{2\pi r_{pi} h_c} + \frac{1}{2\pi k_b} \left(\ln\frac{r_b}{r_{po}} + \frac{k_b - k_s}{k_b + k_s} \ln\frac{r_b^2}{r_b^2 - s^2} \right) \quad (2.21)$$

$$R_{12} = \frac{1}{2\pi k_b} \left(\ln\frac{r_b}{2s} + \frac{k_b - k_s}{k_b + k_s} \ln\frac{r_b^2}{r_b^2 + s^2} \right) \quad (2.22)$$

where k is the thermal conductivity [$W/(m^\circ C)$], r_{pi} and r_{po} are respectively the inner and outer radius of the U-pipe [m], h_c is the convective heat transfer coefficient between the working fluid and the inner wall of the U-pipe [$W/(m^2^\circ C)$] and s is the shank spacing which is defined as half of the distance between the centres of the two legs of the U-pipe.

The calculation of the thermal resistance between the working fluid and the grout (R_{fg}) is calculated using the following equation [67]:

$$R_{fg} = R_p + xR_g \quad (2.23)$$

where R_p is the thermal resistance which includes the convection resistance of the fluid in the pipe and the conduction resistance of the pipe wall, R_g is the conduction resistance of the grout and x is the location of the grout centre of mass. These are calculated using the following equations, respectively:

$$R_p = \frac{1}{2\pi r_{pi} h} + \frac{1}{2\pi k_p} \ln\left(\frac{r_{po}}{r_{pi}}\right) \quad (2.24)$$

$$R_g = \frac{1}{2\pi k_b} \left(\ln\frac{r_b}{r_{po}} + \frac{k_b - k_s}{k_b + k_s} \ln\frac{r_b^2}{r_b^2 - s^2} \right) + \frac{1}{2\pi k_b} \left(\ln\frac{r_b}{2s} + \frac{k_b - k_s}{k_b + k_s} \ln\frac{r_b^2}{r_b^2 + s^2} \right) \quad (2.25)$$

$$x = \frac{\ln\left(\frac{\sqrt{r_b^2 + r_{po}^2}}{2r_{po}}\right)}{\ln\left(\frac{r_b}{r_{po}\sqrt{2}}\right)} \quad (2.26)$$

Eventually, the thermal resistance between the grout and the borehole wall (R_{gb}) and the thermal resistance between different elements of the soil outside the borehole ($R_{s,k}$) are calculated using the following equations:

$$R_{gb} = (1 - x)R_g \quad (2.27)$$

$$R_{s,k} = \frac{1}{2\pi k_s} \ln\left(\frac{r_{s,k}}{r_{s,k-1}}\right) \quad (2.28)$$

where Δr is the dimension of the discretized element in the radial direction outside the borehole [m] and $r_{s,k}$ is the radial distance of the inner face of the k^{th} node outside the borehole [m]. The radial distance $r_{s,k}$ can be calculated as follows:

$$r_{s,k} = r_b + \frac{\Delta r}{2} + (k - 1)\Delta r \quad (2.29)$$

For the first node outside the borehole, the thermal resistance is given by

$$R_{s,1} = \frac{1}{2\pi k_s} \ln\left(\frac{r_{s,1}}{r_b}\right) \quad (2.30)$$

The convective heat transfer coefficient which describes the convective heat transfer mechanism that occurs between the heat transfer fluid and the inner wall of the U-pipe is calculated using the Dittus-Boelter correlation [68] described by Equation 2.31

$$h_c = 0.023Re^{0.8}Pr^n \frac{k_f}{2r_{pi}} \quad (2.31)$$

where $n = 0.3$ for cooling, $n = 0.4$ for heating, Re is the Reynolds number and Pr is the Prandtl number. In general, these can be calculated as shown in Equation 2.32 and 2.33.

$$Re = \frac{4\dot{m}}{\pi\mu d} \quad (2.32)$$

$$Pr = \frac{c_{p_f}\mu}{k_f} \quad (2.33)$$

where \dot{m} is the working fluid mass flow rate (kg/s), μ is the dynamic viscosity of the working fluid ($Pa \cdot s$).

Numerical solution Discretization of the energy balance equations provided above is done using a fully implicit numerical method in order to ensure that the numerical model is stable. In particular, as mentioned above, the Crank-Nicolson method is used as suggested by [66] since it guarantees high accuracy and it is unconditionally stable.

In the Crank-Nicolson method, for any time step j we have that

$$T_{j+1} = T_j + \left\{ \left[\frac{dT}{dt} \right]_{T=T_j, t=t_j} + \left[\frac{dT}{dt} \right]_{T=T_{j+1}, t=t_{j+1}} \right\} \frac{\Delta t}{2} \quad (2.34)$$

that is, the time rate of change for the time step is estimated based on the average of its value at the beginning and at the end of the time step.

This method will be applied on each energy balance equation obtained above (Equations 2.15, 2.16, 2.17 and 2.18)

Starting with the i^{th} element inside tube-u, the Crank-Nicolson equation can be written as

$$T_{f_u,i}^{j+1} = T_{f_u,i}^j + \left\{ \left[\frac{dT_{f_u}}{dt} \right]^j + \left[\frac{dT_{f_u}}{dt} \right]^{j+1} \right\} \frac{\Delta t}{2} \quad (2.35)$$

The term $\frac{dT_{f_u}}{dt}$ at both time j and $j+1$ can be obtained rearranging Equation 2.15. Substituting this term into Equation 2.35 we get the following:

$$\begin{aligned} T_{f_u,i}^{j+1} = T_{f_u,i}^j + \left\{ \frac{T_{f_v,i}^j - T_{f_u,i}^j}{M_f c_{p_f} R_{ff}/\Delta z} + \frac{T_{g,i}^j - T_{f_u,i}^j}{M_f c_{p_f} R_{fg}/\Delta z} + \frac{\dot{m}_f}{M_f} (T_{f_u,i-1}^j - T_{f_u,i}^j) + \right. \\ \left. + \frac{T_{f_v,i}^{j+1} - T_{f_u,i}^{j+1}}{M_f c_{p_f} R_{ff}/\Delta z} + \frac{T_{g,i}^{j+1} - T_{f_u,i}^{j+1}}{M_f c_{p_f} R_{fg}/\Delta z} + \frac{\dot{m}_f}{M_f} (T_{f_u,i-1}^{j+1} - T_{f_u,i}^{j+1}) \right\} \frac{\Delta t}{2} \quad (2.36) \end{aligned}$$

In order to be able to solve this equation using MATLAB, this equation needs to be rearranged in matrix form as follows:

$$\begin{aligned} -\frac{\dot{m}_f \Delta t}{2M_f} T_{f_u,i-1}^{j+1} + \left[1 + \frac{\Delta t}{2} \left(\frac{1}{M_f c_{p_f} R_{ff}/\Delta z} + \frac{1}{M_f c_{p_f} R_{fg}/\Delta z} + \frac{\dot{m}_f}{M_f} \right) \right] T_{f_u,i}^{j+1} - \frac{\Delta t}{M_f c_{p_f} R_{ff}/\Delta z} T_{f_v,i}^{j+1} - \frac{\Delta t}{M_f c_{p_f} R_{fg}/\Delta z} T_{g,i}^{j+1} = \\ = \frac{\dot{m}_f \Delta t}{2M_f} T_{f_u,i-1}^j + \left[1 - \frac{\Delta t}{2} \left(\frac{1}{M_f c_{p_f} R_{ff}/\Delta z} + \frac{1}{M_f c_{p_f} R_{fg}/\Delta z} + \frac{\dot{m}_f}{M_f} \right) \right] T_{f_u,i}^j \quad (2.37) \end{aligned}$$

The same procedure is followed for all the other domains of the borehole heat exchanger. The final equations rearranged in matrix form for the i^{th} fluid element inside tube-v, for the i^{th} grout element and for the k^{th} soil element outside the borehole, are given by Equations 2.38, 2.39 and 2.40, respectively.

$$\begin{aligned} \left[1 + \frac{\Delta t}{2} \left(\frac{1}{M_f c_{p_f} R_{ff}/\Delta z} + \frac{1}{M_f c_{p_f} R_{fg}/\Delta z} + \frac{\dot{m}_f}{M_f} \right) \right] T_{f_v,i}^{j+1} - \frac{\dot{m}_f \Delta t}{2M_f} T_{f_v,i+1}^{j+1} - \frac{\Delta t}{M_f c_{p_f} R_{ff}/\Delta z} T_{f_u,i}^{j+1} - \frac{\Delta t}{M_f c_{p_f} R_{fg}/\Delta z} T_{g,i}^{j+1} = \\ = \left[1 - \frac{\Delta t}{2} \left(\frac{1}{M_f c_{p_f} R_{ff}/\Delta z} + \frac{1}{M_f c_{p_f} R_{fg}/\Delta z} + \frac{\dot{m}_f}{M_f} \right) \right] T_{f_v,i}^j + \frac{\dot{m}_f \Delta t}{2M_f} T_{f_v,i+1}^j \quad (2.38) \end{aligned}$$

$$\left[1 + \frac{\Delta t}{2} \left(\frac{2}{M_g c_{p_g} R_{fg} / \Delta z} + \frac{1}{M_g c_{p_g} R_{gb} / \Delta z} \right)\right] T_{g,i}^{j+1} - \frac{\Delta t}{2} \left(\frac{1}{M_g c_{p_g} R_{fg} / \Delta z} T_{f_v,i}^j + \frac{1}{M_g c_{p_g} R_{fg} / \Delta z} T_{f_u,i}^j + \frac{1}{M_g c_{p_g} R_{gb} / \Delta z} T_{b,i}^j \right) = \left[1 - \frac{\Delta t}{2} \left(\frac{2}{M_g c_{p_g} R_{fg} / \Delta z} + \frac{1}{M_g c_{p_g} R_{gb} / \Delta z} \right)\right] T_{g,i}^j + \frac{\Delta t}{2} \left(\frac{1}{M_g c_{p_g} R_{fg} / \Delta z} T_{f_v,i}^j + \frac{1}{M_g c_{p_g} R_{fg} / \Delta z} T_{f_u,i}^j + \frac{1}{M_g c_{p_g} R_{gb} / \Delta z} T_{b,i}^j \right) \quad (2.39)$$

$$- \frac{\Delta t}{2 M_{s,k} c_{p_s} R_{s,k} / \Delta z} T_{s,k-1}^{j+1} + \left[1 + \frac{\Delta t}{2} \left(\frac{1}{M_{s,k} c_{p_s} R_{s,k} / \Delta z} + \frac{1}{M_{s,k} c_{p_s} R_{s,k+1} / \Delta z} \right)\right] T_{s,k}^{j+1} + \frac{\Delta t}{2 M_{s,k} c_{p_s} R_{s,k+1} / \Delta z} T_{s,k+1}^{j+1} = \frac{\Delta t}{2 M_{s,k} c_{p_s} R_{s,k} / \Delta z} T_{s,k-1}^j + \left[1 - \frac{\Delta t}{2} \left(\frac{1}{M_{s,k} c_{p_s} R_{s,k} / \Delta z} + \frac{1}{M_{s,k} c_{p_s} R_{s,k+1} / \Delta z} \right)\right] T_{s,k}^j + \frac{\Delta t}{2 M_{s,k} c_{p_s} R_{s,k+1} / \Delta z} T_{s,k+1}^j \quad (2.40)$$

Boundary and initial conditions The following boundary conditions (BC) and initial conditions (IC) will be applied to the numerical model:

I.C. The initial temperature of the working fluid, the grout and the soil is equal to the undisturbed ground temperature

$$T_0$$

$$[T_{f_u}^0 = T_{f_v}^0 = T_g^0 = T_b^0 = T_s^0 = T_0]$$

B.C. The temperature of the working fluid in the upper node of tube-u (i=0) will be equal to the inlet temperature of the fluid inside the tube

$$[T_{f_u,0} = T_{f,in}]$$

B.C. The temperature of the working fluid inside the tube-u at the last node (i=M) is equal to the temperature of the fluid entering the tube-v

$$[T_{f_u,M} = T_{f_v,M+1}]$$

2.4.2. Heat Pump model

The model of the heat pump cycle is based on energy and mass balances between the different thermodynamic stages of the cycle. The chosen configuration for the heat pump cycle is shown in the flow sheet in Figure 2.14

Compared to the basic four-stage cycle shown in Figure 2.2, in the flow sheet we can notice the presence of an internal heat exchanger (IHX). Even though the addition of an IHX implies a higher initial cost, it can increase significantly the COP of the heat pump because the working fluid is superheated using the heat coming from the further subcooling. This results in a higher temperature of the refrigerant entering the condenser and therefore a higher COP [69].

In the flow sheet we can also see the subdivision of the condenser into three separate heat exchangers, namely desuperheater, condenser and sub-cooler. These are the three stages of the condensation.

In the desuperheater the high temperature refrigerant coming from the compressor is cooled down to the condensation temperature.

In the condenser only latent heat is transferred to the sink stream. In this stage the refrigerant condenses. The sink stream is heated up while the temperature of the refrigerant remains constant.

In the subcooler, the entering refrigerant is in liquid form and it is further cooled down exchanging more heat with the sink stream.

These three stages will be modelled separately.

The compressor will be modelled considering the isentropic efficiency characteristic curve of the compressor. In case the compressor pressure ratio is too high, a two stage compressor can be considered.

In order to determine the relevant thermodynamic states of the refrigerant at each stage of the cycle, the software REFPROP [70] will be used. If two of the thermodynamic properties of the refrigerant are known, the software allows to calculate the remaining thermodynamic properties of the fluid.

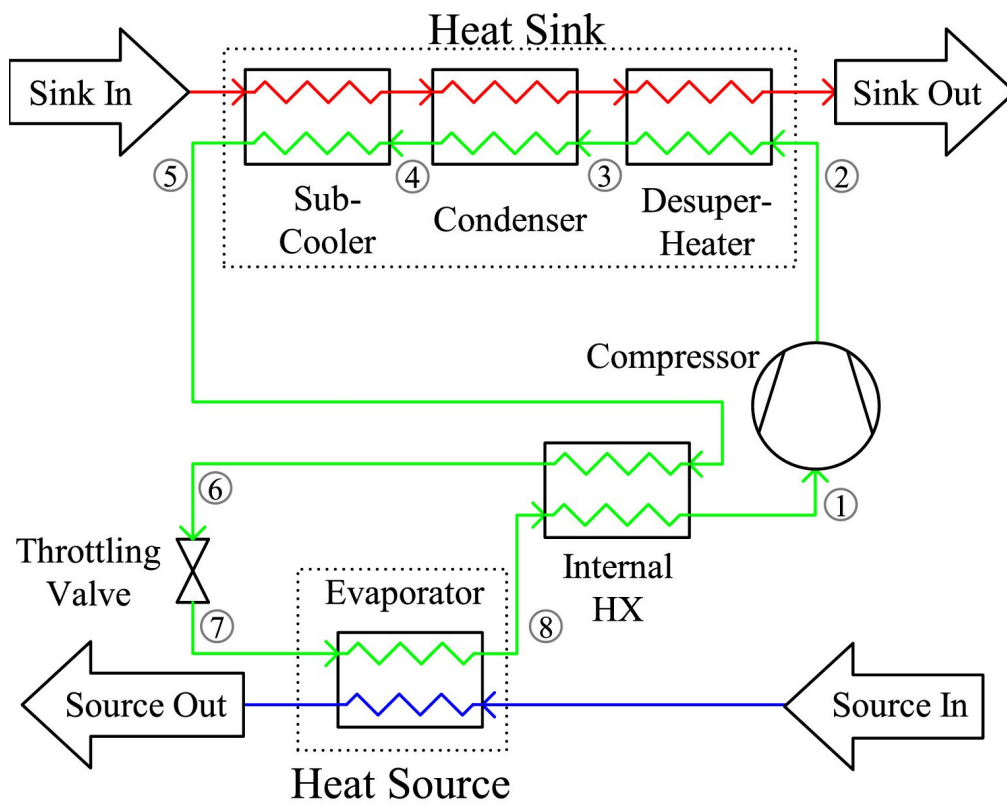


Figure 2.14: Flow sheet of the heat pump cycle

[69]

3

Components - Design, Model and Validation

The design choices together with the model implementation for each main component of the system are reported in this section.

Here we try to answer to research question no. 4 provided in section 1.2 by showing how the different components of the SAGSHP system are designed and how the equations to model each separate sub-system have been implemented.

3.1. Heat Pump

3.1.1. HP design

The heat pump design has been done following certain parameters and different design choices came out during the process.

General cycle layout

In Figure 3.1 we can see the general layout of the heat pumps for both SH and DHW. A first design choice was to split the DHW and space heating production since the temperature requirements for DHW are higher than the temperature requirements for SH. In particular, the water stored in DHW tanks requires to reach a temperature of 65°C in order to prevent legionella growth while for SH a much lower temperature is sufficient. Therefore, dividing these two processes using two heat pumps makes it possible to have a SH HP with a higher COP since T_{cond} is reduced for the SH HP. Additionally, the fact that DHW needs to be drinkable while SH water doesn't need that, makes the separation a convenient way to reduce the amount of drinkable water that needs to be used. With these considerations in mind, the final design has been done as shown in Figure 3.1. Here we can see that a booster heat pump is used to produce DHW. This HP uses the final heat delivered by the SH condenser as the heat source. This is possible since the heat required by DHW is much less than the SH heat load and in this way the condensation temperature of the DHW HP is higher but however quite close to the evaporation temperature, hence giving high COP values.

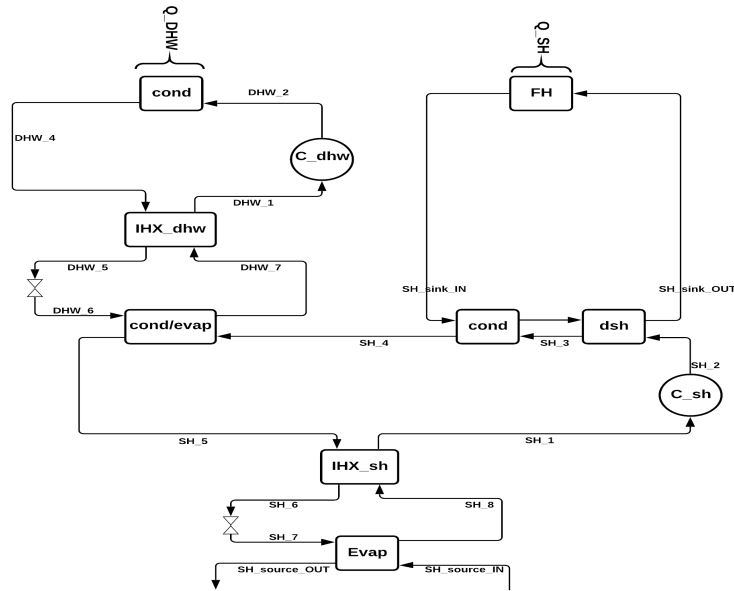


Figure 3.1: Layout of the heat pump cycle

Refrigerant selection

The refrigerant has been chosen following the guidelines presented in the literature review. The basic idea is to choose a refrigerant which has a very low GWP, zero ODP and low flammability. Amongst the HFOs and the inorganic refrigerants, the chosen refrigerant is R1234ze since it has a very low GWP (7), zero ODP and the ASHRAE safety group A2L (low flammability and no toxicity).

Assumptions

The assumptions made in the design of the SH and DHW HPs are the following

- The pressure drop through the heat exchangers and pipes has been assumed to be negligible since the evaporating pressure of the refrigerant is still quite high and such pressure drops wouldn't affect much the HP performance;
- A constant enthalpy process has been considered for the valve in both SH and DHW HPs ($h_{DHW_6} = h_{DHW_5}$ and $h_{SH_7} = h_{SH_6}$);
- Some states were considered to be in saturated conditions, namely SH_8 , SH_3 , DHW_7 and DHW_3 are in saturated vapour conditions while SH_5 and DHW_4 are in saturated liquid conditions;
- For the compressor, the heat loss was considered negligible, the motor efficiency ($\eta_{SH_{motor}}$) has been set to 95% while the volumetric efficiency ($\eta_{SH_{comp_{vol}}}$) to 90%.
- The overall heat transfer coefficients were assumed constant for each heat exchanger:

$$- U_{cond} = 800 \text{ (W/(m}^2 \cdot \text{K))}$$

$$- U_{dsh} = 200 \text{ (W/(m}^2 \cdot \text{K))}$$

$$- U_{evap} = 700 \text{ (W/(m}^2 \cdot \text{K))}$$

$$- U_{ihx} = 200 \text{ (W/(m}^2 \cdot \text{K))}$$

- The design conditions assumed for the design calculations are reported in Table 3.1

Table 3.1: Design conditions

Description	Parameter	Value	Unit
SH peak load	$\dot{Q}_{SH_{peak}}$	4000	W
DHW peak load	$\dot{Q}_{DHW_{peak}}$	500	W
Ambient temperature	T_{amb}	-10	°C
SH source inlet temperature	$T_{SH_{sourceIN}}$	7	°C
SH source outlet temperature	$T_{SH_{sourceOUT}}$	4	°C
SH sink outlet temperature	$T_{SH_{sinkOUT}}$	45	°C
SH sink inlet temperature	$T_{SH_{sinkIN}}$	40	°C
DHW sink temperature	$T_{DHW_{sink}}$	65	°C
SH sink pinch temperature	$DT_{pinch_{sinkSH}}$	5	°C
SH source pinch temperature	$DT_{pinch_{sourceSH}}$	3	°C
SH ihx pinch temperature	$DT_{pinch_{ihxSH}}$	5	°C
DHW sink pinch temperature	$DT_{pinch_{sinkDHW}}$	5	°C
DHW source pinch temperature	$DT_{pinch_{sourceDHW}}$	3	°C
DHW ihx pinch temperature	$DT_{pinch_{ihxDHW}}$	5	°C

Design procedure

Here below the steps done to design the heat pumps are reported:

1. The first step is to calculate the evaporation and condensation temperatures of the SH cycle. This is done imposing the minimum pinch temperature on the condenser and on the evaporator. The minimum pinch temperature is inversely proportional to the heat exchanger area. Therefore a trade off between performance (small pinch temperature) and cost (small HX area) needs to be found. The evaporation and condensation temperatures are calculated as follows

$$T_{SH_{evap}} = T_{SH_{sourceOUT}} - DT_{SH_{pinchsource}} \quad (3.1)$$

$$T_{SH_{cond}} = T_{SH_{sink_{OUT}}} - DT_{SH_{pinch_{sink}}} \quad (3.2)$$

where $DT_{SH_{pinch_{source}}} = 3^\circ\text{C}$ and $DT_{SH_{pinch_{sink}}} = 5^\circ\text{C}$

2. Once the evaporation and condensation temperatures are known, evaporation and condensation pressures are calculated using Refprop;
3. From the condensation pressure, states 8, 3 and 5 can be calculated by using Refprop and imposing a vapour quality of 1 for state 8 and state 3, and a vapour quality of 0 for state 5;
4. Knowing T_{SH_5} it is possible to calculate T_{SH_1} by imposing the minimum pinch temperature on the IHX

$$T_{SH_1} = T_{SH_5} - DT_{SH_{pinch_{IHX}}} \quad (3.3)$$

From T_{SH_1} , the rest of the state variables for state 1 can be calculate using Refprop.

5. The next step is to calculate state 6. This can be done calculating the enthalpy first and then using Refprop to calculate the other state variables. The enthalpy was calculated as follows:

$$h_{SH_6} = h_{SH_5} - \frac{\dot{Q}_{SH_{IHX}}}{\dot{m}_{SH}} \quad (3.4)$$

where

$$\frac{\dot{Q}_{SH_{IHX}}}{\dot{m}_{SH}} = h_{SH_1} - h_{SH_8} \quad (3.5)$$

6. Knowing the pressure ratio of the compressor and the state variables of state 1, we can calculate state 2. The first step is to calculate the isentropic efficiency (function of the pressure ratio). Then the isentropic enthalpy is calculated assuming $s_{SH_{2_{is}}} = s_{SH_1}$. From the isentropic entropy, the isentropic enthalpy can be calculated using Refprop. Eventually, knowing the isentropic efficiency and the isentropic enthalpy value, the following equation is used to calculate the actual enthalpy of state 2

$$h_{SH_2} = h_{SH_1} + \frac{h_{SH_{2_{is}}} - h_{SH_1}}{\eta_{SH_{is}}} \quad (3.6)$$

7. Once all state variables are know for state 2, it is possible to calculate the mass flow rate of refrigerant. This can be calculated by imposing that from state 2 to state 5 the heat delivered matches the sum of the SH heat load and a percentage of the DHW heat load. In particular, the following equation is used to calculated the required mass flow rate of refrigerant.

$$\dot{m}_{SH} = \frac{\dot{Q}_{SH_{peak}} + 0.85 * \dot{Q}_{DHW_{peak}}}{(h_{SH_2} - h_{SH_5})} \quad (3.7)$$

8. From the mass flow rate of refrigerant it is possible to calculate the compressor inlet volume ($\dot{V}_{SH_{comp_{IN}}} = \dot{m}_{SH} / \rho_{SH_1}$). From the inlet volume flow rate, the displacement volume flow rate (m^3/s) together with the compressor displacement volume (m^3) are calculated respectively as follows

$$\dot{V}_{SH_{comp_{disp}}} = \frac{\dot{V}_{SH_{comp_{IN}}}}{\eta_{SH_{comp_{vol}}}} \quad (3.8)$$

$$V_{SH_{comp_{disp}}} = \frac{\dot{m}_{SH}}{(\eta_{SH_{comp_{vol}}} * \rho_{SH_1} * n_{SH_{comp}})} \quad (3.9)$$

9. Once the refrigerant mass flow rate is known, enthalpy of state 4 can be calculated as follows:

$$h_{SH_4} = h_{SH_2} - \dot{Q}_{SH_{peak}} / \dot{m}_{SH} \quad (3.10)$$

And from here all the other state variables of state 4 can be calculated using Refprop;

10. Then state 7 is calculated by imposing $h_{SH_7} = h_{SH_6}$ and then using Refprop to find the all other state variables;

11. Once all the states are known, the work load of the electrical motor ($W_{SH_{motor}} = W_{SH_{comp}} / \eta_{SH_{motor}}$) is calculated. Using this results together with the sink heat load ($\dot{Q}_{SH_{sink}} = \dot{Q}_{SH_{dsh}} + \dot{Q}_{SH_{cond}} + \dot{Q}_{SH_{condevap}}$), the COP is calculated as shown by the following equation

$$COP_{SH} = \frac{\dot{Q}_{SH_{sink}}}{W_{SH_{motor}}} \quad (3.11)$$

12. The last step is to calculate the heat exchanger's area. For each HX the same procedure is followed. First the logarithmic mean temperature difference is calculated and then the area is defined using the following equation

$$A = \frac{\dot{Q}}{DT_{lm} * U} \quad (3.12)$$

where each heat exchanger had different values of \dot{Q} , U and DT_{lm} ;

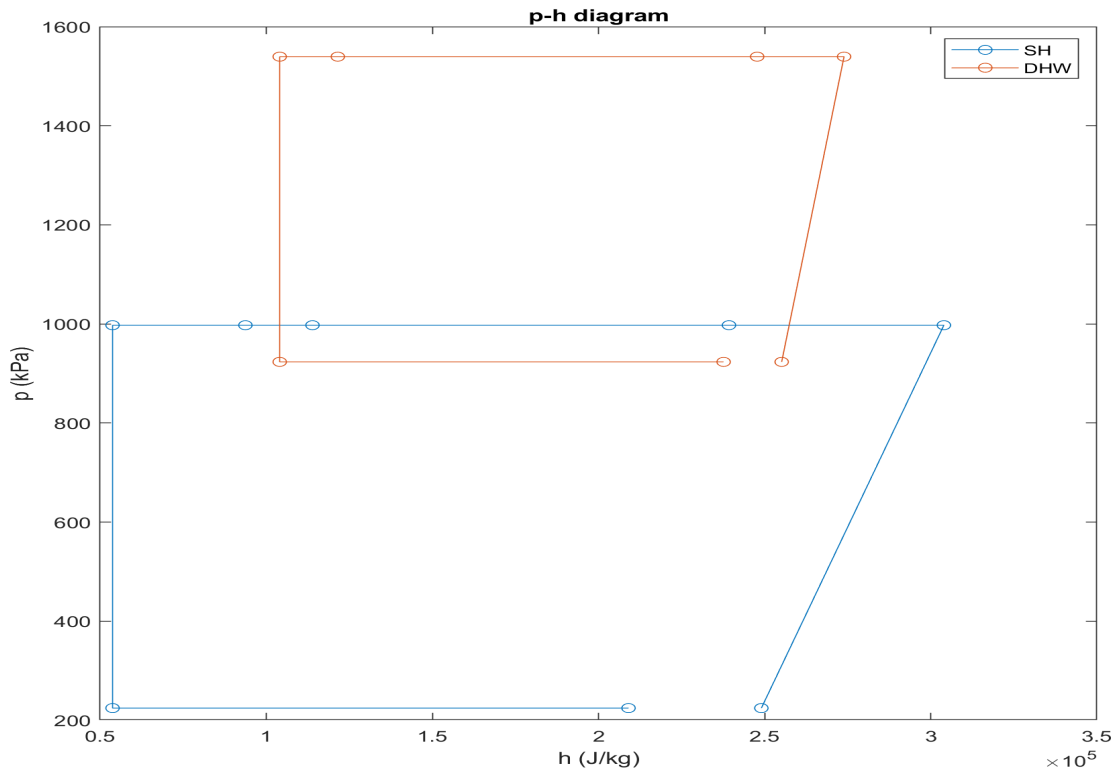
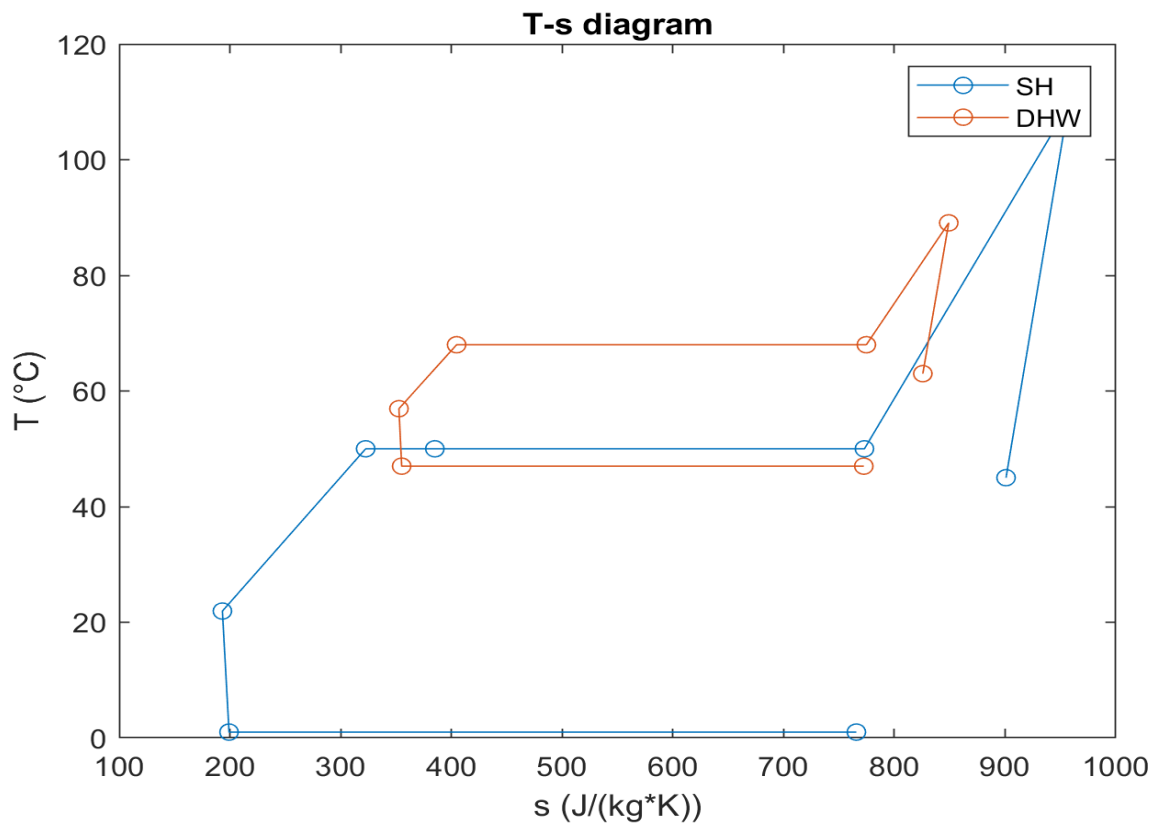
The same procedure is followed to design the booster DHW heat pump. The only thing that needs to be specified regarding the design of the booster DHW heat pump is that the inlet and outlet source temperatures are given by the results of the design of the SH heat pump. In particular, $T_{DHW_{sourceIN}} = T_{SH_4}$ and $T_{DHW_{sourceOUT}} = T_{SH_5}$. Additionally, it is important to state that the water temperature in the DHW storage tank (the sink side) is considered to be homogeneous and constant as specified above in the assumptions.

From the design calculations, the obtained heat exchanger areas are the following:

- $A_{sink_{SH}} = 0.906 \text{ m}^2$
- $A_{ihx_{SH}} = 0.357 \text{ m}^2$
- $A_{source_{SH}} = 1.136 \text{ m}^2$
- $A_{sink_{DHW}} = 0.421 \text{ m}^2$
- $A_{ihx_{DHW}} = 0.044 \text{ m}^2$
- $A_{source_{DHW}} = 0.202 \text{ m}^2$

Where $A_{sink_{SH}}$ is given by the sum of $A_{SH_{cond}}$ and $A_{SH_{dsh}}$.

In Figure 3.2a and Figure 3.2b the results of the design calculations are reported. These figures show respectively the obtained p - h diagram and T - s diagram for both heat pumps.

(a) p - h diagram(b) T - s diagramFigure 3.2: p - h and T - s diagrams for design conditions using refrigerant R1234ze

Apart from the areas of the heat exchangers and the p - h and T - s diagrams, other design conditions that are obtained from the design calculations are reported in Table 3.2:

Table 3.2: Results of design calculations

Description	Parameter	Value	Unit
Refrigerant mass flow rate SH	\dot{m}_{SH}	0.0218	kg/s
Refrigerant mass flow rate DHW	\dot{m}_{DHW}	0.0031	kg/s
Source mass flow rate SH	$\dot{m}_{sourceSH}$	0.2732	kg/s
Sink mass flow rate SH	\dot{m}_{sinkSH}	0.1914	kg/s
Pressure ratio SH	$p_{ratioSH}$	3.5	
Pressure ratio DHW	$p_{ratioDHW}$	1.9	
Coefficient of performance SH	COP_{SH}	4.27	
Coefficient of performance DHW	COP_{DHW}	6.42	
Compressor displacement volume SH	V_{dispSH}	42.03	cm ³
Compressor displacement volume DHW	$V_{dispDHW}$	1.82	cm ³

3.1.2. HP model

Once the design conditions are defined and the required surface area of the heat exchangers is fixed, the HP model for both SH and DHW heat pump can be developed.

Assumptions

Some assumptions have been made while developing the model. These assumptions are reported here below:

- The heat delivered by the heat pump (\dot{Q}_{SH}) is assumed to be proportional to the ambient temperature and the following relationship has been used in the model:

$$\dot{Q}_{SH} = \frac{T_{room} - T_{amb}}{DT_{max}} * \dot{Q}_{SH_{peak}} \quad (3.13)$$

As we can see from Equation 3.13, the heat delivered by the main heat pump is equal to $Q_{SH_{peak}}$ when the temperature difference between the room temperature and ambient temperature is equal to DT_{max} which is equal to the maximum temperature difference when the outside temperature is -10 °C. The heat delivered by the main heat pump to the house is equal to zero when the temperature difference between the room temperature and ambient temperature is equal to zero.

- The values of the overall heat transfer coefficients have been assumed to be constant over time to simplify the physics behind the model. This has been done since the influence of this change has been considered to be small enough and negligible;
- The rotational speed of the DHW heat pump has been assumed to be fixed at a constant speed or to be zero if no DHW heating is needed;

Model implementation

Two separate models have been developed for the two heat pumps, namely SH heat pump and DHW heat pump. The heat pumps have been modelled using Matlab. In Figure 3.3 and Figure 3.4 the algorithm followed by the two models, respectively, is reported in a flow diagram.

In both cases, the model starts with initial assumptions based on the design conditions initially and on the previous time step later on. These assumed values are used to calculate all the thermodynamic states of the HP cycle. However, since the calculations are based on assumed values, it is required to iterate the different initial assumptions. This is done by matching the calculated HX areas with the areas defined in the design conditions. For each iteration, assumed values are adjusted until the areas match and then the programme goes forward with the next HX area until all the areas match the design values.

This is the basic principle used to model the heat pumps.

As we can see from the diagrams in Figure 3.3 and 3.4, there is a difference between the algorithm developed for the SH heat pump and the one used for the DHW heat pump. This is due to the fact that the DHW heat pump has as heat source part of the condenser of the SH heat pump. This implies that some of the outlets of the SH heat pump are used as inputs to the DHW heat pump. Therefore, once we enter the DHW heat pump model, the heat delivered by the SH heat pump to the DHW heat pump through the DHW evaporator is already calculated in the SH heat pump model. For this reason, the last iteration that we can see in the DHW heat pump flow chart is required to adjust the DHW refrigerant mass flow rate so that the heat delivered by the SH heat pump and the heat absorbed by the DHW heat pump through the evaporator are matched. This is the last iteration and it happens only once all other iterations have been performed. Once all requirements are matched, the heat exchanged through the DHW evaporator are compared and if they don't match the DHW refrigerant mass flow rate is adjusted so that heat flow rates match. Then the compressor rotational speed is adjusted accordingly and sent back at the beginning of the flow chart to re-do the calculations once again but with the correct compressor rotational speed.

SH heat pump Starting with the SH heat pump model, the inputs to the model are the following:

- $T_{BHE_{out}}$, which is equal to $T_{source_{in_{SH}}}$;
- T_{amb} and T_{room} which are needed to determine the heat load (\dot{Q}_{SH});
- $m_{flow_{BHE}}$ coming from the borehole;
- $DHW_{on/off}$ conditions

The useful outputs of the SH heat pump model are the following:

- COP_{SH} , the coefficient of performance of the heat pump;
- $Q_{cond_{evap}}$, the heat exchanged between SH heat pump and the DHW heat pump through the condenser/evaporator;
- Q_{SH} , the provided to the house;
- $T_{BHE_{in}}$, the temperature going back into the BHE which corresponds to the stream coming out from the SH evaporator;

In the specific case when either the DHW or the SH load is zero, the model of the SH heat pump is changed as reported in Table 3.3:

Table 3.3: Specific cases model variations

Conditions	Changes
$T_{room} < T_{room_{set}}$, $\dot{Q}_{DHW} = 0$	state 4 is at saturation $x=0$, iterate on $n_{comp_{SH}}$ to match $Q_{SH} = Q_{cond_{SH}} + Q_{dsh_{SH}}$
$T_{room} > T_{room_{set}}$, $\dot{Q}_{DHW} > 0$	$n_{comp_{SH}} = 400$
$T_{room} > T_{room_{set}}$, $\dot{Q}_{DHW} = 0$	$n_{comp_{SH}} = 0$, $T_{SH} = T_{amb}$ and $COP_{SH} = NaN$

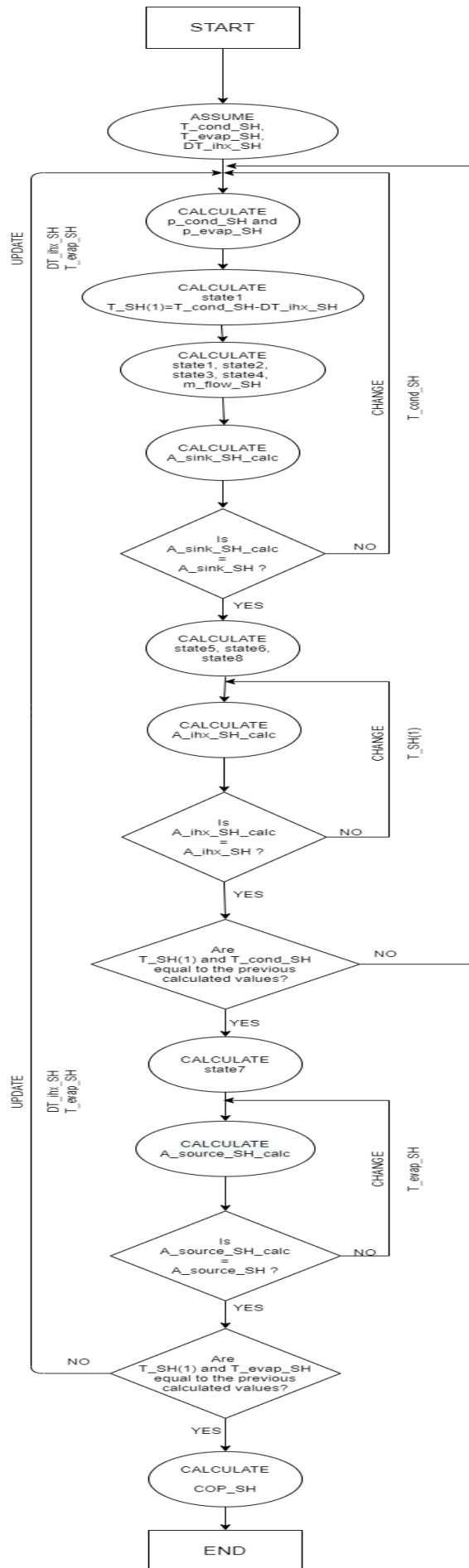


Figure 3.3: SH Flow Chart

DHW heat pump When considering the DHW heat pump model, things are slightly different compared to the SH heat pump model. It is important to state that the DHW heat pump model doesn't have a load requirement. The calculations are done based on matching the heat delivered from the heat source and in turn this allows us to calculate the heat delivered to the DHW storage tank.

The inputs to the DHW heat pump model are the following:

- $Q_{cond_{evap}}$, the heat exchanged between SH heat pump and the DHW heat pump through the condenser/evaporator;
- $T_{water_{tank}}$, the average temperature of the water in the storage tank for DHW;
- $T_{SH_{cond_{evap}_{in}}}$, the temperature of the SH stream entering the condenser/evaporator which corresponds to the DHW source inlet temperature;
- $DHW_{on/off}$ conditions

The outputs of the model are the following:

- COP_{DHW} , the coefficient of performance of the heat pump;
- Q_{DHW} , the heat delivered to the DHW storage tank;
- $T_{cond_{DHW}}$, the condensation temperature of the heat pump;

Model Validation

The model has been validated using the performance data of the W/W heat pump 5G - 4.5 kW individual source from Ithodaalderop [71].

The performance data are reported in Table 3.4:

Table 3.4: Performance data W/W heat pump 5G-4.5 kW individual source from Ithodaalderop

Type of refrigerant	R134a
Nom. flow rate source	0.33 l/s
Nom. flow rate sink	0.35 l/s
COP at 10/35 °C (W10/W35) according to EN 14511	5.9

The model shows similar results, the only thing worth noticing is that to obtain such high COP at 10/35 °C an isentropic efficiency of about 85% is required. Therefore, the model is considered validated with the consideration that the data reported in Table 3.4 are obtained assuming a very high isentropic efficiency for the compressor. The obtained T - s and p - h diagrams for the validation conditions are reported in Figure 3.5b and Figure 3.5a

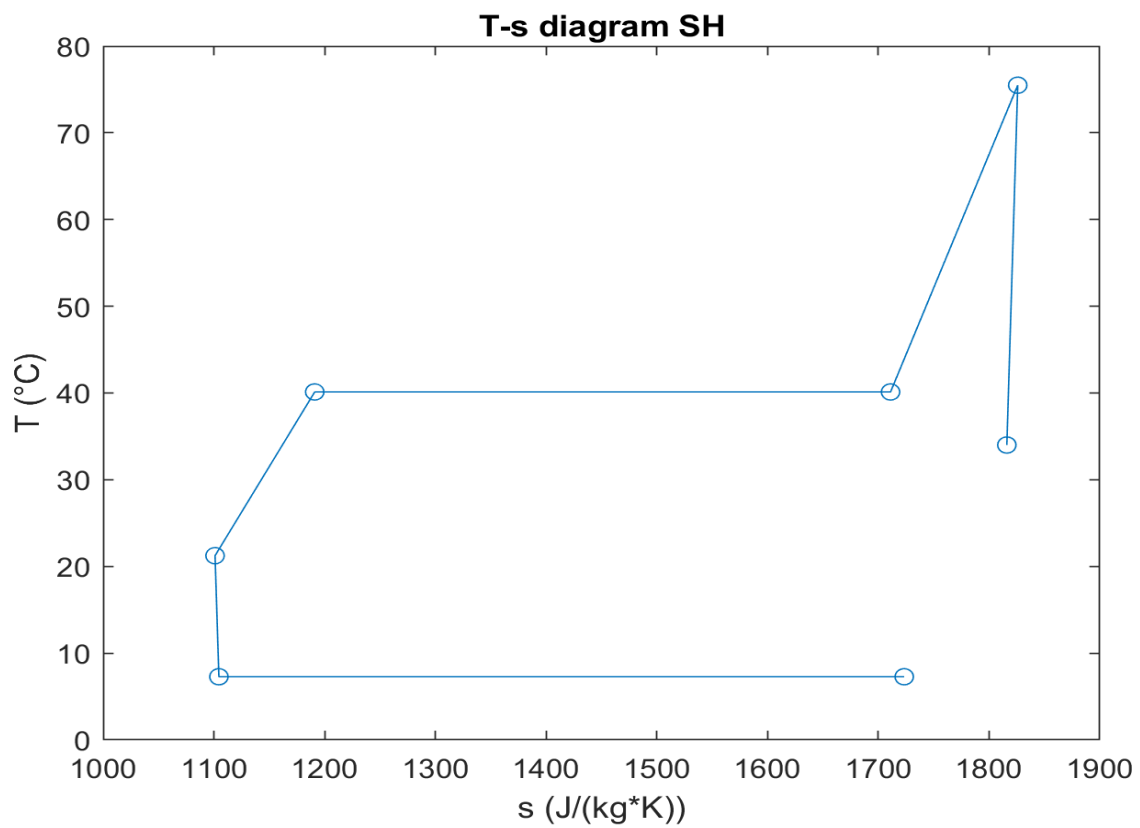
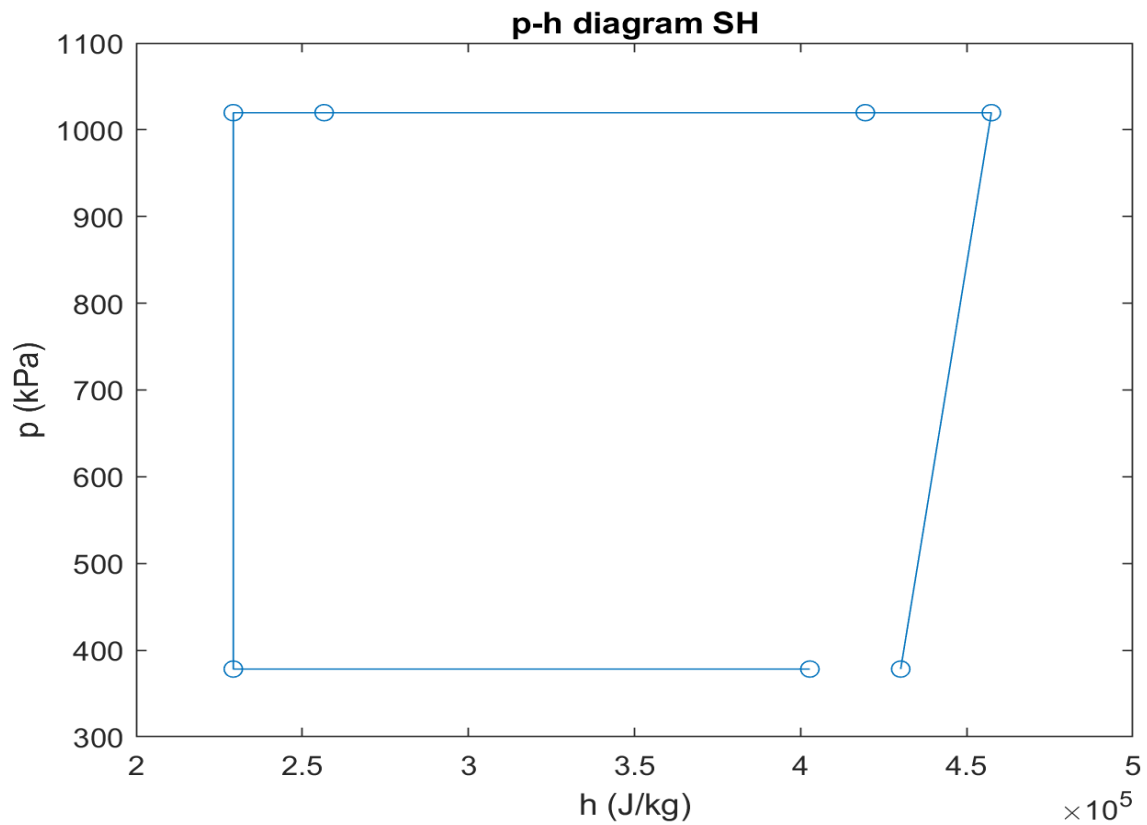


Figure 3.5: *p-h* and *T-s* diagrams for validation using refrigerant R134a

3.2. Borehole Heat Exchanger

3.2.1. BHE design

The design conditions of the BHE and the properties of the material used are reported in Table 3.5.

Table 3.5: Values of thermal properties and parameters used in the BHE model

Description	Symbol	Value	Unit
Borehole depth	H	180	m
Shank spacing	s	0.038	m
Borehole radius	r_b	0.3	m
U-tube pipe outer radius	r_{po}	0.016	m
U-tube pipe inner radius	r_{pi}	0.008	m
U-tube (HDPE pipe) thermal conductivity	k_p	0.39	$W/(mK)$
Grout (WC05-SC05) thermal conductivity	k_g	1.5	$W/(mK)$
Ground (soil) thermal conductivity	k_s	0.81	$W/(mK)$
Working fluid mass flow rate	\dot{m}_f	0.2732	kg/s
Grout (WC05-SC05) specific heat capacity	c_{pg}	1500	$J/(kgK)$
Ground (soil) specific heat capacity	c_{ps}	2016	$J/(kgK)$
Grout (WC05-SC05) density	ρ_g	1984	kg/m^3
Ground (soil) density	ρ_s	2500	kg/m^3
Undisturbed ground temperature	T_0	10	$^{\circ}C$

Some parameters, such as working fluid properties (i.e. thermal conductivity, specific heat and density), vary with fluid's temperature therefore it was not possible to report these in the table above. All parameters reported in Table 3.5 are considered constant over time and not changing with temperature. The working fluid used in the system is a mixture of water and ethylene-glycol (40% by volume). This is needed to avoid freezing of the working fluid during winter time since it is the same fluid that runs through the solar collector array. The water ethylene-glycol mixture freezes at $-23.5^{\circ}C$ at ambient pressure, hence there is no risk of freezing of the working fluid during the winter period.

3.2.2. BHE model

The BHE model has been developed following the equations described in section 2.4.1. An iterative process has been used to make sure boundary and initial conditions are satisfied. The process is described below and graphically explained in Figure 3.7. Figure 3.6 is reported from section 2.4.1 to make it easier for the reader to understand the grid element division of the borehole domain.

1. The first step is to assume the temperature value of the first grid element in the v-tube.
2. Then it is possible to simultaneously solve all the equations for the first grid elements in vertical direction and for the second grid element of the v-tube.
3. Once all the temperatures for the first grid elements are calculated, the same procedure is repeated for the second grid element and so on.
4. Once the temperature of the last grid elements is calculated, the boundary condition $T_{fu}(N) = T_{fv}(N + 1)$ is checked. If these temperatures don't match, then the value of $T_{fv}(1)$ is adjusted accordingly and the process is repeated until this condition is matched.

For each line of grid elements ($i=1,2,3,\dots,N$) the following matrix equation is used:

$$Ax = B \quad (3.14)$$

where A, x and B are given as follows:

$$A = \begin{bmatrix} (1-a+b+c) & 0 & -c & 0 & 0 & 0 & 0 & 0 \\ -b & a & -c & 0 & 0 & 0 & 0 & 0 \\ -d & 0 & (1+2d+e) & -e & 0 & 0 & 0 & 0 \\ 0 & 0 & -l & (1+l+g) & -g & 0 & 0 & 0 \\ 0 & 0 & 0 & -f & (1+f+g) & -g & 0 & 0 \\ 0 & 0 & 0 & 0 & -f & (1+f+g) & -g & 0 \\ 0 & 0 & 0 & 0 & 0 & -f & (1+f+g) & -g \end{bmatrix} \quad (3.15)$$

$$x = \begin{bmatrix} T_{fu}(i) \\ T_{fv}(i+1) \\ T_g(i) \\ T_s(i,1) \\ T_s(i,2) \\ T_s(i,3) \\ T_s(i,4) \\ T_s(i,5) \end{bmatrix} \quad (3.16)$$

$$B = \begin{bmatrix} (1+a-b-c)T_{fu_{old}}(i) - a(T_{fu}(i-1) + T_{fu_{old}}(i-1)) + b(T_{fv}(i) + T_{fv_{old}}(i)) + c * T_{g_{old}}(i) \\ (-1+a-b-c)T_{fv}(i) + (1+a-b-c)T_{fv_{old}}(i) - a * T_{fv_{old}}(i+1) + b * T_{fu_{old}}(i) + cT_{g_{old}}(i) \\ (1-2d-e)T_{g_{old}}(i) + d(T_{fv_{old}}(i) + T_{fu_{old}}(i) + T_{fv}(i)) + e * T_{s_{old}}(i,1) \\ (1-l-g)T_{s_{old}}(i,1) + l * T_{g_{old}}(i) + g * T_{s_{old}}(i,2) \\ (1-f-g)T_{s_{old}}(i,2) + f * T_{s_{old}}(i,1) + g * T_{s_{old}}(i,3) \\ (1-f-g)T_{s_{old}}(i,3) + f * T_{s_{old}}(i,2) + g * T_{s_{old}}(i,4) \\ (1-f-g)T_{s_{old}}(i,4) + f * T_{s_{old}}(i,3) + g * T_{s_{old}}(i,5) \\ (1-f-g)T_{s_{old}}(i,5) + f * T_{s_{old}}(i,4) + g * T_{s_{old}}(i,6) \end{bmatrix} \quad (3.17)$$

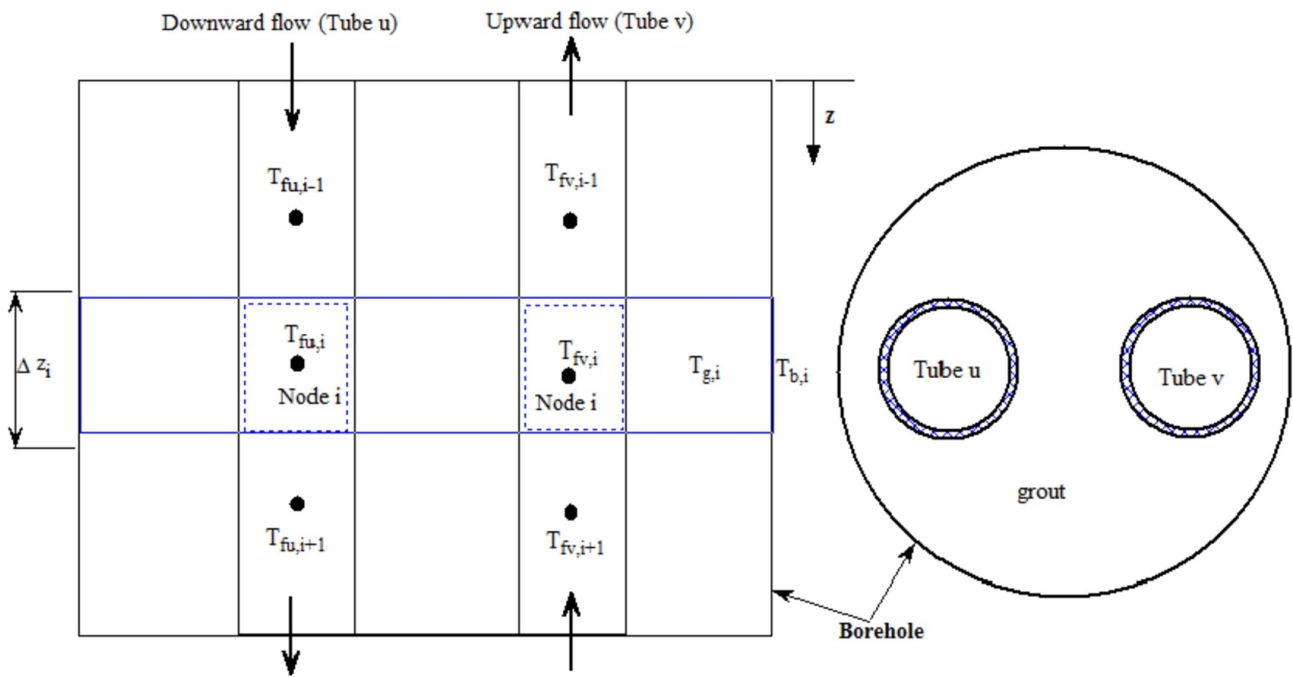


Figure 3.6: Schematic diagram of borehole and grid scheme inside the borehole [66]

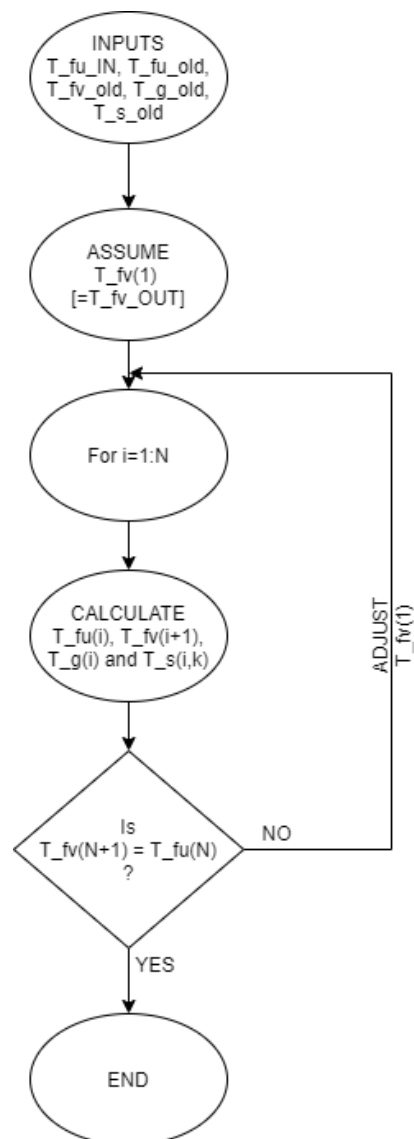


Figure 3.7: BHE model - Flow Chart

In Equation 3.14, x is the vector of unknown temperature values at present time step of the different grid elements at the same height, A is the matrix of constant parameters which multiply the unknown values of vector x , and B is the matrix of known parameters which is made of temperature values at previous time steps and already calculated temperatures at the present time step.

For every grid elements line, the temperature values at the present time step are calculated solving Equation 3.14 for x , as showed in the following equation:

$$x = A^{-1}B \quad (3.18)$$

The values of a, b, c, d, e, f, g and l are reported below

$$a = \frac{\Delta t}{2} \frac{\dot{m}_f}{M_f} \quad (3.19)$$

$$b = \frac{\Delta t}{2} \frac{1}{M_f C p_f R_{ff} / \Delta z} \quad (3.20)$$

$$c = \frac{\Delta t}{2} \frac{1}{M_f C p_f R_{fg} / \Delta z} \quad (3.21)$$

$$d = \frac{\Delta t}{2} \frac{1}{M_g C p_g R_{fg} / \Delta z} \quad (3.22)$$

$$e = \frac{\Delta t}{2} \frac{1}{M_g C p_g (R_{gb} + R_{s,1}) / \Delta z} \quad (3.23)$$

$$f = \frac{\Delta t}{2} \frac{1}{M_{s,k} C p_s R_{s,k} / \Delta z} \quad (3.24)$$

$$g = \frac{\Delta t}{2} \frac{1}{M_{s,k} C p_s R_{s,k+1} / \Delta z} \quad (3.25)$$

$$l = \frac{\Delta t}{2} \frac{1}{M_{s,1} C p_s (R_{gb} + R_{s,1}) / \Delta z} \quad (3.26)$$

Model Validation

The model has been validated comparing the obtained results with the results from [66] as shown in Figure 3.8

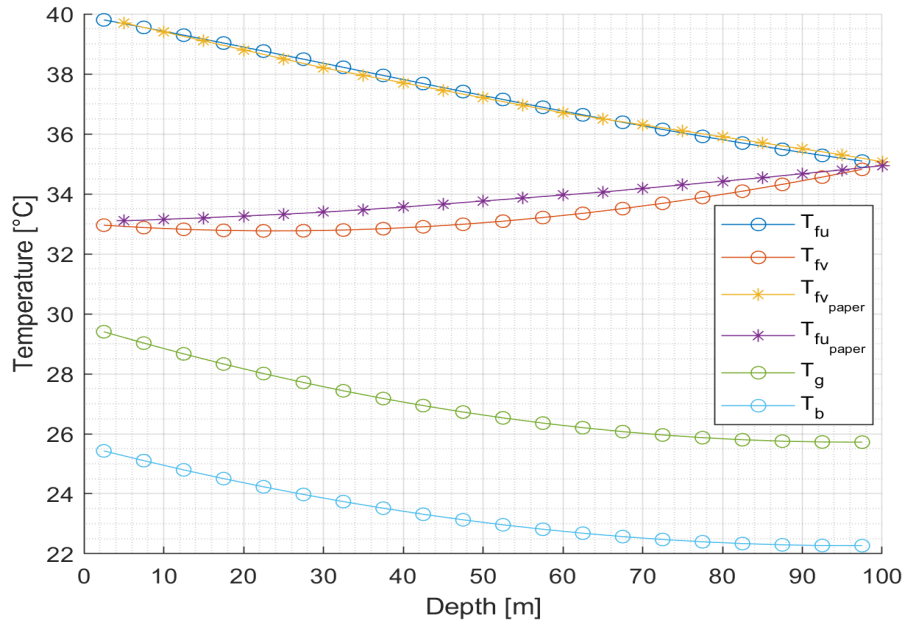


Figure 3.8: BHE model - Results and model validation

As we can see from the plot, the downward fluid pipe temperatures match the values from the paper. However, the upward fluid pipe temperatures are slightly different from the paper results. This mismatch is believed to be caused by an oversimplification of the model. In this work, for sake of simplicity, the mass of grout in between the two legs of the tube has been considered interacting with the pipes the same way the rest of the grout region is. Of course, the thermal resistance of the grout region in between the two tubes is different and this is believed to be the reason for the slight mismatch. In particular, with this simplification, all the heat flows from the hot branch directly to the colder branch since the heat accumulated in the grout between the two branches has been neglected. Still, the model gives sufficiently accurate results to be used in the system.

3.3. Evacuated Tube Collectors

3.3.1. ETC design

The ETC system is used throughout the year and all the heat obtained from the solar collectors is redirected into the ground to raise the average ground temperature and therefore increasing the efficiency of the HP system. The selected ETC that will be used in this work is the ETC-10 solar collector from Apricus. The basic specifications of this solar collector as provided by the manufacturer are reported in Table 3.6.

Table 3.6: Specifications of ETC-10 solar collector from Apricus

Dimensions (LxWxH)	2005x796x136 mm
Peak output	671 W
Aperture area	0.947 m ²
Gross Area	1.59 m ²
Gross Dry Weight	35 kg
Fluid capacity	310 ml
Flow rate	0.7 L/min
Max operating pressure	800 kPa

3.3.2. ETC model

The overall heat input from the solar collectors array is calculated as follows:

$$\dot{Q}_{ETC} = \eta A_{aperture} G \quad (3.27)$$

where $\eta = \eta_0 - \frac{a_1(T_{amb} - T_{coll_{avg}}) + a_2(T_{amb} - T_{coll_{avg}})^2}{G}$.

Here $T_{coll_{avg}} = (T_{coll_{IN}} + T_{coll_{OUT}})/2$ is the average collector temperature, η_0 is the maximum efficiency, G is the global irradiance intensity (W/m^2), a_1 and a_2 are two experimental parameters. a_1 ($W/(m^2K)$) is the heat transfer coefficient and is used to describe the thermal losses (the higher a_1 , the more the thermal losses). a_2 (W/m^2K^2) is the temperature dependent heat transfer coefficient.

In our specific case, the chosen evacuated tube solar collector ETC-10 from Apricus has the following characteristics:

- $\eta_0 = 0.710$
- $A_{aperture} = 0.947 m^2$
- $a_1 = 1.737 W/(m^2K)$
- $a_2 = 0.008 W/(m^2K^2)$

In the model, to calculate the efficiency of the solar collector, the collector average temperature $T_{coll_{avg}}$ is estimated using the collector stream outlet temperature of the previous time step. Once the efficiency is known, the heat flow is calculated and eventually the actual collector outlet temperature can be calculated as well using the following equation:

$$T_{coll_{OUT}} = T_{coll_{IN}} + \frac{\dot{Q}_{ETC}}{c_{p_{water}} \dot{m}_{ETC}} \quad (3.28)$$

3.4. DHW storage tank

3.4.1. DHW storage tank design

A DHW storage tank is used as buffer for hot water production in order to ensure constant availability of DHW. In this specific system, DHW is produced only by means of the ground-source heat pump, while the summer the heat coming from the evacuated tube solar collectors is always used to heat up the ground to increase the HP efficiency. The storage tank is having an indirect heat exchangers for the heat pump loop. When there is need for it, hot water is taken from the top of the tank and new cold water enters the tank from the bottom. A schematic of the storage tank is given in Figure 3.9 where all the different heat contribution and losses are shown.

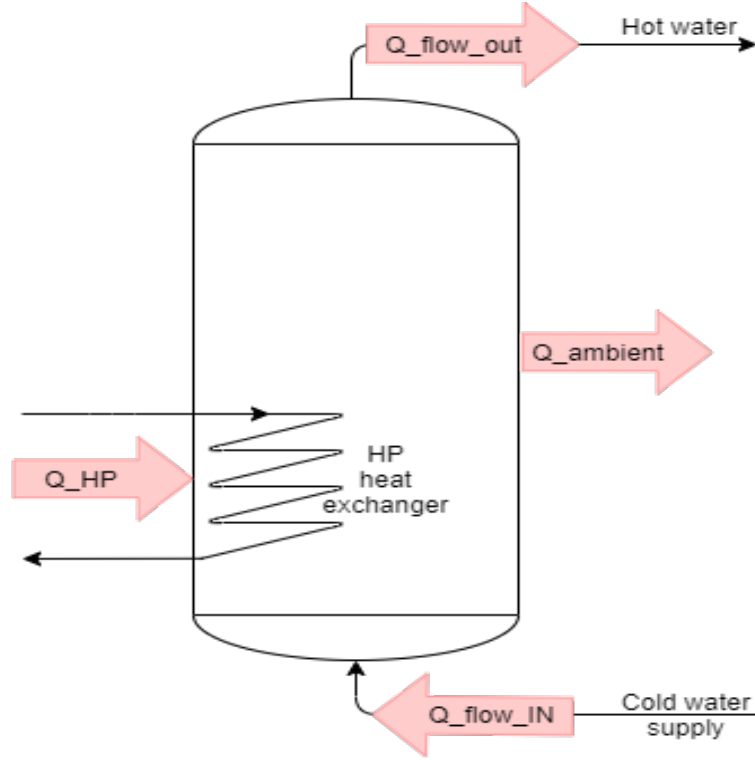


Figure 3.9: DHW storage tank - schematic

To calculate the tank volume, an average showering time of 8 minutes has been considered, with a water mass flow rate of 0.083 l/s ($T_{water} = 40 \text{ }^\circ\text{C}$). Only part of this mass flow rate is hot water at $65 \text{ }^\circ\text{C}$. Therefore, the required water mass flow rate from the DHW tank can be assumed to be about 0.05 l/s . Multiplying this flow rate by the average showering time, we get an average hot water consumption of 20 l per shower. Considering an average of 1.5 showers a day and adding to this the hot water consumption used for other means, we can safely assume a daily water consumption per person of about 40 l . With a number of occupants assumed to be equal to three, a daily hot water consumption of 120 litres is estimated. The dimensions of the tank have been chosen accordingly, selecting the tank radius equal to $r_{tank} = 0.2 \text{ m}$ and the height equal to $h_{tank} = 1 \text{ m}$.

3.4.2. DHW storage tank model

In order to calculate the water temperature in the tank, an energy balance is carried out on the hot water storage tank. In this calculation, the water temperature in the tank is assumed to be homogeneous everywhere hence neglecting the stratification effect. The following contributions are considered in the energy balance of the water tank:

- Heat input from heat pump

$$\dot{Q}_{HP} = U_{cond} * A * DT_{lm} \quad (3.29)$$

where $DT_{lm} = (T_{condensation} - T_{water})$.

- Heat exchanged with outside ambient air

$$\dot{Q}_{ambient} = U(A_{tank_{lateral}} + A_{tank_{base}})DT_{lm} \quad (3.30)$$

where $DT_{lm} = (T_{water} - T_{amb})$ and U_{tank} is assumed to be equal to $0.25 \text{ W/m}^2\text{K}$.

- Heat exchanged with the flow of water entering and exiting the tank

$$\dot{Q}_{flow} = \dot{Q}_{flow_{OUT}} - \dot{Q}_{flow_{IN}} = \dot{m}_{DHW} * c_{p_{water}}(T_{water_{OUT}} - T_{water_{IN}}) \quad (3.31)$$

where \dot{m}_{DHW} is the water flowing out and in of the tank. Here we assumed that the volume of water entering the tank equals the volume of water getting out of it. $T_{water_{IN}} = 10 \text{ }^\circ\text{C}$ and $T_{water_{OUT}} = T_{water}$.

Eventually, the energy balance equation on water storage tank can be written as follows:

$$\rho * c_{p_{water}} V_{tank} \frac{dT_{water}}{dt} = \dot{Q}_{HP} - \dot{Q}_{ambient} - \dot{Q}_{flow} \quad (3.32)$$

In order to determine T_{water} , this first order differential equation is solved directly on Simulink.

3.4.3. DHW consumption hourly profile

The hourly profile of DHW consumption in a house has been assumed to be the one reported in Figure 3.10a and 3.10b:

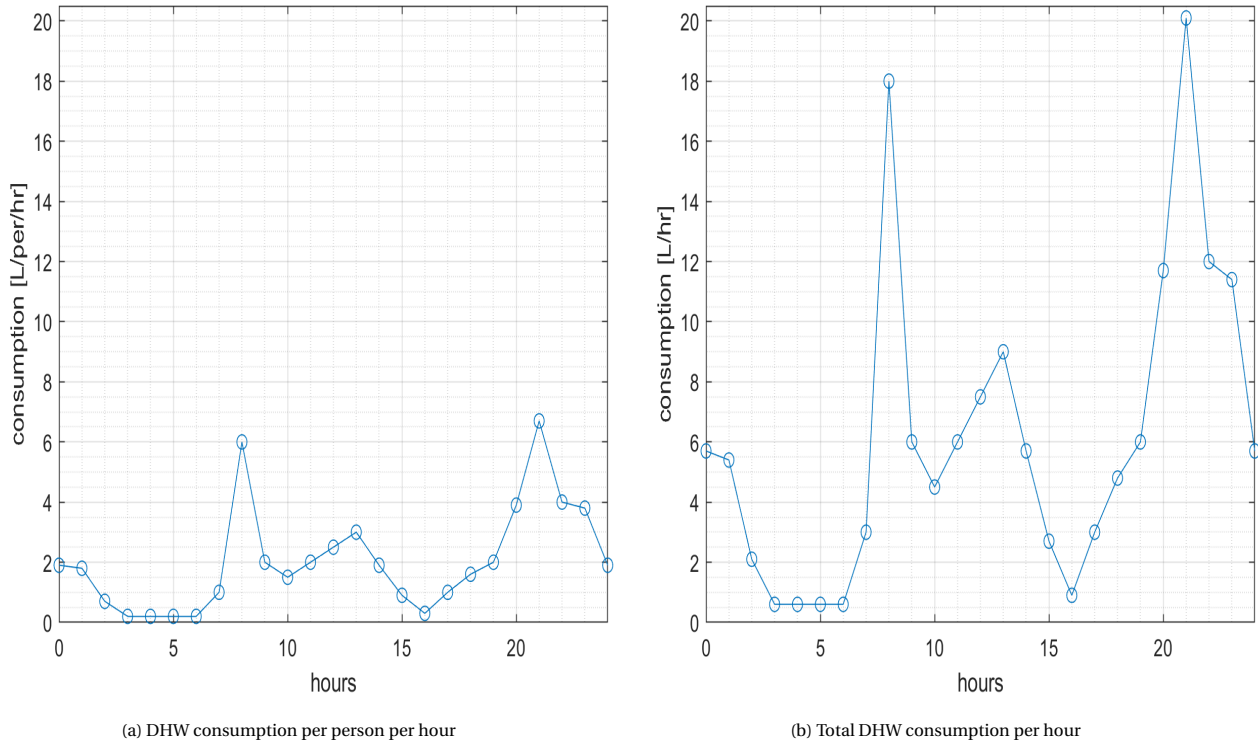


Figure 3.10: DHW consumption profile [72]

Figure 3.10a reports the DHW consumption per person per hour for a general house. In our specific case, the house in consideration is a 3 people terraced house. The graph in Figure 3.10b reports the overall hourly consumption for the house in consideration. This graph has been obtained multiplying the DHW consumption per person per hour by the number of people in the house. It is important to underline that the DHW consumption profile is assumed to be the same throughout the year for the sake of simplifying the model. In reality, there is a difference in DHW consumption profile between weekdays and weekends and between different seasons. The DHW consumption profile used in this work is an average of the consumption profiles in the month of November as proposed by [72]. These profiles refer to the hot water consumption at 40 °C. Since in the DHW tank the temperature is set to 65 °C, the required mass flow rate of DHW reported in Figure 3.10b will be obtained by mixing the hot water in the tank with cold water at 10 °C. Therefore, the required flow rate for the DHW storage tank will be determined depending on the water temperature inside the storage tank and on the DHW mass flow rate requirements.

The following equations are implemented in Simulink to calculate the required mass flow rate from the DHW storage tank. These are the conservation of energy and the conservation of mass, respectively:

$$(\dot{m}_1 c_{p1} + \dot{m}_2 c_{p2}) T_3 = (\dot{m}_1 c_{p1} T_1 + \dot{m}_2 c_{p2} T_2) \quad (3.33)$$

$$\dot{m}_3 = \dot{m}_1 + \dot{m}_2 \quad (3.34)$$

Where, the subscript 1, 2 and 3 are assigned accordingly to what is reported in Figure 3.11.

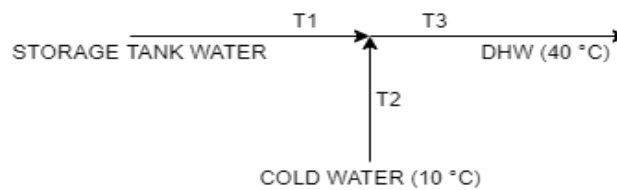


Figure 3.11: Mixing of hot and cold water - schematic

Equations 3.33 and 3.34 are solved for \dot{m}_1 and \dot{m}_2 depending on the variables \dot{m}_3 and T_1 (temperature in the storage tank). c_{p1} is a function of T_1 and all the other variables are constant [$T_2 = 10$ °C, $T_3 = 40$ °C and $c_{p2} = 4195.5$ J/(kg * K)].

3.5. House model

The house has been modelled using a simplified heat balance equation to determine the room temperature at each time step. The contributions considered in the model are reported below while all other contributions have been considered to be negligible for the sake of simplicity.

- Heat load due to temperature difference between room temperature and ambient temperature

$$\dot{Q}_{load} = U_{building} A_{building} * (T_{room} - T_{amb}) \quad (3.35)$$

- The heat exchanged with the building thermal mass

$$\dot{Q}_{thermal_{mass}} = U_{wall} A_{wall} * (T_{room} - T_{wall}) \quad (3.36)$$

- The heat provided by the space heating heat pump which is an output of the SH heat pump model described above

$$\dot{Q}_{HP_{SH}} \quad (3.37)$$

The overall heat balance equation on the house is the following:

$$M_{air} * c_{p_{air}} \frac{dT}{dt} + \dot{Q}_{load} + \dot{Q}_{thermal_{mass}} = \dot{Q}_{HP_{SH}} \quad (3.38)$$

The heat balance is used to calculate the new room temperature starting from the previous time step room temperature. In Equation 3.38 all heat contributions are calculated using the old room temperature. Once calculated, the thermal mass load is used to calculate the new wall temperature using the following equation:

$$\dot{Q}_{thermal_{mass}} = M_{wall} c_{p_{wall}} \frac{T_{wall_{new}} - T_{wall_{old}}}{dt} \quad (3.39)$$

The model initial conditions, $T_{room}(0)$ and $T_{wall}(0)$, have been assumed to be equal to 15 and 19 °C, respectively.

This model has been implemented using Matlab and then combined with the other models in the Simulink environment.

To be noticed that the overall heat transfer coefficient of the wall has been assumed constant and an average value has been used for the sake of simplicity. On the other side, the building overall heat transfer coefficient has been calculated assuming a heat load equal to 3700W when the outside temperature is -10 °C and inside temperature is 20 °C. Eventually, the area and mass of both building and wall have been calculated considering a house with length of 10 m, width of 6 m, wall thickness of 0.1 m and with two floor of 3 m height. The portion occupied by windows and doors has to be removed from the total area calculation for the thermal mass. Assuming that about 1/5 of the wall area is made of windows and doors, a wall perimeter of 26 m has been assumed for the thermal mass calculation.

3.6. Other system components

Apart from the previously mentioned main components of the system, the remaining components to be modelled are pumps and valves.

Pumps The pumps circulating the water in the system have been modelled in Matlab and then combined with the models of the other components in the Simulink environment. The model calculates the pump power consumption based on the water volumetric flow rate and the pressure drop as shown by Equation 3.40

$$P_{pump} = \frac{\dot{m}_{vol} * dp}{\eta_{pump}} \quad (3.40)$$

Where the volumetric flow rate is expressed in m^3/s and the pressure drop in Pa . The pressure drop is calculated using the Darcy-Weisback equation shown below:

$$dp = \frac{1}{2} \epsilon * \rho_{water} * v^2 * l_{tubing} / d_{tube} \quad (3.41)$$

where ϵ is the pipe roughness, v is the average flow velocity, l_{tubing} is the length of the tubing and d_{tube} is the inner diameter of the tube. These values change for the different pumps in the system.

Valves The valves are modelled directly in the Simulink environment using multiple switch blocks to include the different switching conditions of the valves.

4

Overall system - Design and Model

In the following section, the overall system design and layout are described together with the control strategy and the final implementation and interaction of all the models in the Simulink environment.

In this chapter we try to answer to research question no. 5 provided in section 1.2 by showing how the whole system has been designed and modelled.

4.1. Design and Layout

Figure 4.1 shows the overall system layout. Here we can see how all the different components are connected to each other. The main components are the borehole heat exchanger (represented by the U-tube at the bottom of the figure), the heat pump (composed of the main HP and the booster HP), the evacuated tube collector, the storage tank for DHW and the house. Additionally in this schematic we see the pumps and the valves used to direct the water flowing in the system.

Here is a brief explanation of how each system interacts with the others.

Let's start from the bottom of the schematics.

The BHE is used as a heat source for the main HP. The water flowing out of the BHE goes into the main HP evaporator exchanging heat with the heat pump refrigerant.

On the sink side of the main HP we see that the heat delivered by the main HP is divided between the floor heating and the booster HP.

The floor heating water is circulated by the pump P4. Passing through the condenser heat exchanger of the main HP, the heating water flow absorbs heat which then is delivered to the house by circulating through the floor and then it comes back to the heat pump sink.

The last part of the condenser of the main HP heat exchanger is the source heat exchanger of the booster HP. The booster HP needs to heat up the water up to 65°C so using the main HP as the heat source ensures a higher COP of the booster HP compared to using the BHE water since the source and sink temperatures are closer to each other. The booster HP refrigerant absorbs then some heat from the main HP, upgrades it, and on the sink side it heats up the water in the DHW storage tank.

The hot water in the DHW storage tank is then sent to the house through a separate loop where it is mixed with water at about 10°C to reach the required temperature of 40 °C.

The control valve (CV1), depending on the water temperature level of the fluid coming out of the ETC collector, directs the flow into the BHE through valve V4 to exchange heat with the soil and restoring part of the heat balance or it can be directed back into the ETC inlet through V3. If the water stream is sent to the BHE, then once the water comes out of the main HP source HX it is split through valve V2 so that part of it goes back to the BHE through V4 and part goes back to the solar collector.

Each separate loop uses a pump (P1, P2, P3 and P4) to ensure the required flow of water in the loop.

The BHE field includes four different U-tube BHEs that are used to increase the performance of the system and to be able to store all the energy coming from the ETC system. This will of course increase the initial investment of the system, however, this was a design choice made to maximize system performance.

The ETC system includes six solar collectors. These are placed in three parallel arrays each made up of two collectors in series. The parallel configuration ensures a high enough flow rate while the addition of more collectors in series ensure that the outlet temperature is higher. The ETC system configuration has been selected to ensure thermal balance on the BHE temperature.

4.2. Control strategy

In the following system, some components can be switched on and off depending on specific conditions to maximize the heat utilisation in the system. Also the control valve (CV1) is used to ensure that all of the available heat is used at its best. In this section we will list the on/off conditions for each component as well as the valves control strategy and the main HP control mechanism.

DHW storage tank and booster HP The DHW tank water temperature is used to control the booster HP on/off condition.

The DHW tank requires heat from the booster HP only if $T_{water_{tank}} < 65$ °C. Once this temperature is reached, the booster HP is switched off.

The system is turned back on only when $T_{water_{tank}}$ becomes colder than 50 °C. Once this temperature is reached, the booster HP turns on.

ETC The evacuated tube collector can be switched on and off depending on the irradiance level which determines the heat that the ETC would deliver to the system. Hence, if the irradiance is too low, the ETC system is switched off to avoid useless pump power consumption. The heat threshold is set to 300 W.

Main HP The main HP can also be switched on and off depending on both the room temperature (i.e heat requirements from SH) and the booster HP on/off condition.

Only if at the same time the booster HP is off and the room temperature reaches the set point, then the main HP switches off. Otherwise it will be running.

The heat delivered to the house is controlled based on the temperature difference between the room temperature and the ambient air temperature. In particular, with the simplification of neglecting the thermal mass of the floor, the heat delivered to the house is calculated as follows:

$$Q_{HP} = 4000 * (T_{room} - T_{amb}) / DT_{max} \quad (4.1)$$

Where DT_{max} is equal to 30 °C. The compressor speed is proportional to the heat delivered and if the temperature difference between room temperature and ambient temperature gets closer to zero but the booster HP is still on, then the compressor will rotate at its lowest speed (400 rpm).

CV1 The control valve CV1 has the role to ensure that the water coming out from the ETC outlet goes to the BHE only if it has a high enough temperature.

This limit is set to 10 °C to ensure that heat is transferred to the soil. If the water temperature entering the valve is lower than 10 °C, then it is directed to the ETC inlet.

This also ensures that the temperature entering the ETC is closer to the ambient temperature to limit the losses in the ETC due to temperature difference with the environment.

4.3. Model implementation

Once all components have been integrated together in the Simulink environment, then inputs, outputs and initial conditions of the system must be specified. This section is dedicated to explain the details and the behaviour of the model, including characteristic time step of the simulation and general simplifications and assumptions.

Initial conditions (I.C.) Some parameters in the model need to be initialized to allow the model to start simulation from some initial conditions. Here below are listed the various initial conditions of the model which have been assumed as follows:

- **Borehole model I.C.** (based on undisturbed ground temperature)

$$T_b(0) = 10 \text{ °C} ; T_g(0) = 10 \text{ °C} ; T_s(0) = 10 \text{ °C} ; T_{fu}(0) = 10 \text{ °C} ; T_{fv}(0) = 10 \text{ °C}$$

- **House model I.C.**

$$T_{room}(0) = 15 \text{ °C} ; T_{wall}(0) = 19 \text{ °C}$$

- **ETC model I.C.**

$$T_{ETC_{out}}(0) = 15 \text{ °C}$$

General simplifications and assumptions The following simplifying assumptions have been considered in the model:

- The main heat pump works only in heating mode.
This assumption is based on the fact that during the summer period, in the Netherlands, ambient temperature does not reach too high values and thus cooling of the house is usually not required (see Figure 4.4). Therefore, this load has been considered to be negligible allowing the main heat pump to work only in heating mode.
- The DHW consumption has been considered constant throughout the year.
This assumption, already mentioned in the section above about the DHW storage tank model, is a simplifying assumption since there is a variation in the consumption of DHW throughout the year. However, using an average consumption can give sufficiently accurate results for the goal of this work.

Input values The inputs required in the model are the following:

- Ambient temperature [$^{\circ}\text{C}$]
- Irradiance [W/m^2]
- DHW consumption [kg/h]

Both ambient temperature and global irradiance values have been taken from *The Dutch PV portal 2.0 climatological year for Rotterdam* and are based on measurements made available by the Koninklijk Nederlands Meteorologisch Instituut (KNMI).

Two different input values for ambient temperature and irradiance have been used for two different simulations. Both values of temperature and irradiance are hourly average values over a period of 29 years (1991-2020) in one simulation and hourly average values for the year 2010 in the other. This has been done in order to have two different perspectives and to understand how the system performs in two different conditions. The average values between 1991 and 2020 have been taken as a reference values while the values from 2010 have been used since this year was a particularly cold one.

In both cases, data points are available for each hour timeslot in the year. In order to reduce the simulation time step to six minutes (0.1 hour), the hourly data points have been interpolated every six minutes for both temperature and irradiance values. In Figure 4.2 and Figure 4.3 are reported, respectively, the ambient temperature and global irradiance values throughout the year for the average between 1991 and 2020 while in Figure 4.4 and Figure 4.5 are reported, respectively, the ambient temperature and global irradiance values throughout the year 2010. Global irradiance is used as input to the ETC system since ETC can absorb both direct and diffuse radiation [73].

The DHW consumption input values are the ones shown above in the section dedicated to the DHW storage tank model (see Figure 3.10b) and these same values have been used for both simulations.

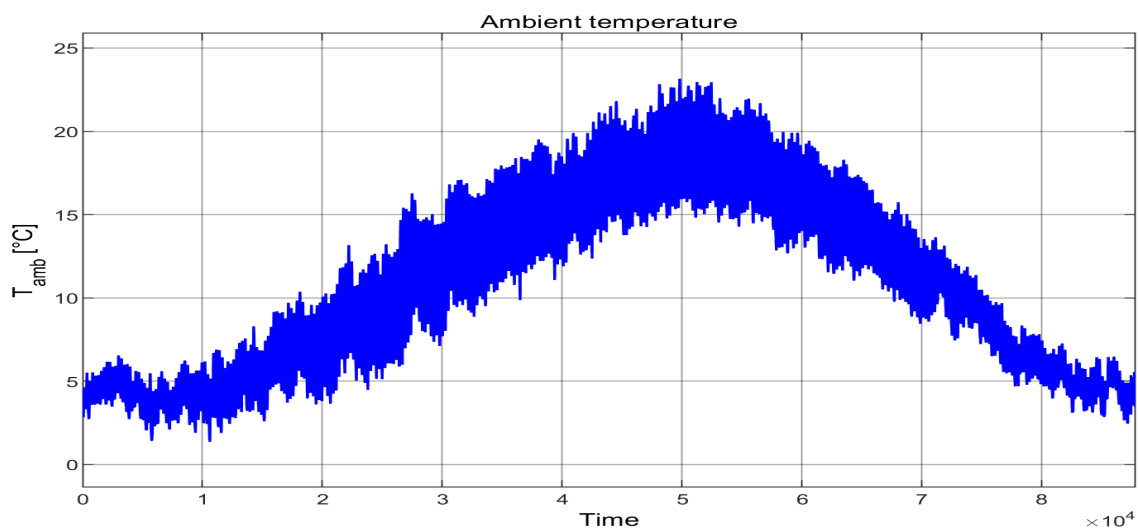


Figure 4.2: Average hourly ambient temperature values throughout the year [Average 1991-2020]

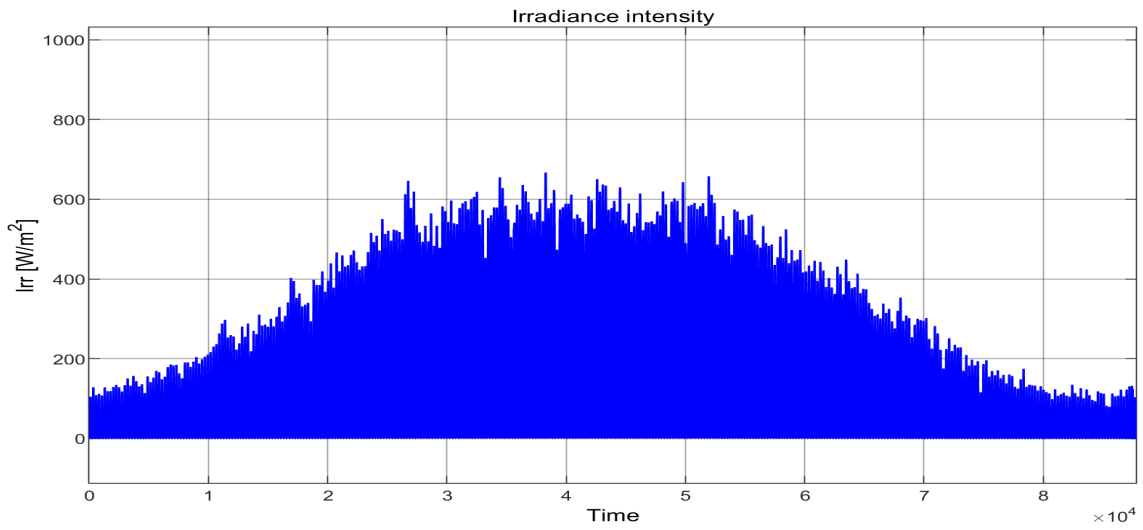


Figure 4.3: Average hourly irradiance values throughout the year [Average 1991-2020]

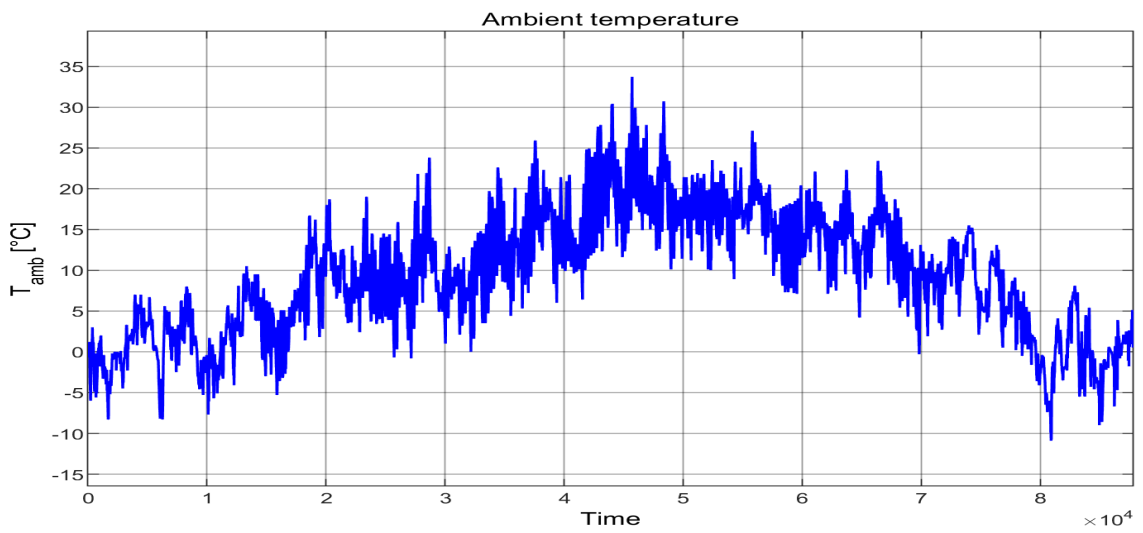


Figure 4.4: Average hourly ambient temperature values throughout the year 2010

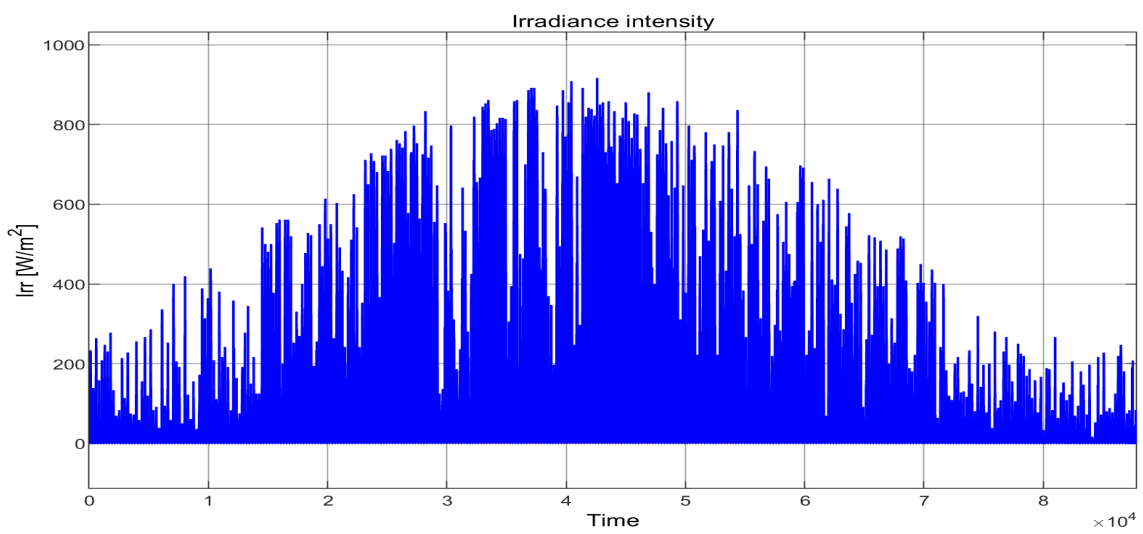


Figure 4.5: Average hourly irradiance values throughout the year 2010

Simulation time step The simulation time step has been set to six minutes (0.1 hour). The input parameters $T_{ambient}$ and $Irradiance$ are obtained interpolating between each hour to calculate the values every six minutes. Of course, it is important to underline that this might be a large time step for some of the processes in the system and the accuracy of the results might then be lower. However, it has been decided to stick to this simulation time step to reduce the amount of calculations and keep this simplification in mind when looking at the results and making conclusions.

5

Results and Discussion

In this section, we are gonna present the results obtained from the SAGSHP model, discuss the main advantages and disadvantages of this system compared to a traditional gas boiler system and present the possible improvements and studies that can be done in this field. Here we will try to answer to research questions 6, 7 and 8 presented in section 1.2 by showing how the system performs and how competitive this is compared to a traditional gas boiler in terms of cost and CO_2 emissions.

Here below, two different result sets are presented for different input parameters.

The first set of results is obtained from a simulation where the inputs (irradiance and ambient temperature) are averaged hourly values over a period of 29 years (1991-2020).

The second set of results focus on a particularly cold year such as 2010.

These two different input datasets have been used in order to compare the system performance when very cold temperatures are registered (2010) as well as based on the average values registered in the last decades. This comparison allows to state whether the system can perform in extreme conditions (2010) as well as assessing the performance of the system based on average values. Therefore, the average values will be used to understand the performance of the system. Last but not least, it give us a basis for comparing two different situations and state in which situation the system performs better in terms of SCOP as well as from an economic point of view.

It is important to keep in mind that in all of the plots shown below the time axis unit of measurement is 0.1h. It goes from 0 to 87840 since in a leap year there are 8784 hours.

5.1. Results for averaged values between 1991 and 2020

HP and house results Let's start by looking at the house model to see the performance of the main heat pump. In Figure 5.1 the heat loads of the house model are reported while Figure 5.2 shows the room temperature variation throughout the year.

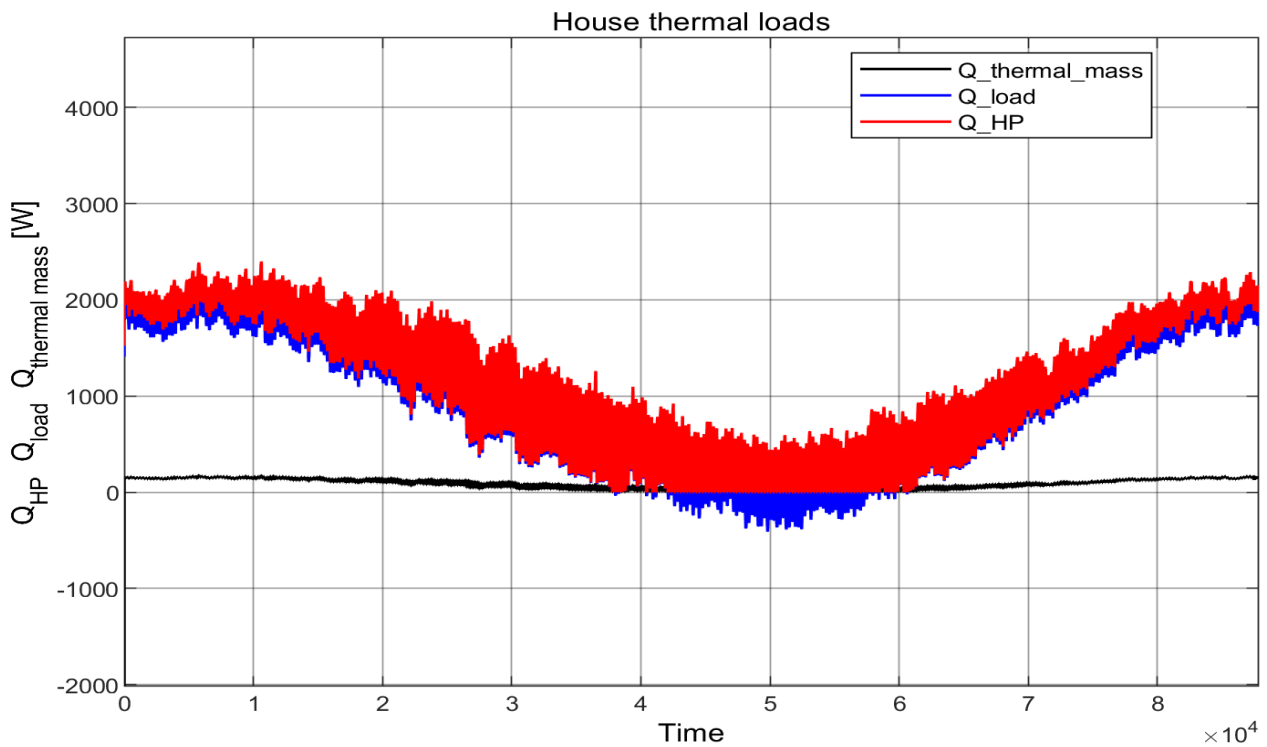


Figure 5.1: Heat loads of the house environment

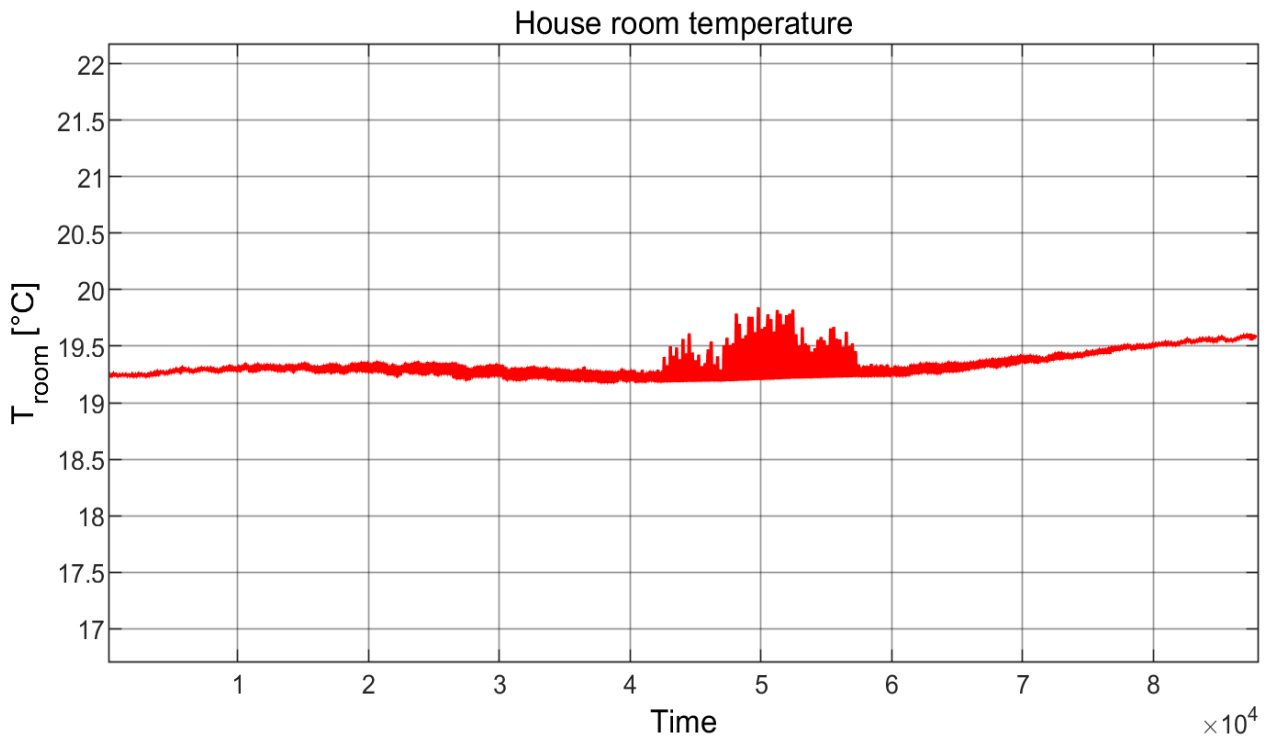


Figure 5.2: Room temperature of the house throughout the year

In Figure 5.1, the blue plot represents the heat exchanged with the environment (i.e. Q_{load}), the black line shows the thermal mass heat load of the house and the red one shows the heat delivered by the heat pump through floor heating. The heat exchanged with the outside environment and the thermal mass heat load are positive when the heat is lost from the room to the ambient environment or to the wall. The heat from the heat pump is positive when heat is given to the house system. In Figure 5.1, we can see how the heat lost to the environment decreases when approaching the summer months and then it goes back up again in the autumn/winter months. We can also see how the heat delivered by the heat pump follows a similar trend. In Figure 5.2 we can see how the temperature of the room air in the house is kept fairly constant around 19.4 °C.

The heat delivered to the house by the heat pump is not all the heat delivered by the main heat pump. By means of a booster heat pump, it also delivers heat to the DHW storage tank. In Figure 5.3 we can see both the heat delivered by the booster heat pump to the DHW tank and the heat loss by the DHW tank to the outside ambient air. The heat loss due to flow of hot water to the house is negative when heat is loss from the tank while the heat delivered by the heat pump system is positive when given to the DHW tank system.

The loads shown in Figure 5.3 can be related to the temperature values of the water in the storage tank reported in Figure 5.4. In both figures, the values are shown for a smaller time period (a bit more than a month) between February and March to show in detail how the DHW loads and the temperature vary accordingly. This same pattern repeats almost identically throughout the year since the same water consumption mass flow rate has been assumed all year long. In Figure 5.3, the heat loss to the environment is not shown since it is negligible compared to the other loads on the DHW tank.

Here it can be clearly seen how the heat pump goes on and off following the water tank temperature. The off threshold temperature is 65 °C and the on threshold temperature is 50 °C. The DHW off period is about 10 hours during the night when the DHW consumption mass flow rate goes to zero. We can clearly see how in the periodical oscillation of the water tank temperature there is a moment when it rises to 61.5 °C and then it drops again to 59 °C before rising back to 65 °C. This happens when the heat loss due to the flow of water for domestic use is higher than the heat delivered by the booster HP. This occurs once a day, when the DHW consumption reaches the maximum. Here the booster HP is still running but it cannot deliver enough heat to avoid the decrease in temperature. The water tank temperature rises again once the DHW consumption decreases.

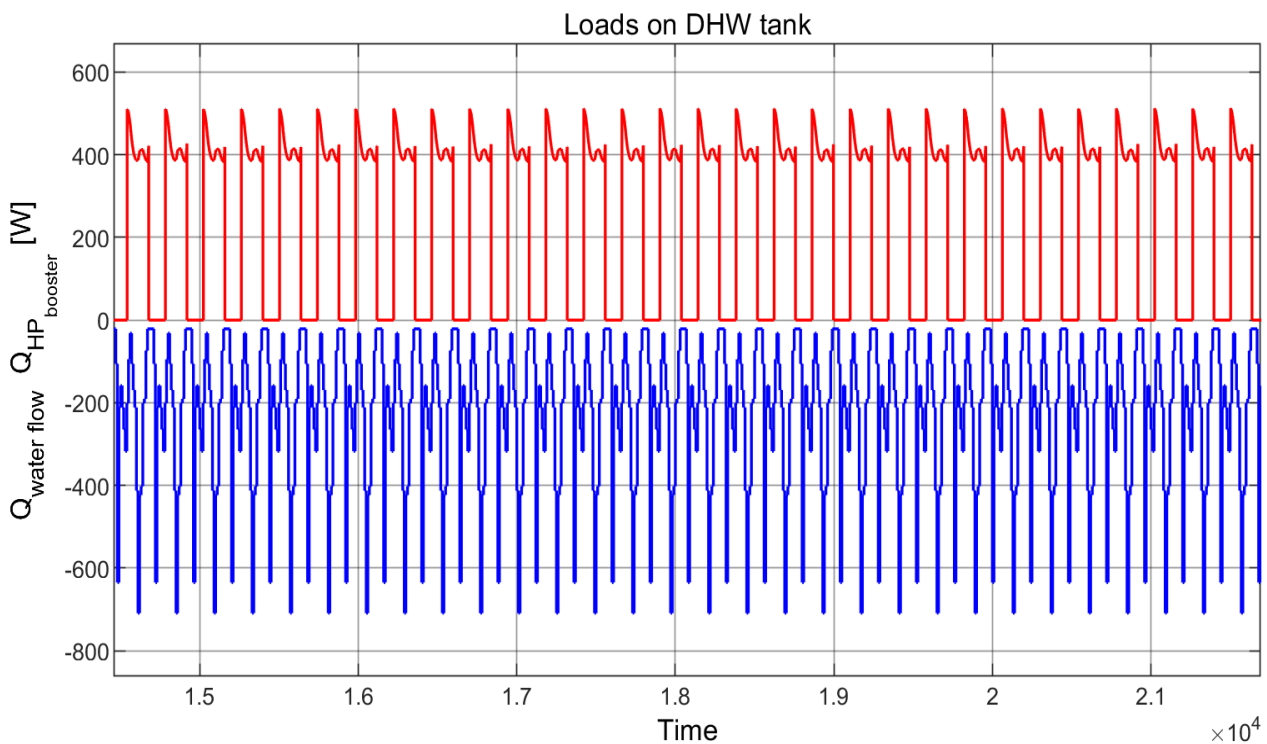


Figure 5.3: DHW tank - Heat loads over a period of one month (March)

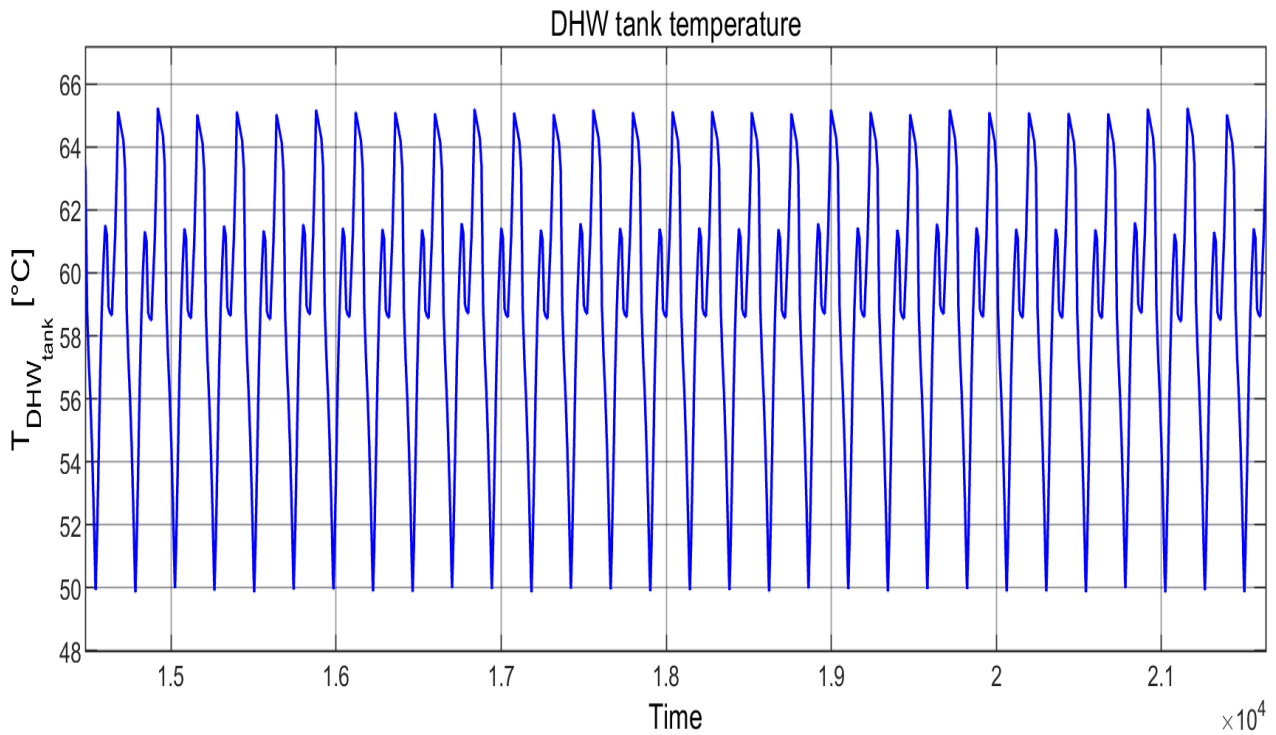


Figure 5.4: DHW tank - Water temperature over a period of one month (March)

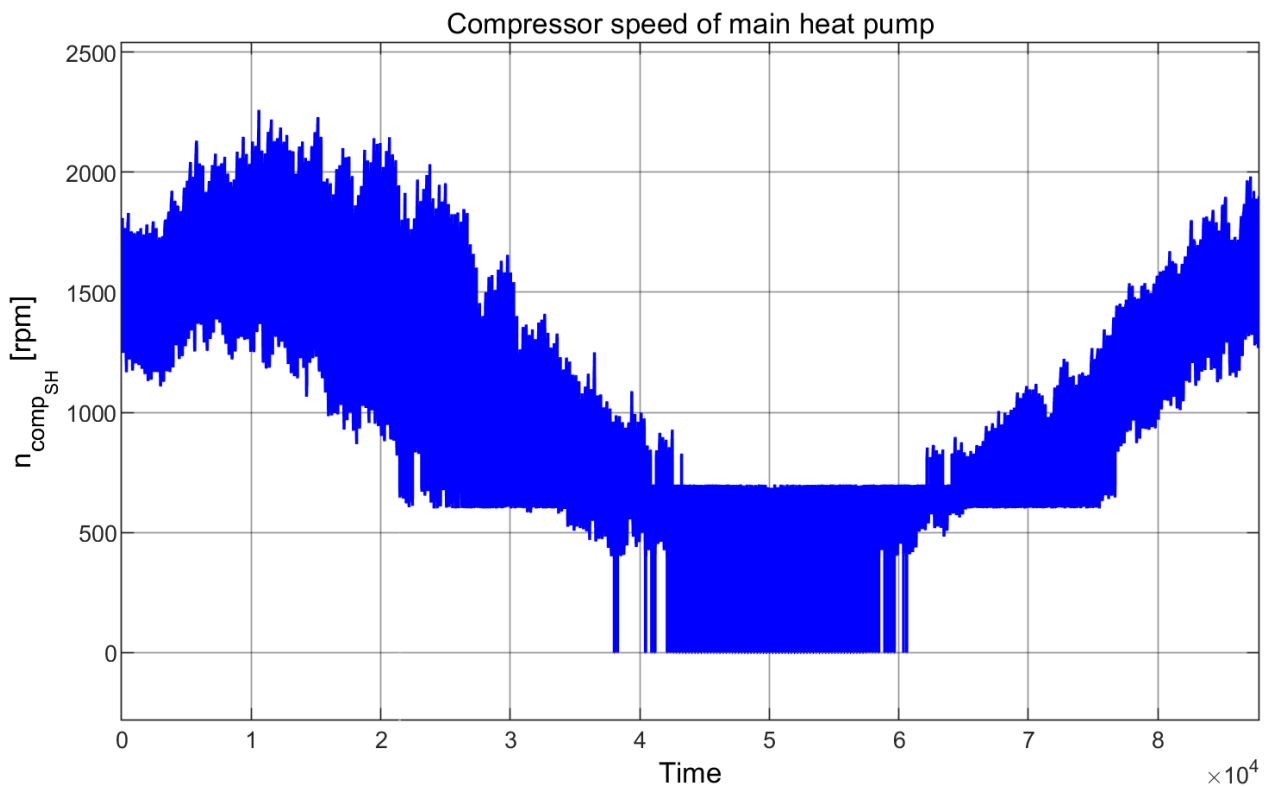


Figure 5.5: Main HP - Compressor rotational speed

Looking more in detail at the heat pump, the rotational speed of the main heat pump compressor is shown in Figure 5.5. Here we can see how the rotational speed of the compressor follows a very similar trend as the one of the heat delivered to the house. It decreases approaching the summer periods and then it gets to the minimum rotational speed in the summer. In Figure 5.5, it can be seen how the compressor speed goes to zero during the summer period.

This happens when both the heat delivered to the house is zero and the DHW tank system switches off. The rest of the summer time the compressor is mostly running at about 500 rpm because one of the two systems (SH or DHW), or both, are on but the total heat requirement is still low. Some peaks occur during the night, when the ambient temperature drops and the heat delivered to the house increases significantly compared to daytime.

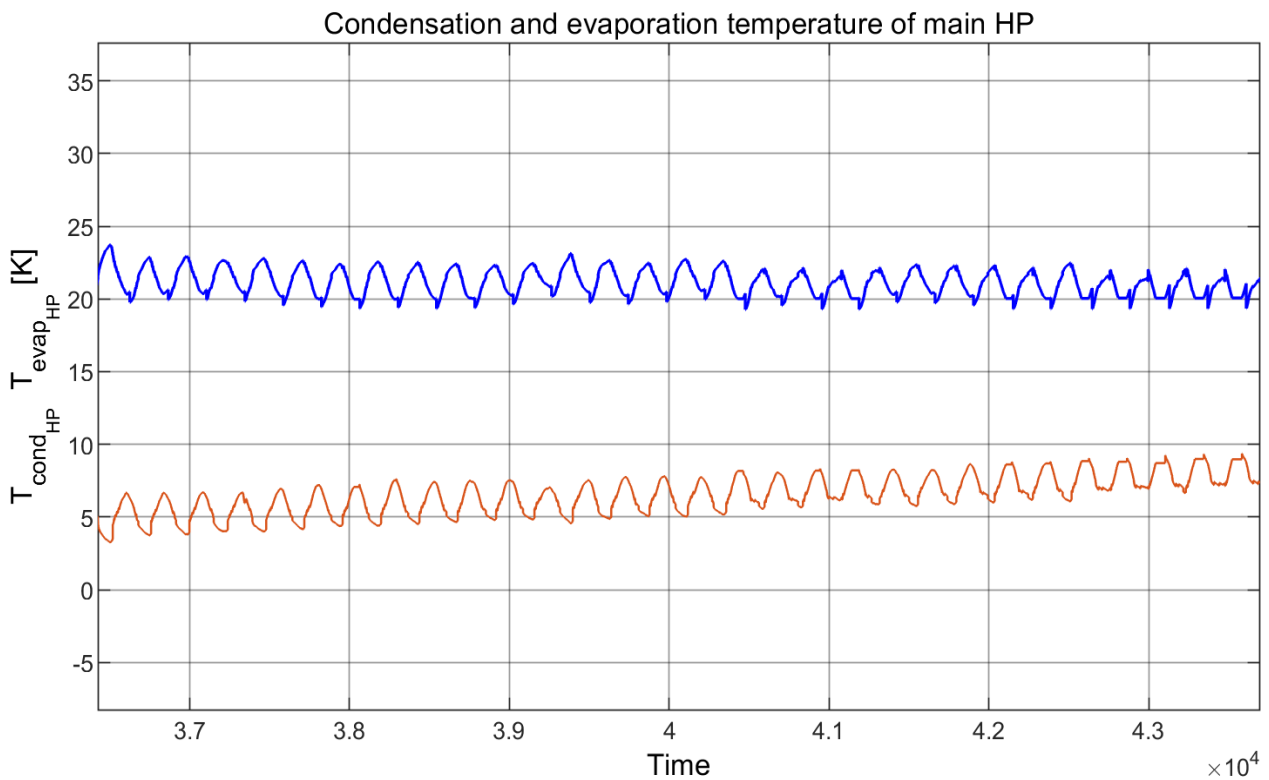
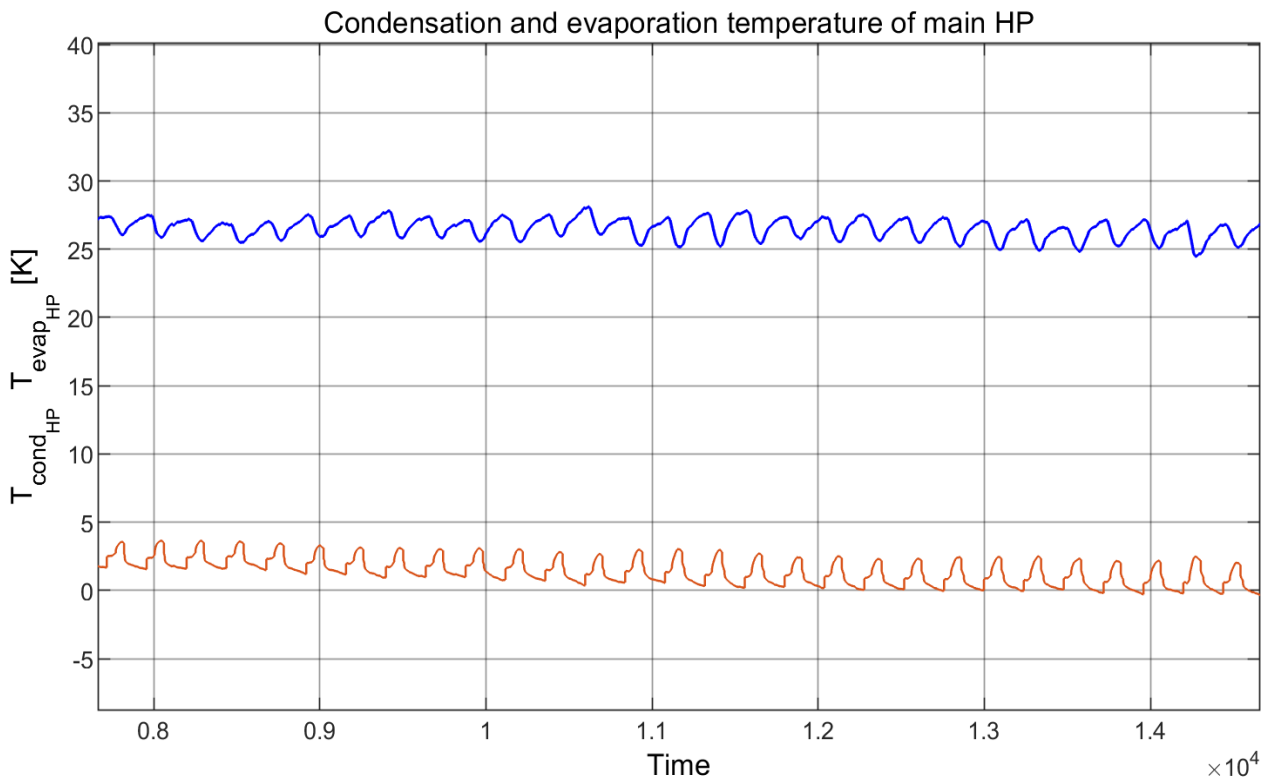


Figure 5.6: Main HP - Condensation and evaporation temperature in the months of February and July

In Figures 5.6 are reported the condensation and evaporation temperatures of the main heat pump. Here, two significant months are reported to give an idea of the condensation and evaporation temperatures of the heat pump in a cold and in a hot month. From these graphs we can notice how the condensation temperature decreases in the month of June compared to February. This can be related to the reduced heat load of the house which required a lower condensation temperature of the heat pump. Looking at the evaporation temperature, we can notice an opposite behaviour compared to the condensation temperature. The evaporation temperature in June is higher compared to February due to the increase in heat source temperature resulting from more utilisation of the ETC system.

The increase in the evaporation temperature during the summer period is clearly related to the source temperature at the inlet of the heat pump evaporator, shown in Figure 5.7.

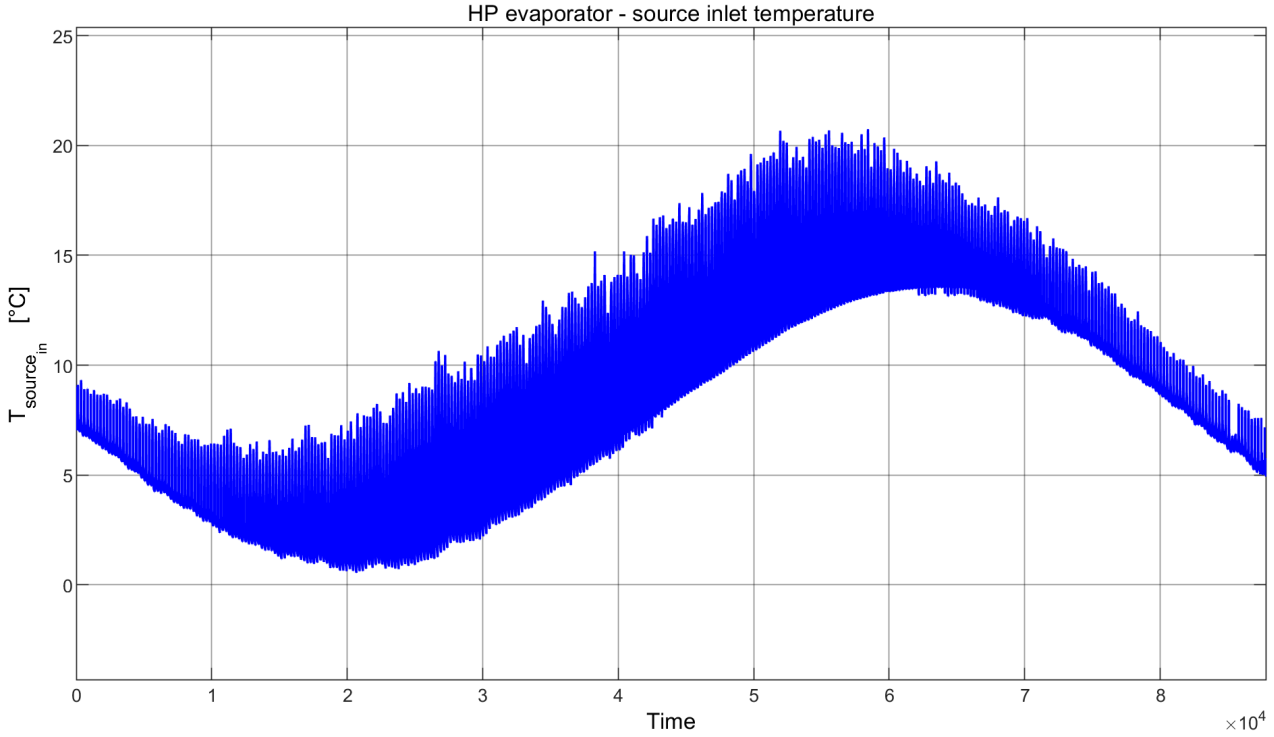


Figure 5.7: Main HP - Heat source temperature at the inlet of the evaporator

Another interesting result regarding the HP system is the SCOP of the HP system. This value is obtained by dividing the overall heat delivered by the heat pump system by the overall energy consumption of the compressor of the HP system as shown in Equation 5.1.

$$SCOP_{HP} = \frac{Q_{HP_{tot}}}{W_{HP_{tot}}} \quad (5.1)$$

where

$$Q_{HP_{tot}} = Q_{sink_{HP}} + Q_{sink_{booster}} \quad (5.2)$$

and

$$W_{HP_{tot}} = W_{comp_{HP}} + W_{comp_{booster}} \quad (5.3)$$

For the specific configuration and model inputs used in the model, the final value obtained for the SCOP of the HP system over a year is reported in Table 5.1

Table 5.1: HP system - Seasonal coefficient of performance

$SCOP_{HP}$	6.2
-------------	------------

BHE results The BHE system behaviour can be analysed looking at the heat extraction or injection rate in the borehole, the borehole temperature, and the inlet and outlet temperature of the borehole working fluid.

Starting with the heat injected and extracted from the borehole during the year, in Figure 5.8 it can be seen how the heat extraction/injection rate changes throughout the year. In this figure, a positive value indicates that heat is

injected in the ground while a negative value means that heat is extracted from the ground. Keeping this in mind, we can see how the first 1000 hours (approximately until the 10th of February) the heat values in the graph are always negative, hence heat is extracted from the ground. Then the heat injection rate starts to increase until it approaches the peak around 4000 hours (15th of June). After 5000 hours (24th of July) the heat injected reduces until the last months of the year, when heat extraction becomes once again more significant compared to heat injection. This trend is following the operation of the ETC system and it is due to a higher heat extraction from irradiation in the summer which is then injected in the ground. It can be noticed that in the summer months, there is still heat extraction from the ground. This happens during the night, when no heat is obtained from the solar collectors and at the same time there is some heating requirement for the house.

This variation during the year of heat injected and extracted from the ground has significant effects on the borehole temperature variation throughout the year. In Figure 5.9 is shown the borehole temperature variation during the year where we can see how the borehole temperature reduces at the beginning of the year up to 2000 hours (24th of March). This can be explained by looking at Figure 5.8, where, in the first months of the year, we can see a larger heat extraction from the borehole compared to the heat injected. The higher heat extraction in the first months of the year causes the initial temperature drop that can be seen in Figure 5.9. However, once the heat injection begins to rise in the spring and summer period, also the temperature of the borehole increases significantly, reaching the peak around 6500 hours (28th of September). After this moment, the heat injected from the ETC system reduces since the amount of irradiation decreases while the heat extraction increases because of the increase in heat requirement from the house. This causes the borehole temperature to decrease in the last months of the year.

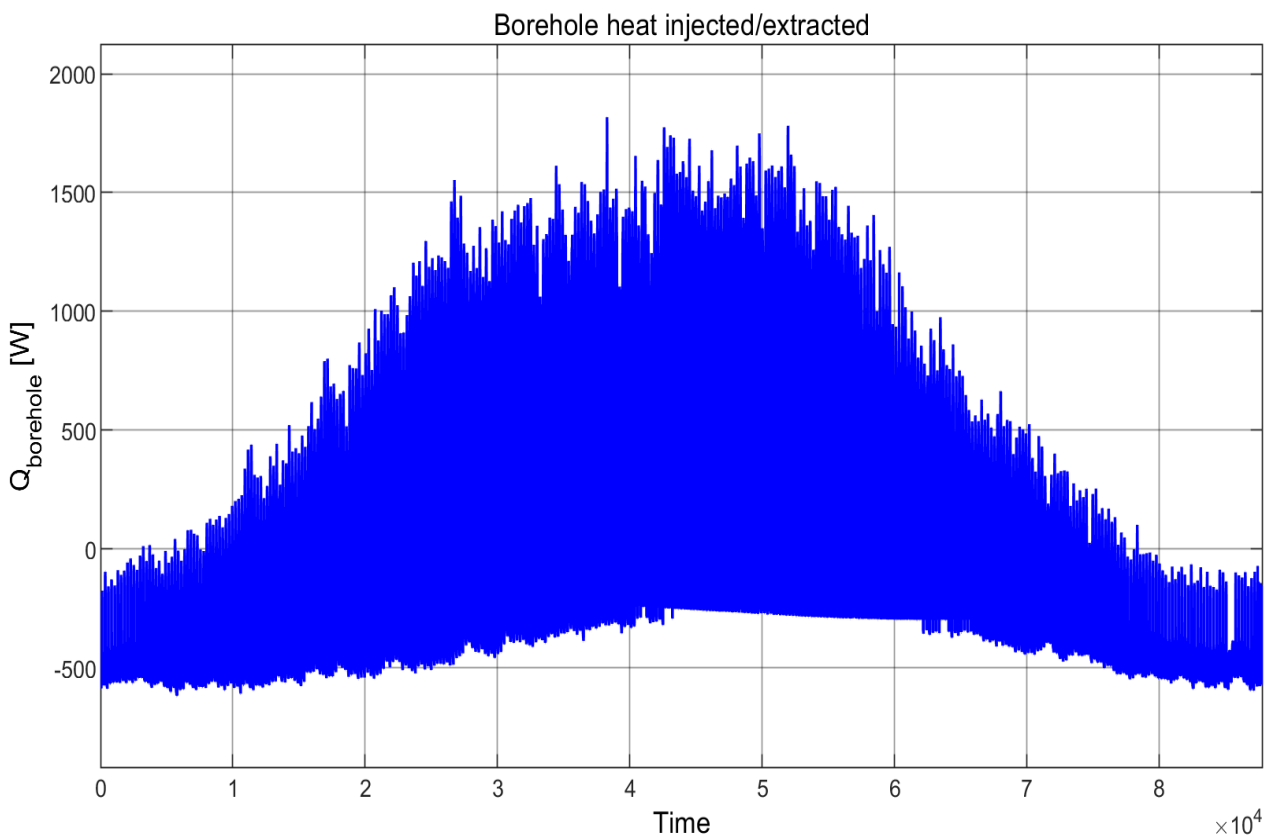


Figure 5.8: BHE system - Heat extraction/injection

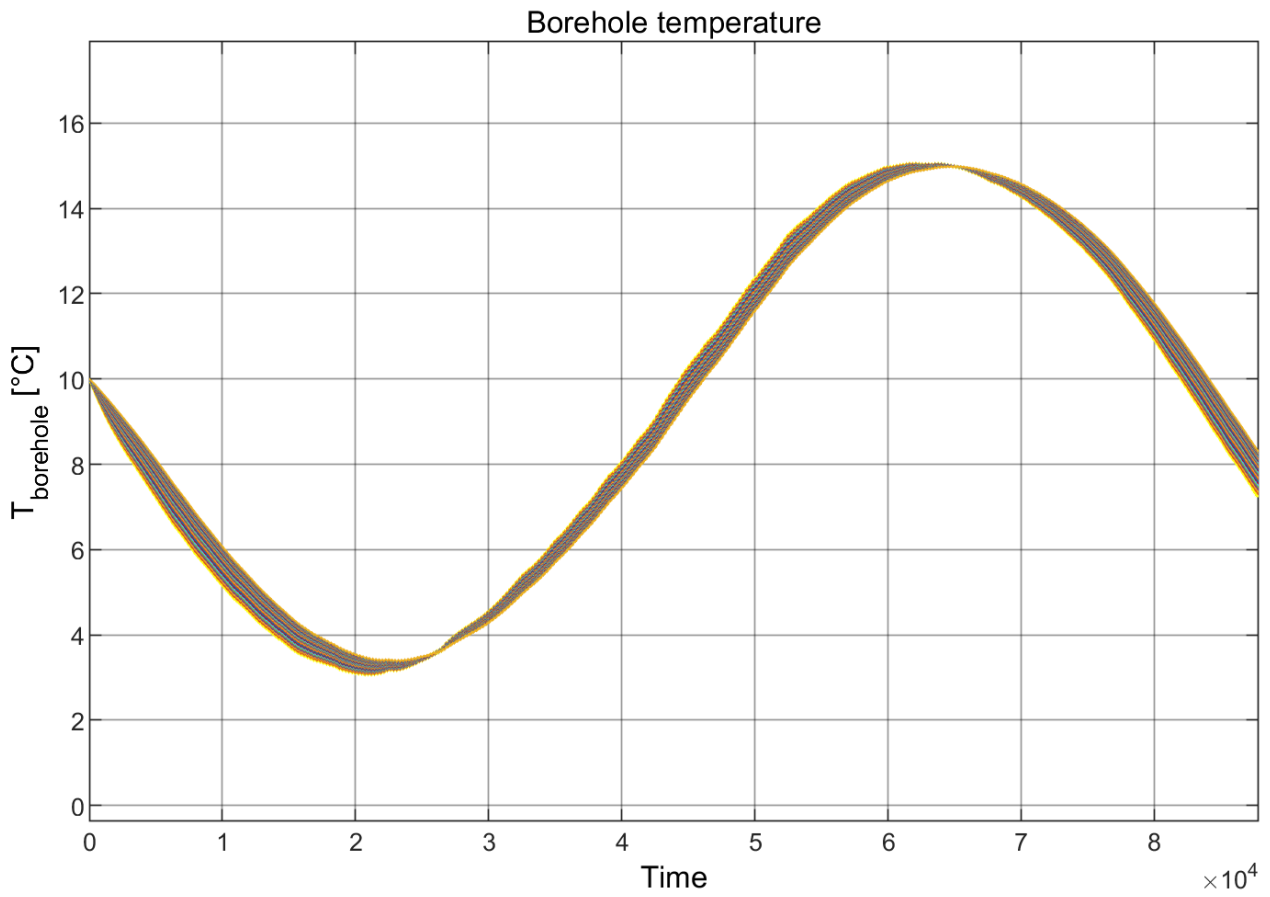


Figure 5.9: BHE system - Temperature at the edge of the borehole

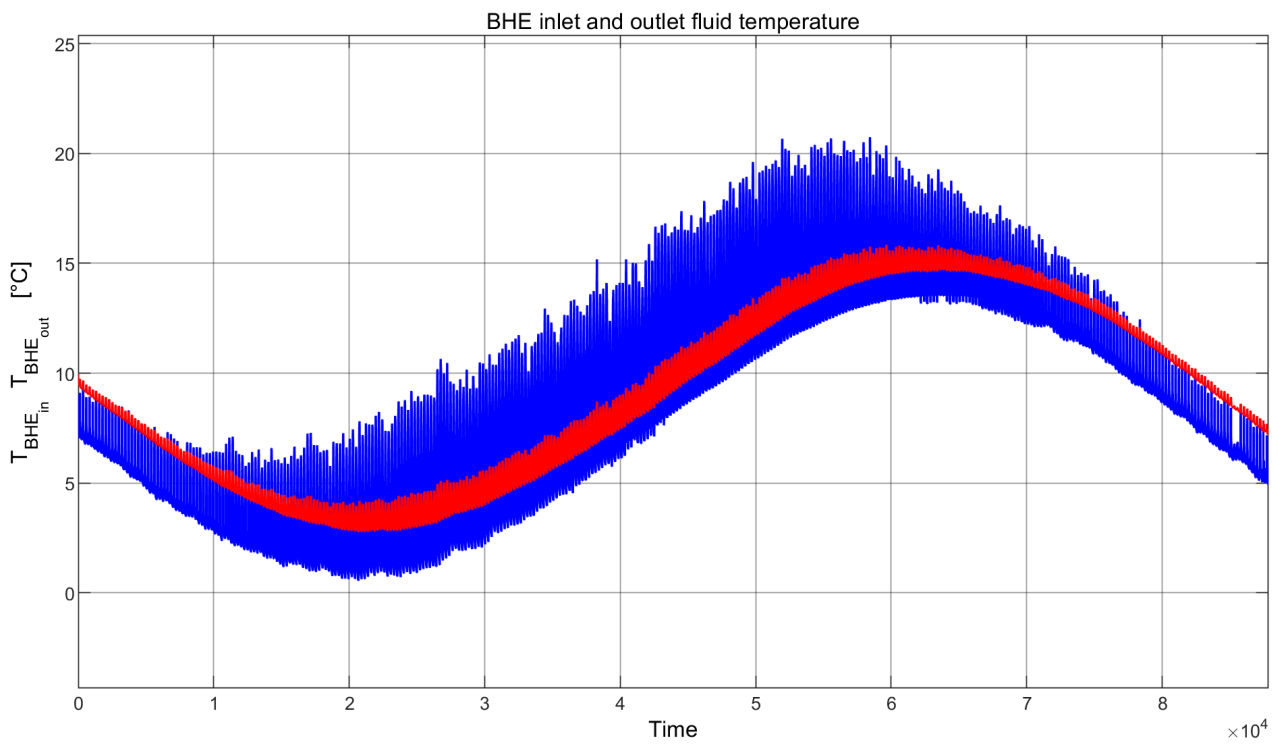


Figure 5.10: BHE system - Inlet (blue) and outlet (red) temperature of the working fluid

Another interesting observation that can be made from Figure 5.9 is that at the end of the year, the borehole temperature is actually lower than when it started at the beginning of the year. This implies that, if this configuration is used, every year the borehole temperature will slightly decrease. This shows that the heat injected from the ETC system should actually be increased to ensure thermal balance of the ground. This can be done by increasing the amount of solar collectors used. However, it must be specified that these results are obtained for input ambient temperature and irradiance values averaged between 1991 and 2020. Therefore, it is important to keep in mind that due to climate change average temperatures will be increasing in the coming year. Therefore, this slight unbalance in the ground temperature is not considered to be an issue, since it is assumed that on average ambient temperature values will be higher than what has been used to run the simulation and this should therefore slightly reduce the heat extracted from the ground making thermal balance of borehole temperature more likely to happen without increasing the number of ETC.

Last but not least, it is interesting to see the variation of inlet and outlet temperature of the working fluid in the BHE system throughout the year reported in Figure 5.10.

In this graph, the blue plot shows the temperature of the working fluid entering the BHE and the red line shows the temperature of the working fluid coming out of the BHE. Also here we can clearly see the effects of the ETC system. As summer approaches, the temperature of the working fluid entering the BHE increases. This happens because the temperature coming from the ETC system is higher in the summer and when it gets mixed with the temperature coming out from the condenser of the main heat pump, it significantly increases its temperature. However, with increasing temperature of the working fluid as we approach the summer, we can also notice a higher oscillation in the temperature value. This can be related to the temperature variation between day and night which increases in the summer period because the temperature during the day is increasing a lot thanks to the mixing with the ETC working fluid while at night the ETC system is off, hence resulting in a BHE inlet temperature much lower than that of the day. The temperature of the working fluid coming out from the BHE and entering the HP evaporator follows the same trend as the inlet temperature. However, the oscillation of the outlet temperature between day and night is less compared to the inlet temperature since part of the heat contained in the working fluid of the ETC system is injected into the ground thus resulting in much lower temperature difference between day and night.

ETC results To have a better understanding of how the ETC system works, we can have a look at the heat obtained from the ETC system as well as at the inlet and outlet temperatures of the system. In Figure 5.11 is shown the heat obtained from the ETC system as a function of time.

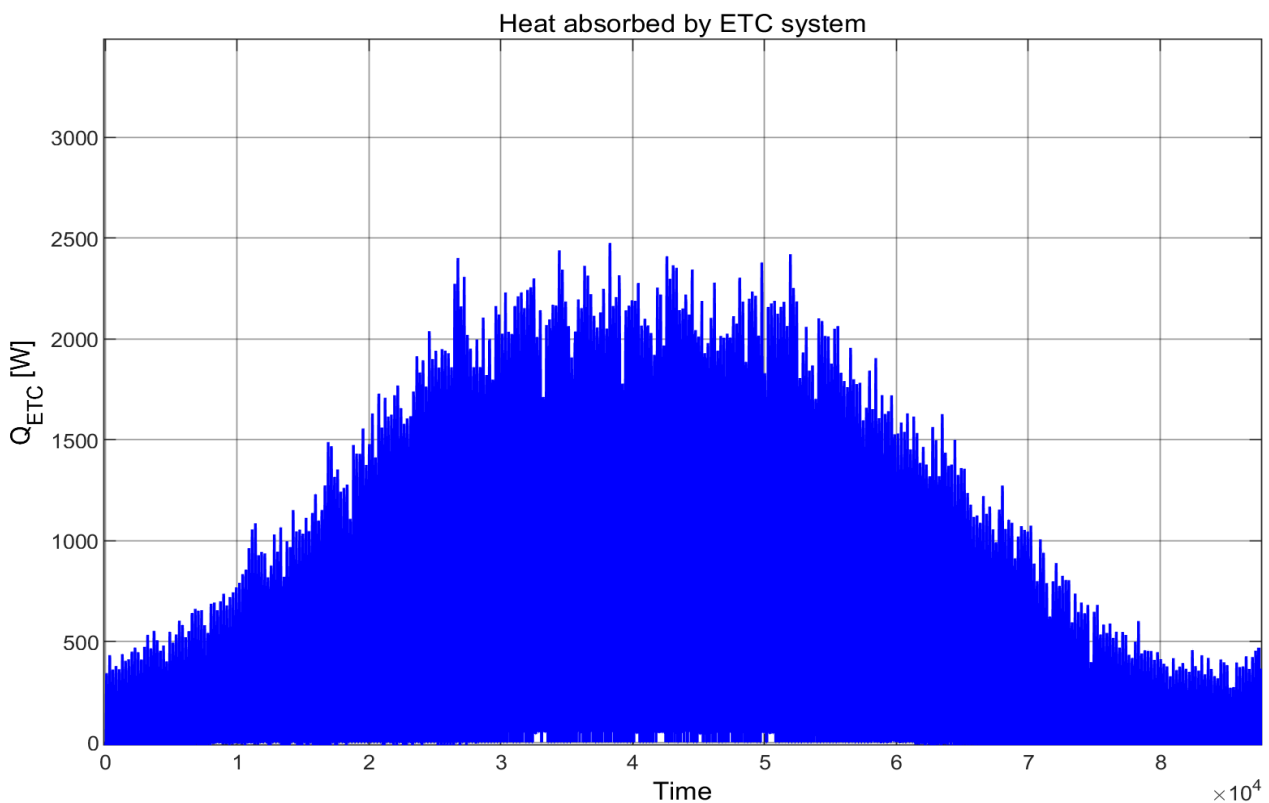


Figure 5.11: ETC system - Heat absorbed

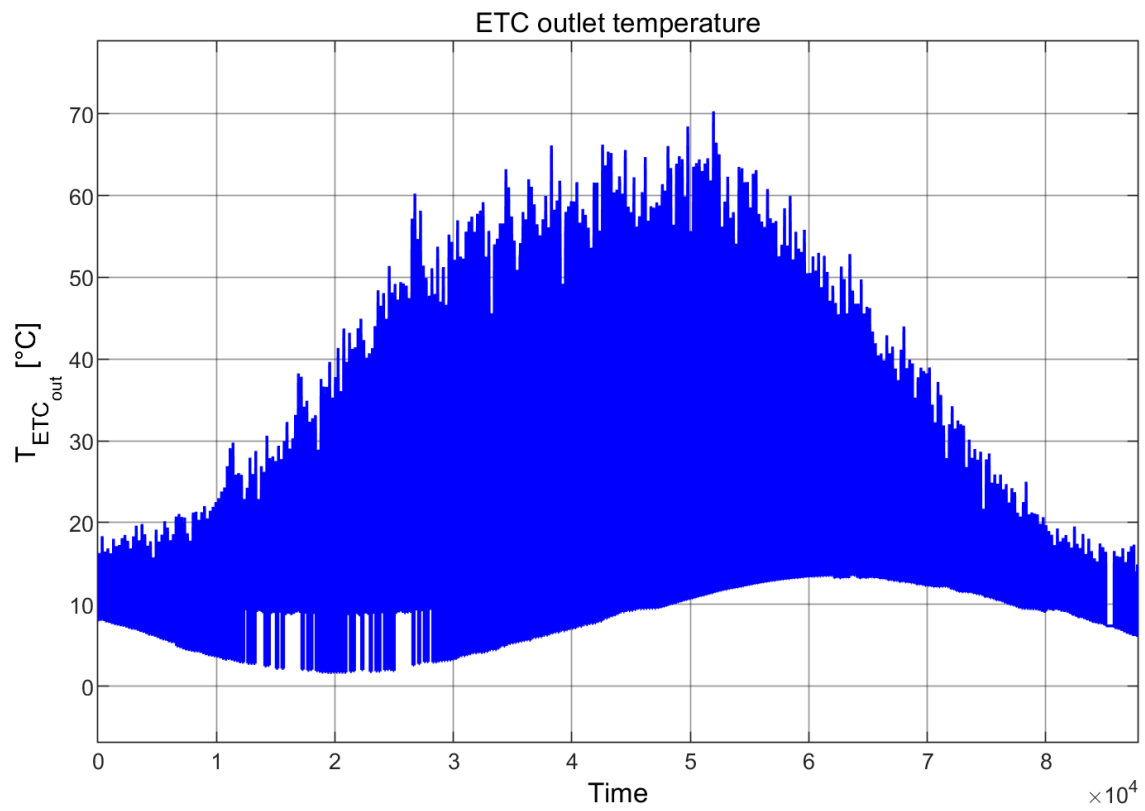


Figure 5.12: ETC system - Outlet temperature

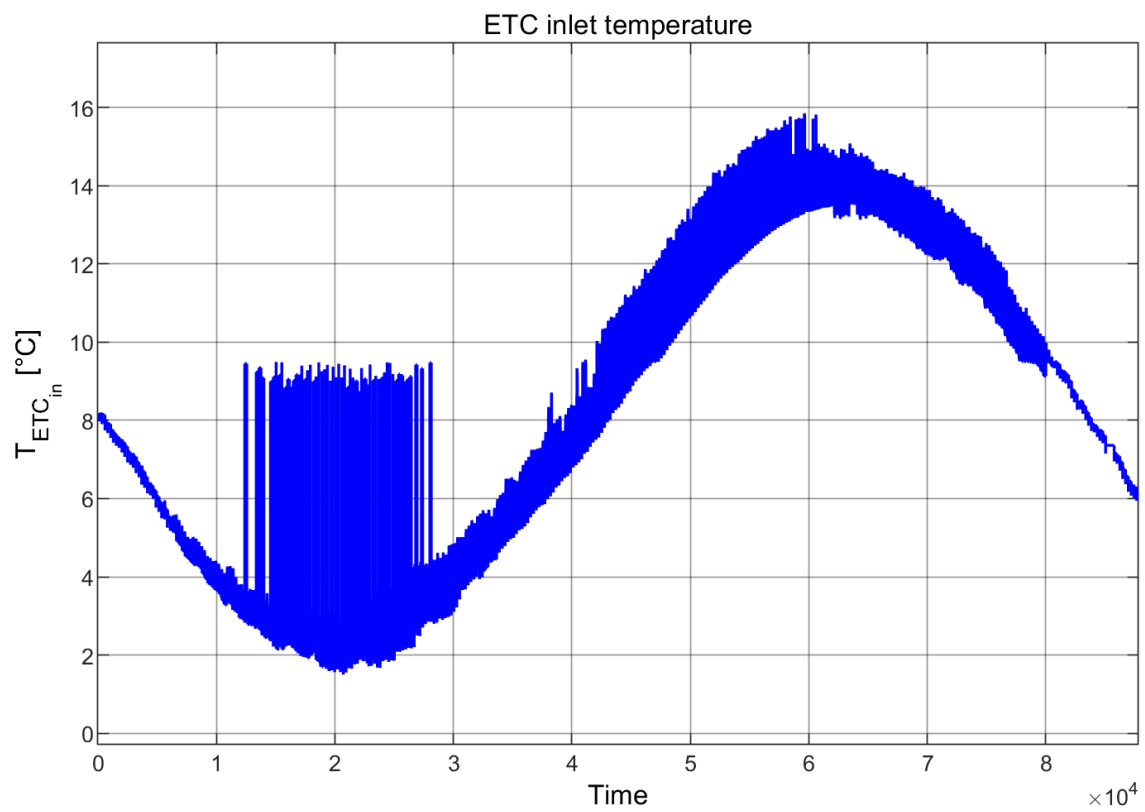


Figure 5.13: ETC system - Inlet temperature

In Figure 5.11 it is clear how the energy obtained from the ETC system is having a trend that follows the irradiance throughout the year shown in Figure 4.3. This variation in heat obtained from the ETC collector is strictly related to the parameter changes during the year that were analysed above. This can also be related to the temperature variation at the outlet of the ETC system, shown in Figure 5.12. On the other side, the ETC system inlet temperature variation during the year, reported in Figure 5.13 is clearly having the same trend of the temperature entering the borehole. This is because, unless $T_{ETC_{out}}$ is lower than 283.15 K, the temperature entering the ETC system is the same as the temperature coming out from the evaporator of the HP system.

Additionally, in Figure 5.13 it can be noted that in the time span between 1000 and 3000 hours there are some peaks occurring. These peaks can be related to the control of the ETC system. In particular, these peaks can be explained since the control valve CV1 directs the stream coming out of the ETC system to the BHE system only if $T_{ETC_{out}} > 10^{\circ}\text{C}$. When this happens, mixing of the two fluids reduces significantly the temperature coming from the outlet of the HP evaporator and this temperature is the one of the fluid entering the ETC system. On the other hand, if $T_{ETC_{out}} < 10^{\circ}\text{C}$, then the ETC outlet stream goes directly back to the inlet of the ETC systems.

Therefore, the peaks occur when the outlet temperature of the ETC system is lower than the threshold of 10°C and therefore the working fluid is not mixed with the BHE working fluid resulting in a much higher inlet temperature to the ETC system.

System results It is interesting to look at the overall system results to understand the competitiveness of the system when compared to a traditional gas boiler.

Considering the overall system, the main results to be looked at are:

- Seasonal System COP (SSCOP)
- Levelized cost of energy (LCOE)
- CO_2 equivalent emissions

The SSCOP is used to determine the overall efficiency of the system. It is calculated as shown in Equation 5.4

$$SSCOP = \frac{Q_{tot}}{P_{tot}} \quad (5.4)$$

Where Q_{tot} is the overall heating energy provided by the system and is calculated as $Q_{tot} = Q_{SH_{tot}} + Q_{DHW_{HP_{tot}}}$. Here $Q_{SH_{tot}}$ is the total energy delivered to the house through the floor heating and $Q_{DHW_{HP_{tot}}}$ is the total energy delivered to the DHW storage tank by the booster HP. These values are calculated by adding together the heat delivered at each time step.

The same is done for P_{tot} , which is the total energy consumed by all pumps and by the heat pump compressors and is calculated as $P_{tot} = P_{pump1_{tot}} + P_{pump2_{tot}} + P_{pump3_{tot}} + P_{pump4_{tot}} + W_{SH} + W_{DHW}(J)$.

The SSCOP obtained for the model is reported in Table 5.2 together with the total power consumption and the total heat delivered to the house (SH or DHW)

Table 5.2: Final SSCOP results

Cumulative heat delivered to the house [GJ]	Cumulative energy consumption [GJ]	SSCOP [-]
44	11.5	3.8

This might be increased by changing the control strategy and minimizing the energy consumption when not needed. A way to increase the SSCOP could be to use part of the heat coming from the ETC to heat up the water tank hence reducing the heat requirement from the booster HP. However, at the same time, this would reduce the borehole outlet temperature entering the evaporator of the main HP hence reducing the performance of the HP system. This is to clarify that, to increase the SSCOP effectively some investigation needs to be carried out in order to understand what is the overall effect of the sum of the effects of different changes in the system. This is just one of the possible ways to investigate to improve the SSCOP.

The levelized cost of energy is calculated using Equation 5.5

$$LCOE = \frac{CRF * CAPEX + OPEX}{Q_{tot}} \quad (5.5)$$

where $CRF = \frac{i*(1+i)^N}{(1+i)^N - 1}$ is the capital recovery factor, CAPEX are the capital expenses (initial investment), OPEX are the operational expenses, Q_{tot} is the total heat delivered to the house in a year (domestic hot water and space heating), i is the interest rate and N is the number of years the system is used. The OPEX value is calculated multiplying the total energy consumption by the cost of energy to obtain the operational cost of the system. Maintenance costs are neglected.

In Table 5.3 are reported values of the initial investment of each single component of the system and in Table 5.4 are reported the costs and the values used to calculate the LCOE of both the SAGSHP system and a traditional boiler system

Table 5.3: Initial investments for each technology

Component	Total initial investment
BHE	€18000
HP	€10000
ETC	€1500
DHW tank	€500
Gas Boiler	€1500

It is important to specify that, since the life span of an heat pump is around 15 years but all other components have much longer life span, for the initial investment of HP it was considered the cost for two heat pumps to be able to run the system for 30 years. Additionally, the DHW tank cost has been considered in the initial investment for both cases and the pipes and smaller components cost has been considered negligible for this calculations.

Table 5.4: LCOE values

Technology	CAPEX [€]	Total energy consumption [kWh]	Total heat provided [kWh]	Cost of energy [€/kWh]	Number of years (N) [-]	Interest rate (i) [%]	LCOE [€/kWh]
SAGSHP	30000	3194.4	12222.2	0.147	30	6	0.21
Gas Boiler	2000	12222.2	12222.2	0.1	30	6	0.11

For what concerns the CO_2 equivalent emissions, it is interesting to understand the advantage of the system in terms of reducing CO_2 emissions. The CO_2 equivalent emissions are calculated multiplying the overall power consumption of the system throughout the year by the CO_2 emission factor. The emission factors related to the different energy sources that could be used for this specific case are reported in Table 5.5. In this work, the energy sources considered are coal, natural gas and renewable energy source. Different energy sources are compared to show that the competitiveness of the system in terms of CO_2 equivalent emission will be largely affected by the choice of energy source used for electricity production. The resulting CO_2 equivalent emissions are reported in Table 5.6

Table 5.5: CO_2 emission factors for different means of electricity production [74]

Energy source	CO_2 emission factor (kg/GJ)
Coal	94.0
Natural Gas	63.1
Renewable energy	0.0

Table 5.6: Comparison of CO_2 equivalent emissions for a gas boiler and for a SAGSHP system [74]

Technology	Total energy consumption [GJ]	CO_2 equivalent emission [kg/year]
Gas boiler	44	2776.4
SAGSHP - Coal	11.5	1081
SAGSHP - Natural gas	11.5	725
SAGSHP - Renewable energy	11.5	0

To summarize the results and to answer the research question no. 6, 7 and 8 presented in section 1.2, the following conclusions can be drawn from the simulation results presented above for the specific case of the averaged values of ambient temperature and irradiance intensity between 1991 and 2020:

- The ETC system helps to keep the ground temperature in balance and can significantly improve the performance of the system by increasing the evaporation temperature of the main heat pump
- The control strategy on how to use the heat coming from the ETC system can be crucial to improve the performance of the system
- A system SSCOP of 3.8 has been obtained for this specific case. This is definitely a high value compared to other kinds of heating systems but is far away from the initial target of 8. A higher value of 6.2 is obtained for the SCOP of the HP system since the power consumption of the ETC system circulation pump does not affect the SCOP of the HP system.
- A LCOE of 0.21 €/kWh has been obtained for the SAGSHP system compared to a LCOE of 0.11 €/kWh for the gas boiler system. This tells us that the investigated system is not competitive with a traditional gas boiler in terms of costs. The high LCOE value is due to the high initial investment of the SAGSHP system.
- The CO_2 equivalent emission calculation showed that the amount of CO_2 emissions produced in a year by a gas boiler is about 2.6 times the amount of emissions produced by a SAGSHP powered by coal and 3.8 times the emission of a SAGSHP powered by natural gas. If the energy to power the SAGSHP is produced using renewable energy sources, then no CO_2 emissions would be produced and compared to a gas boiler system, this would avoid the emission of about 2.8 ton CO_2 /year.

5.2. Results for year 2010

In this subsection, the same path as the one presented in section 5.1 is followed. Here, we will only briefly present the results and compare these to the results presented in section 5.1. Most of the explanation of the graphs in section 5.1 applies also to the graphs the one presented in this section.

HP and house results In Figure 5.14 the heat loads of the house model are reported.

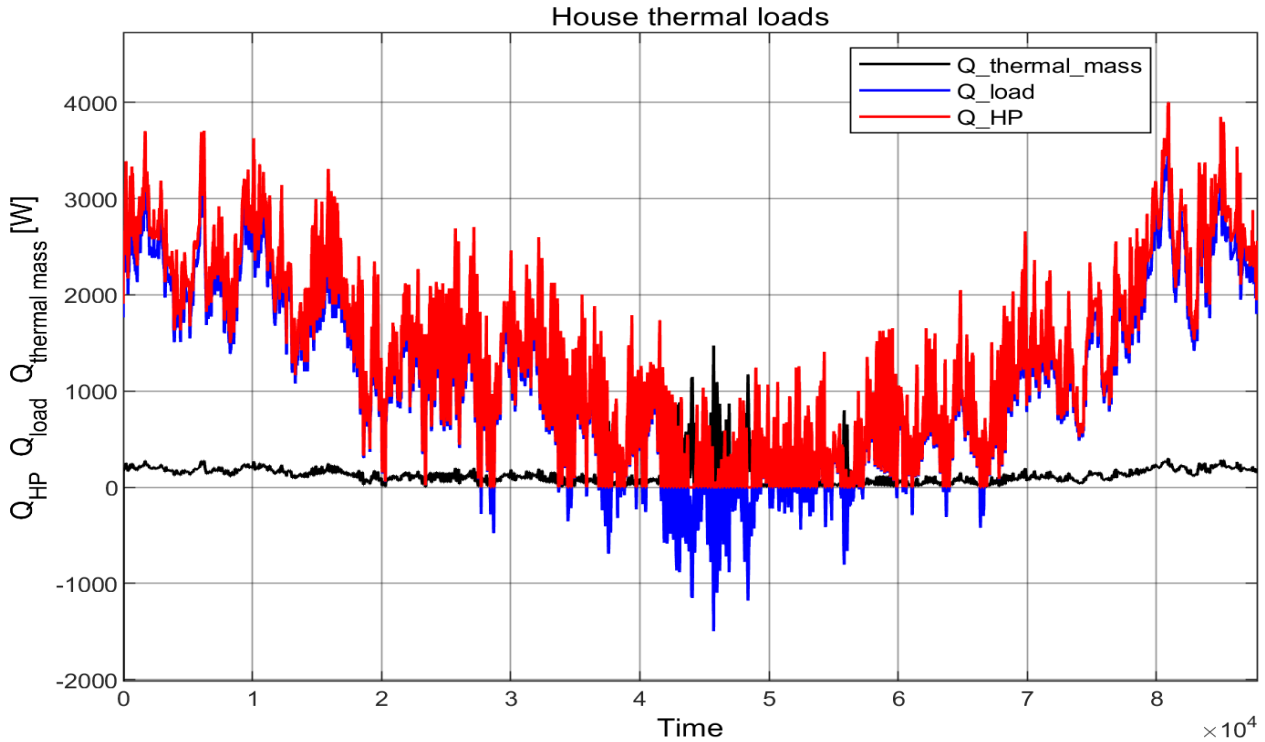


Figure 5.14: Heat loads of the house environment

In Figure 5.14, the heat delivered by the heat pump as well as the heat exchanged with the environment follow a similar trend to what shown in Figure 5.1. Comparing Figure 5.14 with Figure 5.1, we can see how in the case of 2010, shown in Figure 5.14, in the winter period the peak load is much higher (up to 4000W) compared to Figure 5.1 where the peak load is about 2000W. The same happens in the summer period, where in Figure 5.14 the heat exchanged with the environment reaches values up to -1500W while in Figure 5.1 the heat exchanged with the environment in the summer does stay above -500W . This is clearly a consequence of the more extreme conditions of the ambient temperature registered in the year 2010 compared to the averaged value between 1991 and 2020. In 2010 the ambient temperature values, shown in Figure 4.4, go from -10°C in the winter to almost 35°C in the summer while the averaged values between 1991 and 2020 shown in Figure 4.2 reach a minimum value of 2°C in the winter and a maximum value of 23°C in the summer.

In Figure 5.15 the room temperature variation throughout the year is reported. The peaks present in Figure 5.15 occur during the summer, when the outside temperature is much higher than the room temperature of the house. When this happens, the room temperature increases because for our specific case, no cooling mode has been considered for the heat pump system. From Figure 5.14 we can see how in the summer period, when the heat exchanged with the environment (Q_{load}) becomes negative the heat pump heat load is zero. This means that the environment is heating up the room temperature but there is no cooling performed by the HP system. Therefore, since no cooling load is removed from the heat pump system, the house room temperature increased. This was a simplification in the model and it is considered to be reasonable since the room temperature stays within reasonable values. If it would have increase too much, then including the cooling mode in the model would have been needed.

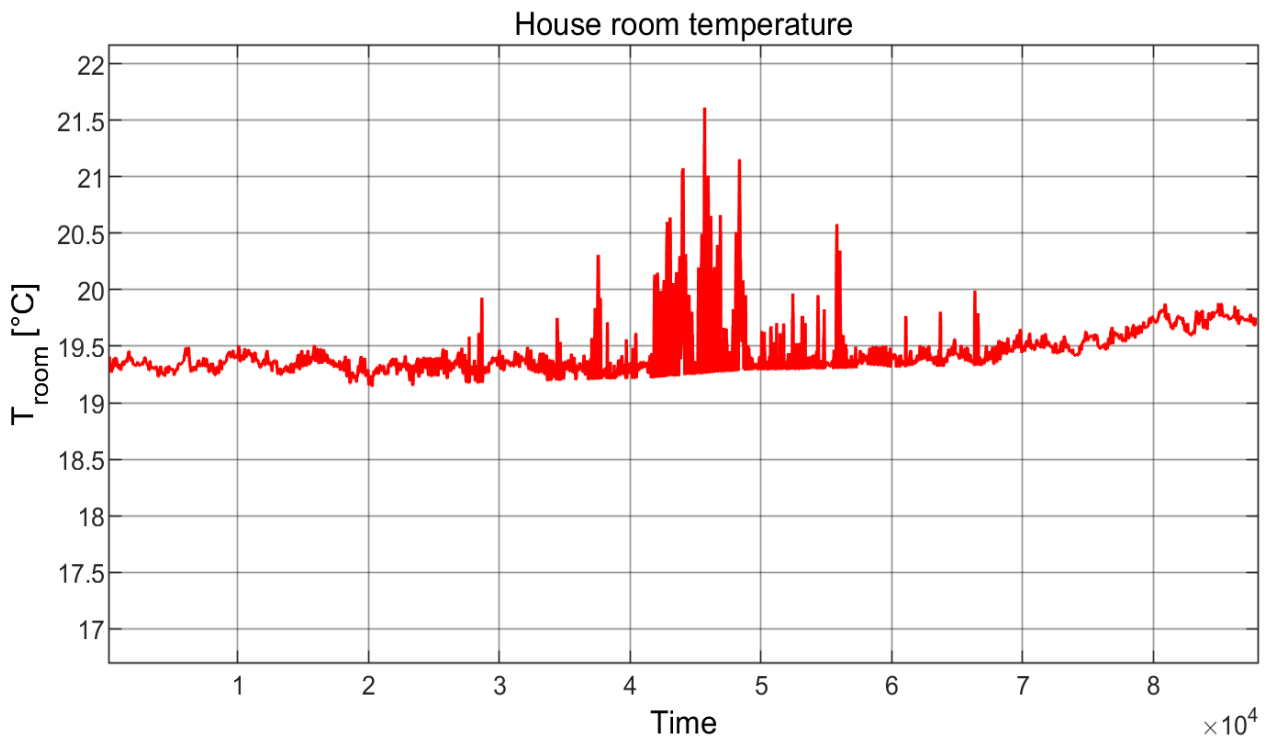


Figure 5.15: Room temperature of the house throughout the year

In Figure 5.16 we can see both the heat delivered by the booster heat pump to the DHW tank and the heat lost by the DHW tank to the outside ambient air.

In Figure 5.17 is reported the tank water temperature variation throughout the year. Here, the same reasoning and discussion applies as the one used for Figures 5.3 and 5.4 since nothing has changed between the two models for what concerns the DHW consumption profile.

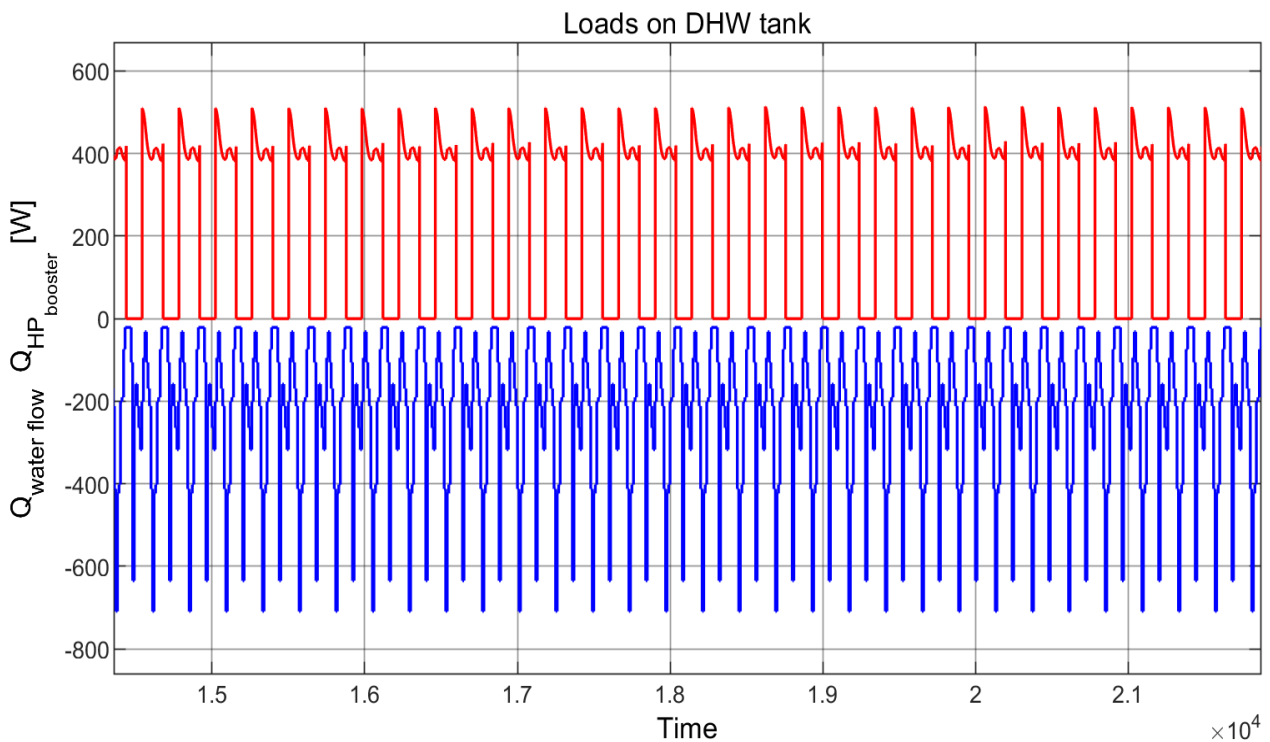


Figure 5.16: DHW tank - Heat loads over a period of one month (March)

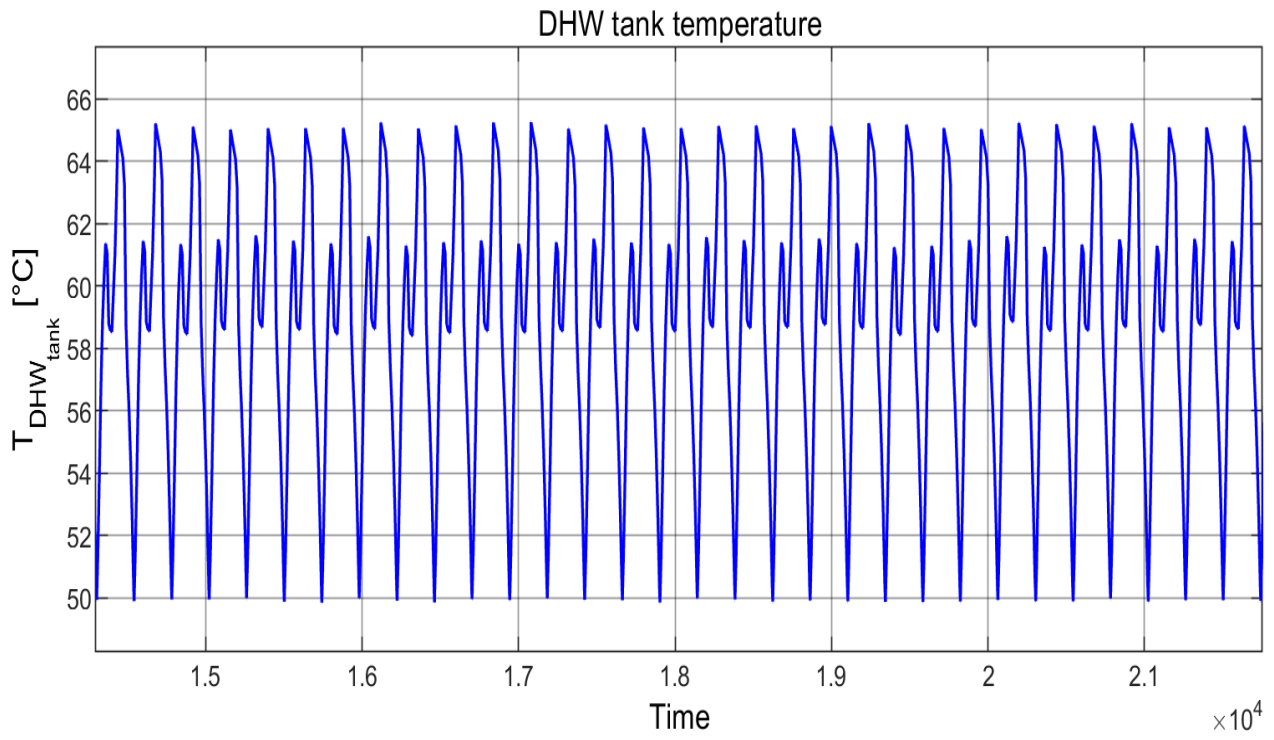


Figure 5.17: DHW tank - Water temperature over a period of one month (March)

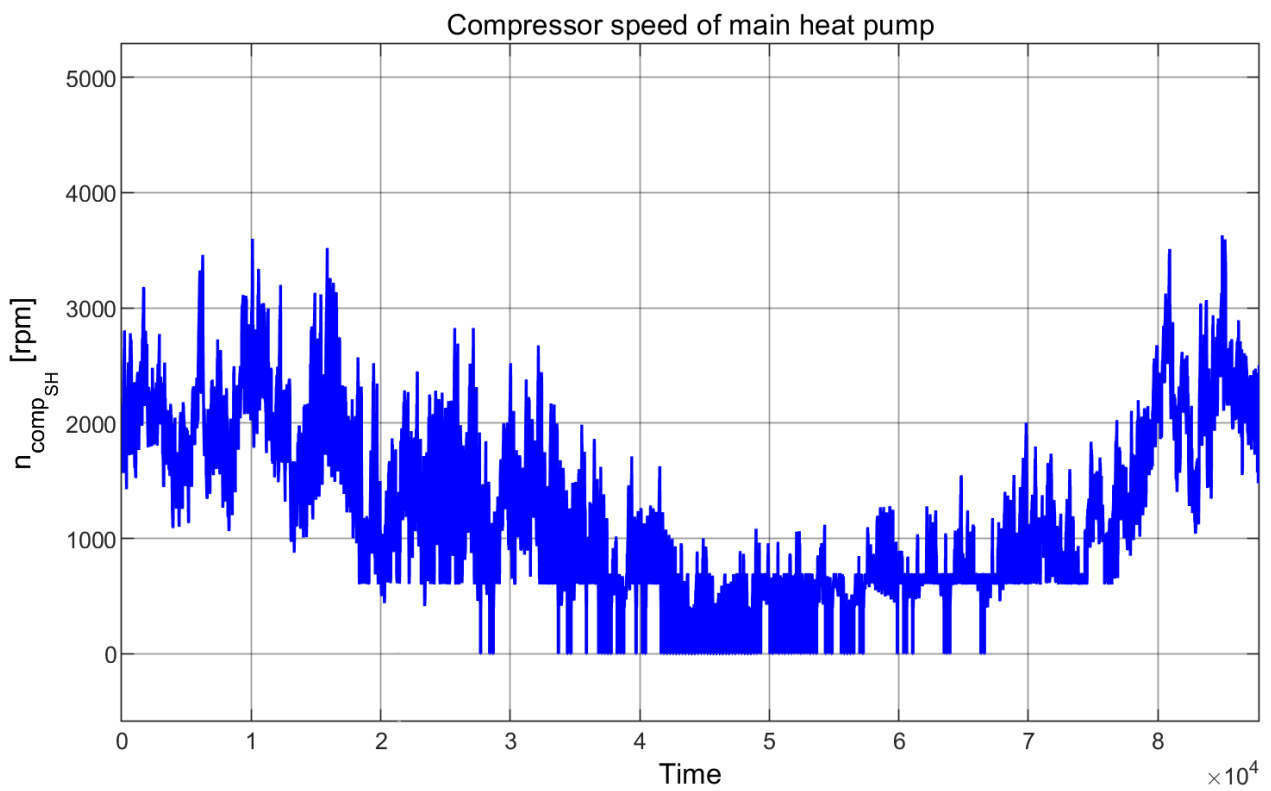
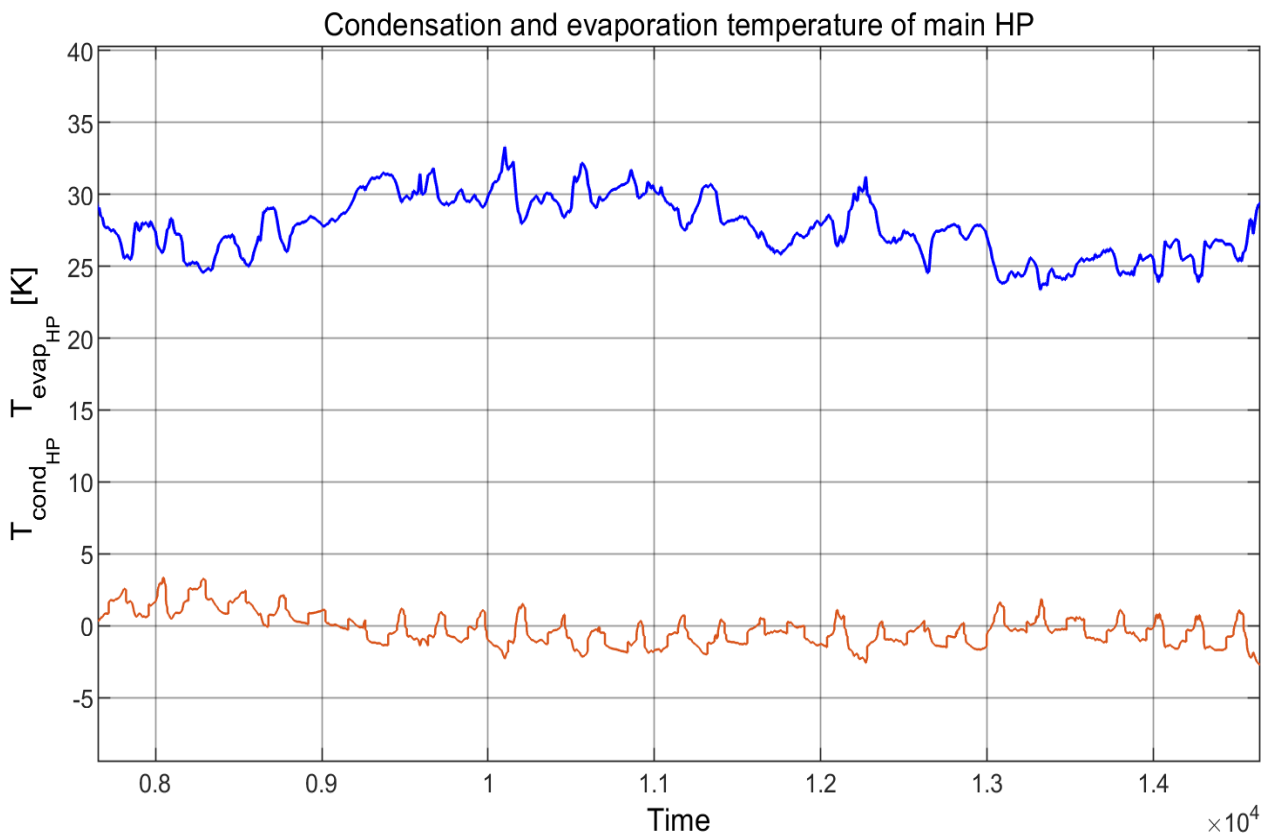
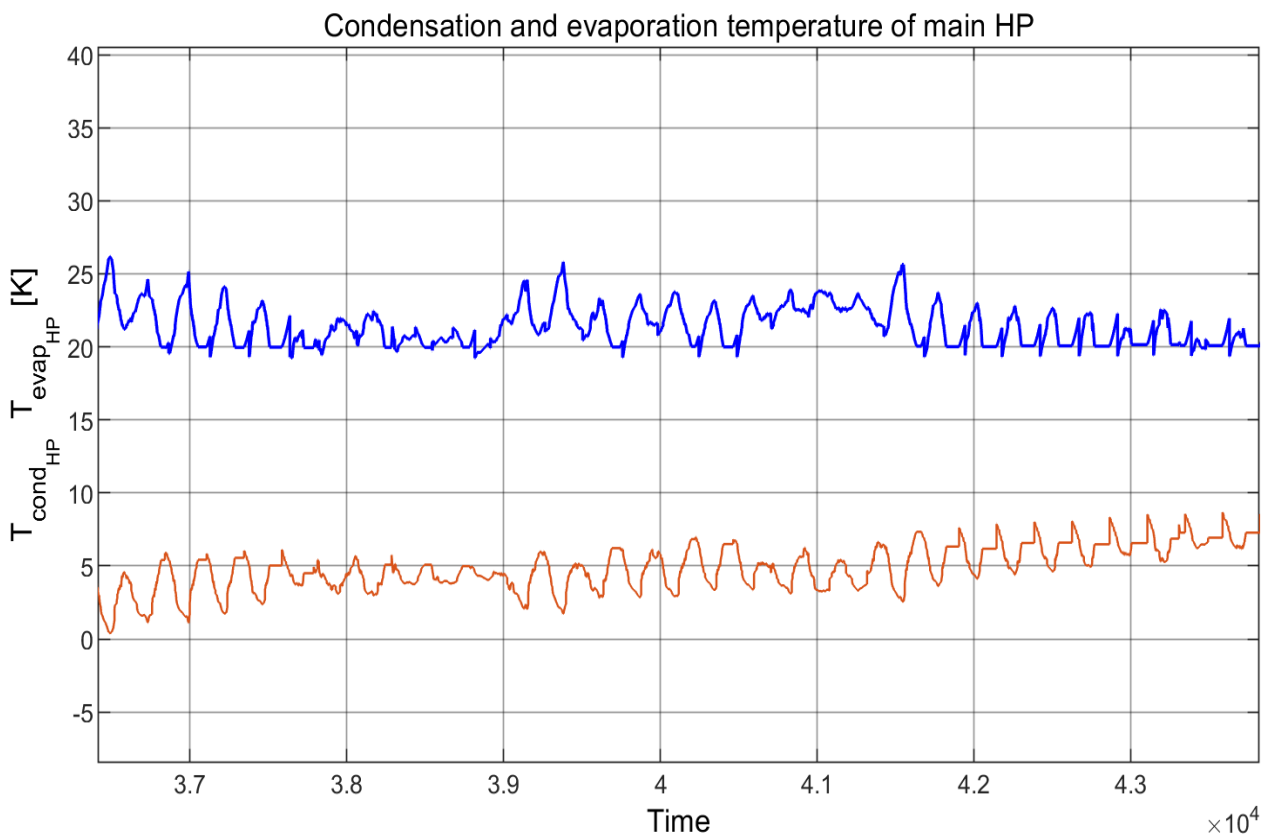


Figure 5.18: Main HP - Compressor rotational speed



(a) Main HP - Condensation (blue) and evaporation (red) temperature in February



(b) Main HP - Condensation (blue) and evaporation (red) temperature in July

Figure 5.19: Main HP - Condensation and evaporation temperature in the months of February and July

In Figure 5.18, we can see how the rotational speed of the compressor throughout the year. Comparing Figure 5.18 with Figure 5.5 we can notice how the rotational speed in the result of 2010 reported in Figure 5.18 reaches much higher values compared to Figure 5.5. This is due to the fact that the rotational speed of the compressor is proportional to the heat delivered to the house. Therefore, since in the year 2010 the heat delivered to the house by the main HP reaches much higher values due to much lower ambient temperature values, the same happens to the rotational speed of the compressor. Another interesting comparison that can be made between the rotational speed of the two different cases, is that in the summer period the time during which the compressor switches off is much longer in the year 2010 compared to the averaged years results. This again can be explained by the lower need of space heating for the house in the summer in the year 2010 since the ambient temperature values of year 2010 are much higher compared to the averaged values over the period 1991-2020.

In Figures 5.19 are reported the condensation and evaporation temperatures of the main heat pump. As before, two significant months are reported to give an idea of the condensation and evaporation temperatures of the heat pump in a cold and in a hot month. We can see in Figure 5.19a that the evaporation temperature of the HP refrigerant drops below zero. However, since a mixture of water and ethylene glycol is used as the working fluid of the BHE system, there is no risk of freezing of the BHE working fluid.

A comparison between Figure 5.19 and Figure 5.6 shows how the condensation temperature is higher in the winter periods of year 2010 compared to the average of the past years because of a higher heat requirement for SH. On the other side, the evaporation temperature is lower in the winter period of 2010 compared to the winter period of the average of the past years since the source inlet temperature of year 2010 shown in Figure 5.20 is lower than the source inlet temperature of the average of the past years shown in Figure 5.7.

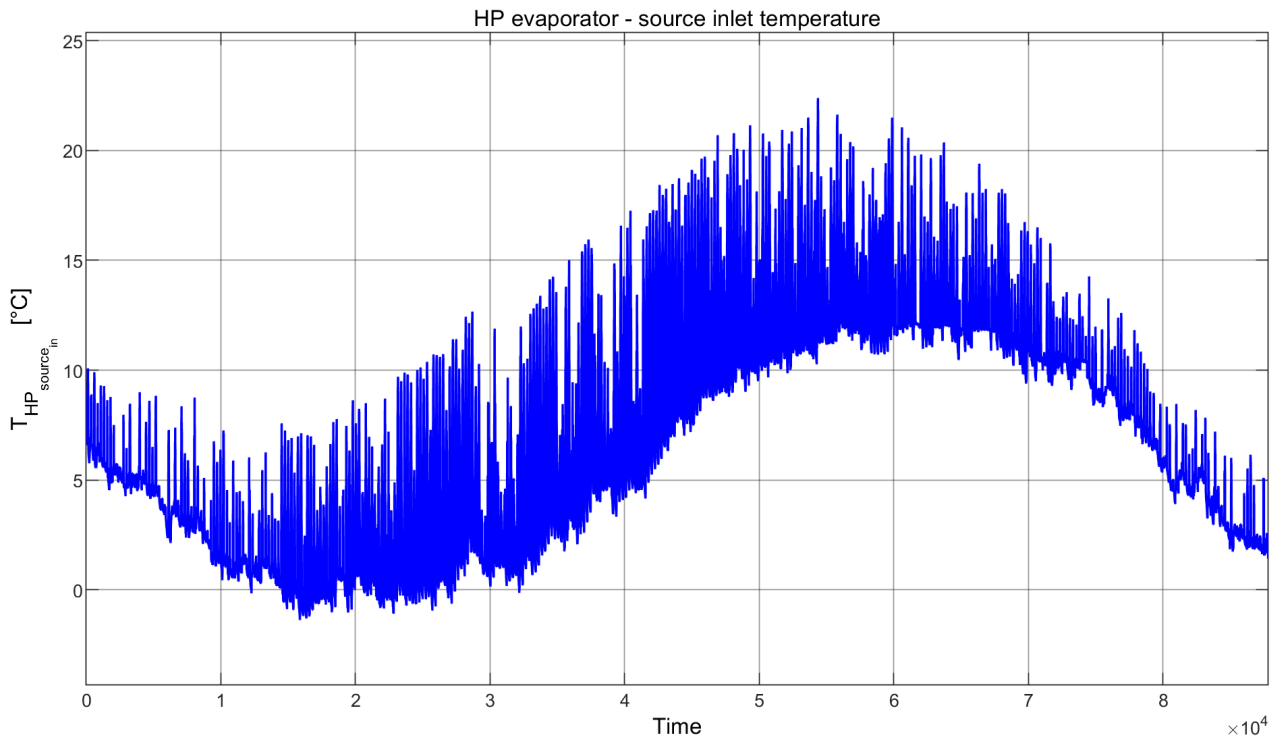


Figure 5.20: Main HP - Heat source temperature at the inlet of the evaporator

Regarding the SCOP of the HP system, the obtained final value for the year 2010 is reported in Table 5.7

Table 5.7: HP system - Seasonal coefficient of performance

$SCOP_{HP}$	5.8
-------------	------------

The obtained value for the year 2010 is lower compared to the value of 6.2 obtained for the average of the past years. This difference can be explained by looking at the difference in condensation and evaporation between the two cases as well as at the SH heat requirement of the house. A lower value of SCOP of the HP system of the simulation for the year 2010 is obtained since the temperature difference between evaporation and condensation temperature of the main heat pump is generally always larger for the year 2010 (Figure 5.19) compared to the temperature difference

between evaporation and condensation temperature for the average of the past years (Figure 5.6). This difference results in a slightly lower SCOP for the year 2010.

BHE results In Figure 5.21 is reported the heat injected and extracted from the borehole during the year.

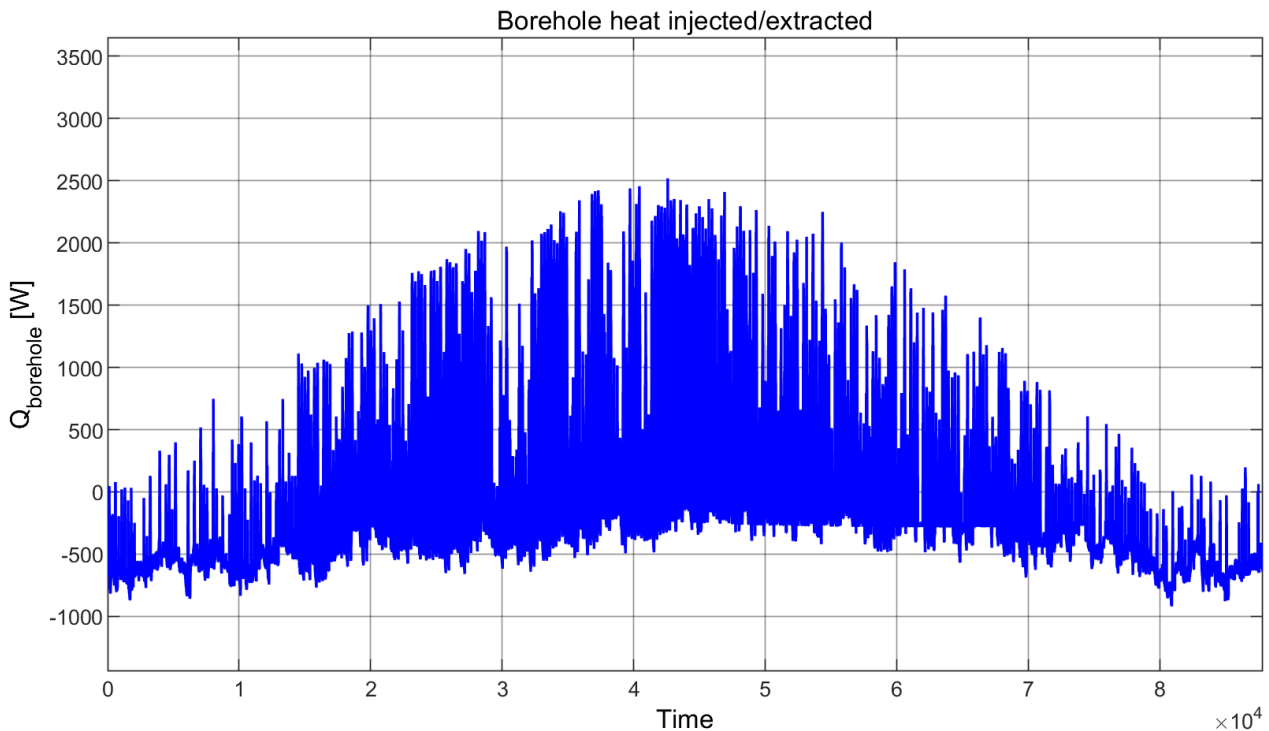


Figure 5.21: BHE system - Heat extraction/injection

Comparing Figure 5.21 with Figure 5.8 we can see that in Figure 5.21 the heat extraction from the borehole is higher (more negative) since the heat requirement for SH is higher for year 2010. At the same time, we can also notice that in Figure 5.21 during the summer months the heat injected in the ground is much higher compared to Figure 5.8. This can be explained by looking at the irradiance input values for the two cases. Looking at Figures 4.5 and 4.3 we can see how the irradiance intensity averaged between 1991 and 2020 (Figure 4.3) has a peak irradiance intensity of about 600 W/m^2 while the irradiance intensity of the year 2010 (Figure 4.5) reaches a peak intensity of more than 800 W/m^2 . And more in general, the irradiance intensity is higher in year 2010 compared to the averaged values between 1991 and 2020. This is the reason of the higher heat injection in the ground in Figure 5.21 compared to Figure 5.8.

In Figure 5.22 is reported the borehole temperature variation during the year. This graph can be easily related to Figure 5.21.

Comparing Figure 5.22 with Figure 5.9 we can see how the final borehole temperature is lower than the initial temperature in both cases, but in Figure 5.22 the temperature difference between initial and final BHE temperature is larger compared to Figure 5.9. The lower final borehole temperature value registered for the year 2010 is caused by larger heat requirements of the house due to lower temperature values in the winter. And even though the larger heat injected in the ground in 2010 counterbalances this difference a bit, still the larger heat requirements of the house results in a more unbalanced borehole temperature after one year.

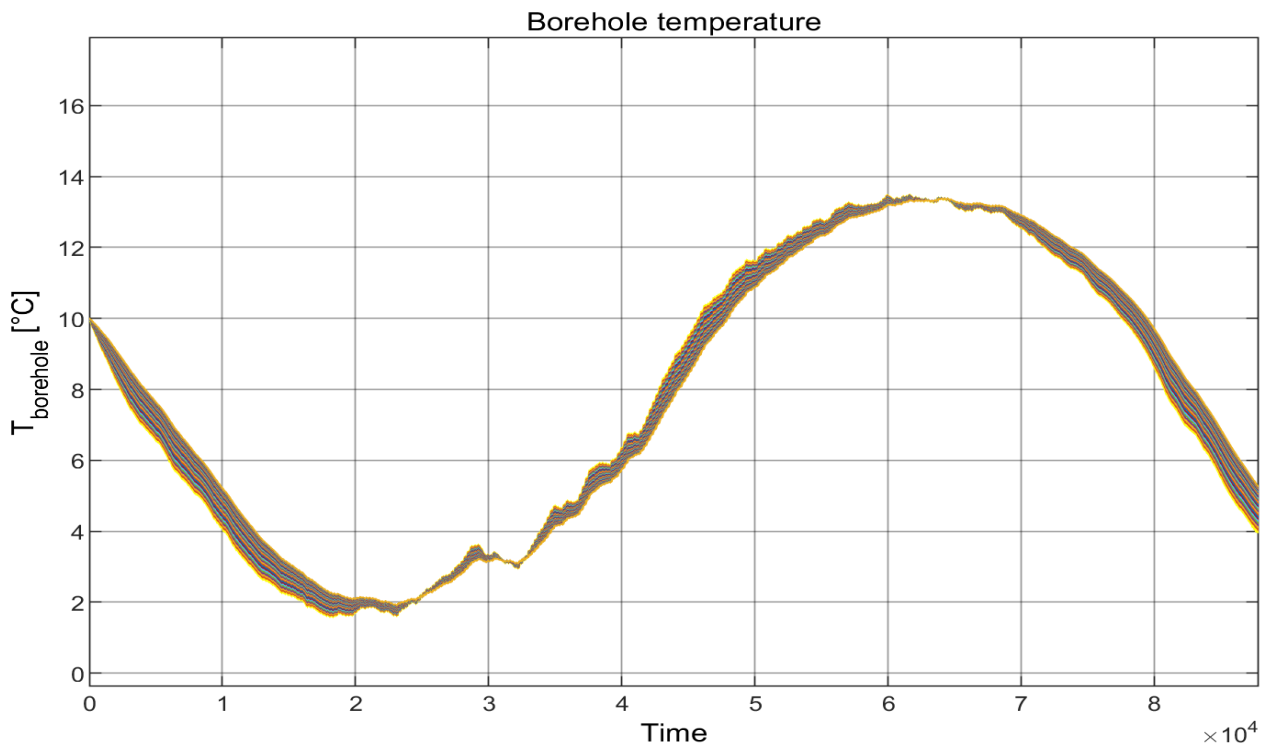


Figure 5.22: BHE system - Temperature at the edge of the borehole

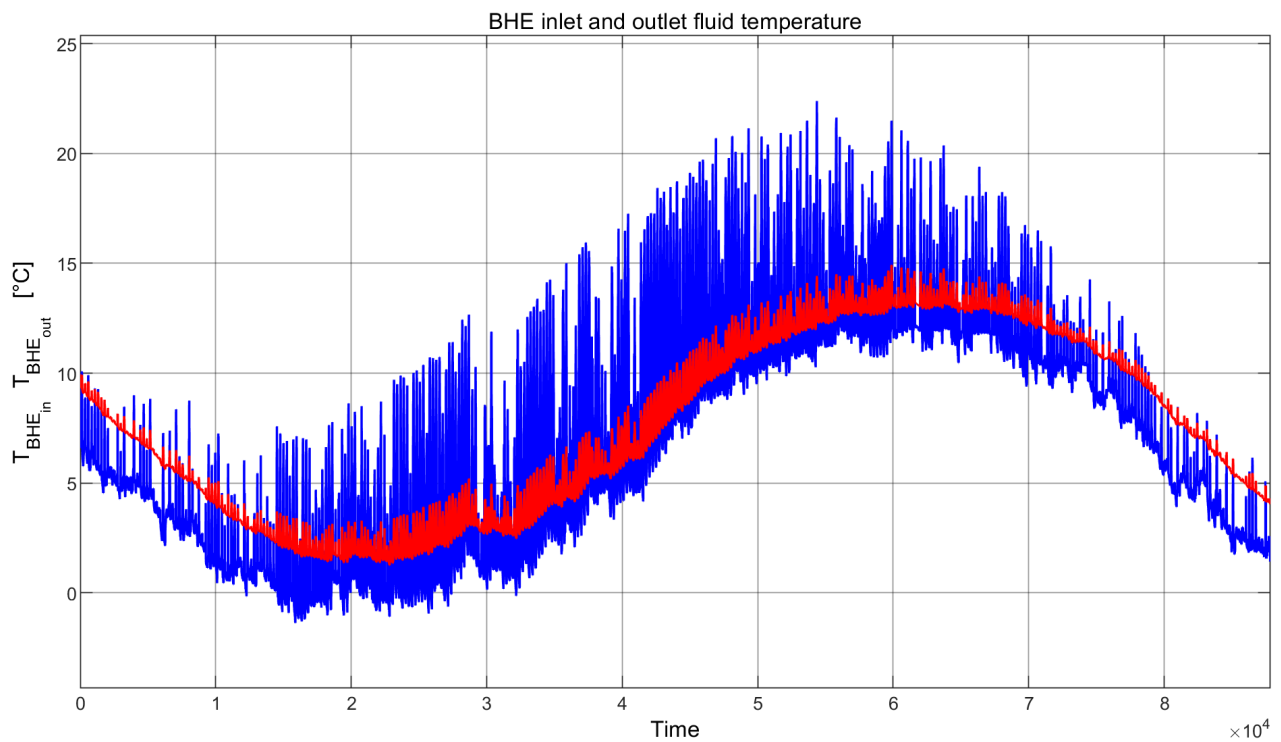


Figure 5.23: BHE system - Inlet (blue) and outlet (red) temperature of the working fluid

In Figure 5.23 are reported the inlet and outlet temperature of the working fluid in the BHE system. In this graph, the blue plot shows the temperature of the working fluid entering the BHE and the red line shows the temperature of the working fluid coming out of the BHE. Also here we can clearly see the effects of the ETC system on the inlet and outlet temperatures of the BHE system.

ETC results In Figure 5.24 is shown the heat obtained from the ETC system as a function of time.

Compared to Figure 5.11, Figure 5.24 shows a higher heat absorbed by the ETC system as a consequence of the higher irradiance intensity registered in the year 2010 compared to the average irradiance intensity between 1991 and 2020. The heat absorbed by the ETC system is clearly related to the temperature variation at the outlet of the ETC system, shown in Figure 5.25. In Figure 5.26 is reported the ETC inlet temperature.

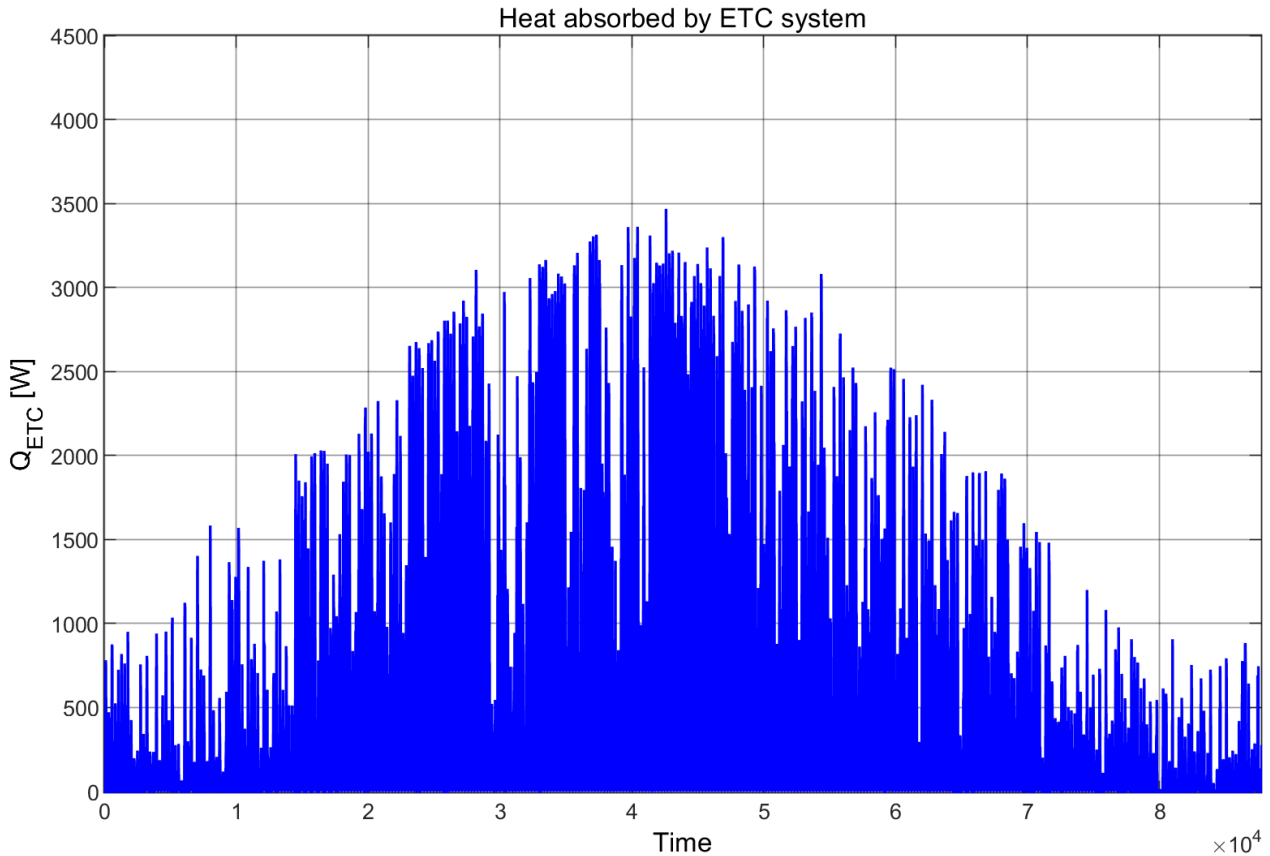


Figure 5.24: ETC system - Heat absorbed

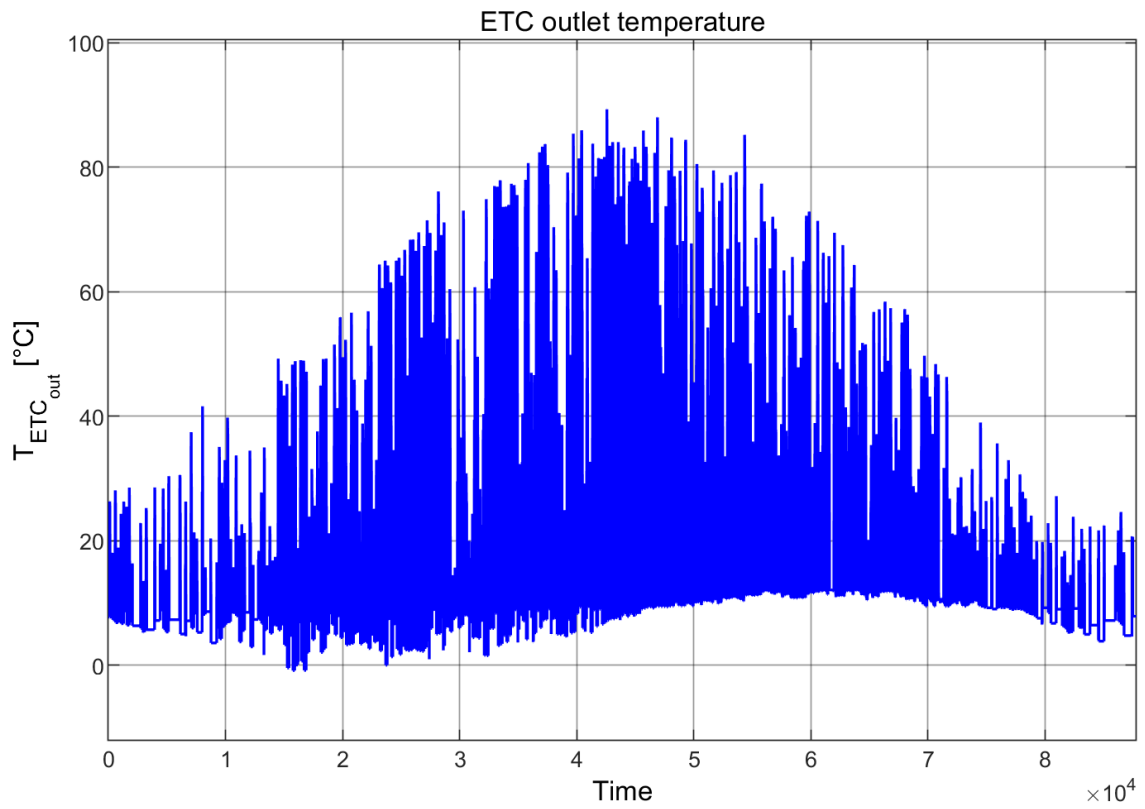


Figure 5.25: ETC system - Outlet temperature

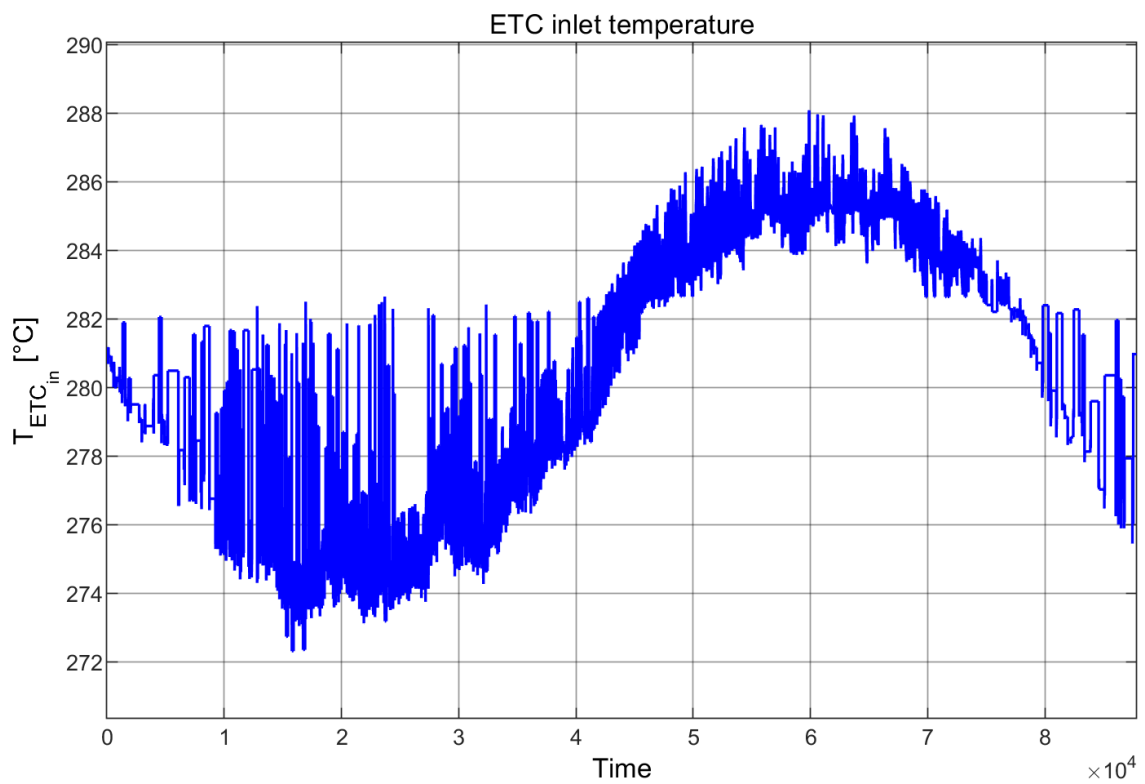


Figure 5.26: ETC system - Inlet temperature

System results Considering the overall system, the main results to be looked at are:

- Seasonal System COP (SSCOP)
- Levelized cost of energy (LCOE)
- CO_2 equivalent emissions

The SSCOP of the system obtained for the model is reported in Table 5.8.

Table 5.8: Final SSCOP results

Cumulative heat delivered to the house [GJ]	Cumulative energy consumption [GJ]	SSCOP [-]
50.5	13	3.9

In general, comparing this result with the SSCOP obtained for the average between 1991 and 2020 we can state that the SSCOP doesn't change much between these two different cases. This could be happening since the positive and negative effects of each case counterbalance each other. For instance, in the year 2010 the cumulative heat delivered to the house is higher than in the previous case but also the cumulative power consumption is higher. Therefore, the increase in cumulative heat delivered to the house is balanced out by the increase in cumulative power consumption of the system.

In Table 5.9 are reported the costs and the values used to calculate the LCOE of both the SAGSHP system and a traditional boiler system. The same assumptions mentioned in the previous section apply also for the year 2010 and the initial investment values for each component are the same in both cases (see Table 5.3).

Table 5.9: LCOE values

Technology	CAPEX [€]	Total energy consumption [kWh]	Total heat provided [kWh]	Cost of energy [€/kWh]	Number of years (N) [-]	Interest rate (i) [%]	LCOE [€/kWh]
SAGSHP	30000	3611.1	14027.8	0.147	30	6	0.19
Gas Boiler	2000	14166.7	14027.8	0.1	30	6	0.11

The emission factors related to the different energy sources that could be used for this specific case are reported in Table 5.5.

The resulting CO_2 equivalent emissions are reported in Table 5.10.

Table 5.10: Comparison of CO_2 equivalent emissions for a gas boiler and for a SAGSHP system [74]

Technology	Total energy consumption [GJ]	CO_2 equivalent emission [kg/year]
Gas boiler	50	3155
SAGSHP - Coal	13	1222
SAGSHP - Natural gas	13	820.3
SAGSHP - Renewable energy	13	0

To summarize the results and to answer the research questions no. 6, 7 and 8 presented in section 1.2 for the specific case of year 2010, the following conclusions can be drawn from the simulation results presented above for the specific case of the year 2010:

- A system SSCOP of 3.9 has been obtained. A higher value of 5.8 is obtained for the SCOP of the HP system since the power consumption of the ETC system circulation pump does not affect the SCOP of the HP system.
- A LCOE of 0.19 €/kWh has been obtained for the SAGSHP system compared to a LCOE of 0.11 €/kWh for the gas boiler system.
- The CO_2 equivalent emission calculation showed that the amount of CO_2 emissions produced in a year by a gas boiler is about 2.58 times the amount of emissions produced by a SAGSHP powered by coal and 3.85 times the emission of a SAGSHP powered by natural gas. If the energy to power the SAGSHP is produced using renewable energy sources, then no CO_2 emissions would be produced and compared to a gas boiler system, this would avoid the emission of 3.16 ton CO_2 /year.

Therefore, from the results presented above in sections 5.1 and 5.2 we can state that the analysed SAGSHP system proves to be competitive in terms of performance (SCOP) and in reducing the amount of CO_2 emissions generated. However, for 30 years of utilisation, the system shows a LCOE value which is rather high and thus making it not economically competitive to a gas boiler system.

Additionally, it can be concluded that this system is economically more competitive when used in colder climates. This is the case since the colder the climate, the higher the total heat provided and the higher the OPEX of the boiler system which in turns increases the LCOE of the boiler system reducing therefore the gap between the two different LCOE.

Eventually, in terms of CO_2 emission reduction, there is not a big difference between the two cases. In general we can say that if the SAGSHP system runs completely on renewable energy sources, then the reduction in CO_2 emissions would be larger for systems in colder climates since the amount of CO_2 emissions of a gas boiler would be larger due to a larger heat load in colder climates.

6

Conclusions and future recommendations

In this thesis work, the performance of a SAGSHP system for domestic heating applications in a typical Dutch terraced house has been investigated. After understanding what is the state of the art of SAGSHP systems and what are the different components that are used in these systems, a choice has been made on the different main components of the system for the specific case of Dutch climatic conditions. In particular the following system has been selected for the specific case fo Dutch terraced houses:

- Vapour compression heat pump using HFO or inorganic refrigerants
- Vertical borehole heat exchanger with a single U-tube pipe configuration using water glycol-ethylene mixture as working fluid
- Heat pipe evacuated tube solar collectors

Each of this components has been modelled separately. In particular the BHE has been modelled in Matlab using a numerical unsteady heat transfer model to predict short-term responses from the system and the HP has been modelled in Matlab using an iterative approach. All the other components have been modelled directly in a Simulink environment, including the house model and the DHW storage tank model. Eventually, the different sub-models have been combined together in Simulink to model the whole system. A simulation period of one year has been used for the model. The input values of ambient temperature and irradiance level have been taken from two different data sets: the first set of inputs is the hourly average values of ambient temperature and irradiance intensity averaged over a period of 20 years (1991-2020); the second set of inputs are hourly average values from the year 2010 which has been an extremely cold year. Here, the results obtained from the input values averaged over a period of twenty years are the ones that will be used to assess the performance of the system. The results obtained from the inputs of year 2010 are used to establish if the system can perform in extreme conditions. Eventually, having two different simulation results gives us a basis for comparing two different situations and state in which situation the system performs better in terms of SCOP as well as from an economic point of view

The results of the simulation show that the following holds for this specific system:

- The ETC system has significant impact on the performance of the system and the control strategy used to direct the heat from the ETC system can be crucial in improving the system performance
- The seasonal coefficient of performance is lower than the goal of 8 stated in the research questions. A final value of 6.2 is obtained during a period of one year for the SCOP of the HP system while a SSCOP of 3.8 is obtained for the whole system.
- The competitiveness of this system in terms of cost is still low compared to a traditional gas boiler system due to the high initial investment cost associated with the SAGSHP system. Over a period of 30 years, the LCOE of the SAGSHP system is 0.21 €/kWh compared to the 0.11 €/kWh.
- The reduction of CO_2 emissions that would occur if a SAGSHP system is used instead of a traditional gas boiler highly depends on the energy source from which the electricity to run the SAGSHP system is produced. While when using coal the CO_2 emissions are reduced by 61% and with natural gas are reduced by 74%, when using renewable energy sources to power the SAGSHP system the CO_2 emissions will be reduced by 100% avoiding the emission of 2.8 kton CO_2 /year.

- Comparing the results obtained for the extremely cold conditions of 2010 with the base simulation, we can notice that:
 1. While the SCOP of the HP system is reduced to 5.8 due to the lower evaporation temperature of the main HP, the SSCOP is basically unchanged since the increased cumulative heat delivered to the house is counterbalanced by an increased cumulative power consumption. The SSCOP of the system for the year 2010 slightly increases (3.9) since the increase in total heat delivered to the house (+14.77%) is slightly higher than the increase in cumulative energy consumption (+13.04%).
 2. The LCOE of the system is reduced, getting closer to the LCOE of a traditional gas boiler system. This happens since the total heat delivered to the house increases for the cold year 2010. At the same time, also the OPEX of the system increases. However, the increase in total heat delivered to the house has a higher influence on the LCOE resulting in a reduced LCOE. Therefore, the colder the ambient temperature values throughout the year the more competitive the system will be in terms of cost.
 3. The relative CO_2 emission reduction are similar for the two different cases. The absolute CO_2 emission reduction is higher for the case of year 2010. This is the case since the overall heat consumption is higher, therefore leading to higher CO_2 emissions for the gas boiler system which in turns increases the absolute CO_2 emission reduction of the SAGSHP systems.

From this conclusions, we can state that the modelled SAGSHP system has a high performance and can have a significant impact in reducing CO_2 emissions, especially if renewable energy sources are used to power the SAGSHP system. On the other hand, the costs of the system are high compared to a traditional gas boiler system. This introduces economical barriers to the development of the chosen system. Compared to a gas boiler system, this technology should still be preferred even if more expensive because our priority should be to get to net-zero CO_2 emissions as soon as possible. Governments should incentivize people to install such a system in their homes by providing financial incentives or other means to overcome the economical barrier of SAGSHP systems.

However, this investigation is just a limited research which can still be expanded and improved in many different directions to move towards a more efficient and less expensive system. This was a small initial step in the investigation of the potential of SAGSHP technology. There is still lots to be done. The next steps that could be taken in future works and research about this topic could focus on the following points to study different options and compare performance and costs:

- Understand the effects of different control strategies on the performance of the system by using different operating modes. Some possible strategies that could be interesting to investigate are
 - Utilize ETC heat for DHW tank by giving priority to the ETC system with respect to the booster HP. This could increase the SSCOP by reducing the work of the booster HP but at the same time this could be having negative effects on the main HP since the booster HP would switch on and off more often
 - Utilizing the ETC system only during the summer. This should allow the use of pure water as working fluid for both the ETC and BHE systems since there is no risk of freezing which in turn should increase the performance of the system.
- Do a sensitivity analysis of different system's parameters to see how each parameters affects the cost and the performance of the system.
 - Try different layouts and different working fluids for the HP system
 - See the effects that changing number of boreholes, length and working fluid has on the system performance and cost
 - See how the number of ETC as well as the configuration and other parameters of the ETC system affect the overall system performance and cost
- Investigate other possible system layout and compare performance and cost.
 - Consider the use of the return flow from the BHE to further subcool the refrigerant before the flow enters the evaporator
 - Use a single heat pump to heat up water in a the water storage tank that is used for both SH and DHW
- Improve model's accuracy to have more accurate results by
 - Reducing the simulation time step even further

- Use different water consumption profiles for different months of the year
- Include also the HP cooling mode in the model
- Define more accurate house heat requirements considering a specific case study
- Include floor heating thermal mass
- Include maintenance cost when calculating LCOE

Bibliography

- [1] The Paris Agreement | UNFCCC. <https://unfccc.int/process-and-meetings/the-paris-agreement/the-paris-agreement>, 2016.
- [2] Paris agreement - status of ratification | UNFCCC. <https://unfccc.int/process/the-paris-agreement/status-of-ratification>, 2020.
- [3] European Green Deal Communication. https://ec.europa.eu/info/sites/info/files/european-green-deal-communication_en.pdf, 2019.
- [4] S.L. Wong, Kevin K.W. Wan, Danny H.W. Li, and Joseph C. Lam. Impact of climate change on residential building envelope cooling loads in subtropical climates. *Energy and Buildings*, 42(11):2098 – 2103, 2010. ISSN 0378-7788.
- [5] Heating and cooling | Energy. https://ec.europa.eu/energy/topics/energy-efficiency/heating-and-cooling_en?redir=1, 2020.
- [6] Yong Geng, Wei Chen, Zhe Liu, Anthony S.F. Chiu, Wenyi Han, Zhiqing Liu, Shaozhuo Zhong, Yiyang Qian, Wei You, and Xiaowei Cui. A bibliometric review: Energy consumption and greenhouse gas emissions in the residential sector. *Journal of Cleaner Production*, 159:301 – 316, 2017. ISSN 0959-6526.
- [7] Energy Report Transition to Sustainable Energy | The Netherlands. <https://www.government.nl/documents/reports/2016/04/28/energy-report-transition-to-sustainable-energy>, 2016.
- [8] National climate agreement - The Netherlands. <https://www.klimaatkoord.nl/documenten/publicaties/2019/06/28/national-climate-agreement-the-netherlands>, 2019.
- [9] Cor Leguijt, Nanda Naber, Frans Rooijers, and Benno Schepers. Towards a climate-neutral built environment 2050 - CE Delft. https://www.ce.nl/publicatie/op_weg_naar_een_klimaatneutrale_gebouwde_omgeving_2050/1638, 2015.
- [10] K.J. Chua, S.K. Chou, and W.M. Yang. Advances in heat pump systems: A review. *Applied Energy*, 87(12):3611 – 3624, 2010. ISSN 0306-2619.
- [11] Ioan Sarbu and Calin Sebarchievici. Chapter 1 - introduction. In Ioan Sarbu and Calin Sebarchievici, editors, *Ground-Source Heat Pumps*, pages 1 – 5. Academic Press, 2016. ISBN 978-0-12-804220-5.
- [12] D.A. Chwieduk. 3.15 - solar-assisted heat pumps. In Ali Sayigh, editor, *Comprehensive Renewable Energy*, pages 495 – 528. Elsevier, Oxford, 2012. ISBN 978-0-08-087873-7.
- [13] Walter Grassi. *Heat Pumps: Fundamentals and Applications*. Springer, 2017. ISBN 3319621998, 9783319621999.
- [14] Anurag Goyal, Marcel A. Staedter, and Srinivas Garimella. A review of control methodologies for vapor compression and absorption heat pumps. *International Journal of Refrigeration*, 97:1 – 20, 2019. ISSN 0140-7007.
- [15] Y. H. Venus Lun and S. L. Dennis Tung. *Heat Pumps for Sustainable Heating and Cooling*. 2019. ISBN 3030313875, 9783030313876.
- [16] F. Reda. *Solar Assisted Ground Source Heat Pump Solutions: Effective Energy Flows Climate Management*. SpringerBriefs in Applied Sciences and Technology, 2016. ISBN 3319496980, 9783319496986.
- [17] Cordin Arpagaus, Frédéric Bless, Jürg Schiffmann, and Stefan S. Bertsch. Multi-temperature heat pumps: A literature review. *International Journal of Refrigeration*, 69:437 – 465, 2016. ISSN 0140-7007.
- [18] Edward Xu. *Green Energy Island Integration and Operation Optimization Research*. PhD thesis, 06 2018.
- [19] Mengjie Song, Shiming Deng, Dongmei Pan, and Ning Mao. An experimental study on the effects of downwards flowing of melted frost over a vertical multi-circuit outdoor coil in an air source heat pump on defrosting performance during reverse cycle defrosting. *Applied Thermal Engineering*, 67(1):258 – 265, 2014. ISSN 1359-4311.

- [20] Rao Martand Singh, Abubakar Kawuwa Sani, and Tony Amis. 15 - an overview of ground-source heat pump technology. In Trevor M. Letcher, editor, *Managing Global Warming*, pages 455 – 485. Academic Press, 2019. ISBN 978-0-12-814104-5.
- [21] Mohamad Kharseh, Lobna Altorkmany, Mohammed Al-Khawaja, and Ferri Hassani. Analysis of the effect of global climate change on ground source heat pump systems in different climate categories. *Renewable Energy*, 78:219 – 225, 2015. ISSN 0960-1481.
- [22] Giti Nouri, Younes Noorollahi, and Hossein Yousefi. Solar assisted ground source heat pump systems – a review. *Applied Thermal Engineering*, 163:114351, 2019. ISSN 1359-4311.
- [23] S. Rinne and S. Syri. Heat pumps versus combined heat and power production as CO₂ reduction measures in finland. *Energy*, 57:308 – 318, 2013. ISSN 0360-5442.
- [24] Messaoud Badache, Parham Eslami-Nejad, Mohamed Ouzzane, Zine Aidoun, and Louis Lamarche. A new modeling approach for improved ground temperature profile determination. *Renewable Energy*, 85:436 – 444, 2016. ISSN 0960-1481.
- [25] Yanping Yuan, Xiaoling Cao, Liangliang Sun, Bo Lei, and Nanyang Yu. Ground source heat pump system: A review of simulation in china. *Renewable and Sustainable Energy Reviews*, 16(9):6814 – 6822, 2012. ISSN 1364-0321.
- [26] Ioan Sarbu and Calin Sebarchievici. Chapter 3 - substitution strategy of non-ecological refrigerants. In Ioan Sarbu and Calin Sebarchievici, editors, *Ground-Source Heat Pumps*, pages 27 – 45. Academic Press, 2016. ISBN 978-0-12-804220-5.
- [27] Y. Heredia-Aricapa, J.M. Belman-Flores, A. Mota-Babiloni, J. Serrano-Arellano, and Juan J. García-Pabón. Overview of low gwp mixtures for the replacement of hfc refrigerants: R134a, r404a and r410a. *International Journal of Refrigeration*, 111:113 – 123, 2020. ISSN 0140-7007.
- [28] Byeongsu Kim, Sang Hun Lee, DongChan Lee, and Yongchan Kim. Performance comparison of heat pumps using low global warming potential refrigerants with optimized heat exchanger designs. *Applied Thermal Engineering*, 171:114990, 2020. ISSN 1359-4311.
- [29] Adrián Mota-Babiloni, Joaquín Navarro-Esbrí, Ángel Barragán-Cervera, Francisco Molés, and Bernardo Peris. Analysis based on eu regulation no 517/2014 of new hfc/hfo mixtures as alternatives of high gwp refrigerants in refrigeration and hvac systems. *International Journal of Refrigeration*, 52:21 – 31, 2015. ISSN 0140-7007.
- [30] Regulation (eu) no 517/2014. https://eur-lex.europa.eu/legal-content/EN/TXT/?uri=uriserv:OJ.L_.2014.150.01.0195.01.ENG, 2014.
- [31] Naeem Abas, Ali Raza Kalair, Nasrullah Khan, Aun Haider, Zahid Saleem, and Muhammad Shoaib Saleem. Natural and synthetic refrigerants, global warming: A review. *Renewable and Sustainable Energy Reviews*, 90:557 – 569, 2018. ISSN 1364-0321.
- [32] Xi Wu, Chaobin Dang, Shiming Xu, and Eiji Hihara. State of the art on the flammability of hydrofluoroolefin (hfo) refrigerants. *International Journal of Refrigeration*, 108:209 – 223, 2019. ISSN 0140-7007.
- [33] Refrigerants environmental gwps. <https://bit.ly/39vRKzq>, 2013.
- [34] Giuseppe Emmi, Angelo Zarrella, Michele De Carli, and Antonio Galgaro. Solar assisted ground source heat pump in cold climates. *Energy Procedia*, 82:623 – 629, 2015. ISSN 1876-6102.
- [35] Renato M. Lazzarin. Dual source heat pump systems: Operation and performance. *Energy and Buildings*, 52:77 – 85, 2012. ISSN 0378-7788.
- [36] Farzin M. Rad, Alan S. Fung, and Wey H. Leong. Feasibility of combined solar thermal and ground source heat pump systems in cold climate, canada. *Energy and Buildings*, 61:224 – 232, 2013. ISSN 0378-7788.
- [37] Luca Evangelisti, Roberto De Lieto Vollaro, and Francesco Asdrubali. Latest advances on solar thermal collectors: A comprehensive review. *Renewable and Sustainable Energy Reviews*, 114:109–318, 2019. ISSN 1364-0321.
- [38] Strategic research priorities for solar thermal technology, renewable heating and cooling. https://www.rhc-platform.org/content/uploads/2019/05/Solar_thermal_SRP.pdf, 2012.
- [39] Giovanni Barone, Annamaria Buonomano, Cesare Forzano, and Adolfo Palombo. Chapter 6 - solar thermal collectors. In Francesco Calise, Massimo Dentice D’Accadia, Massimo Santarelli, Andrea Lanzini, and Domenico Ferrero, editors, *Solar Hydrogen Production*, pages 151 – 178. Academic Press, 2019. ISBN 978-0-12-814853-2.

- [40] Ritvik Dobriyal, Prateek Negi, Neeraj Sengar, and Desh Bandhu Singh. A brief review on solar flat plate collector by incorporating the effect of nanofluid. *Materials Today: Proceedings*, 21:1653 – 1658, 2020. ISSN 2214-7853.
- [41] Kate Hudon. Chapter 20 - solar energy – water heating. In Trevor M. Letcher, editor, *Future Energy (Second Edition)*, pages 433 – 451. Elsevier, Boston, second edition edition, 2014. ISBN 978-0-08-099424-6.
- [42] Mahmud Jamil Muhammad, Isa Adamu Muhammad, Nor Azwadi Che Sidik, and Muhammad Noor Afiq Witri Muhammad Yazid. Thermal performance enhancement of flat-plate and evacuated tube solar collectors using nanofluid: A review. *International Communications in Heat and Mass Transfer*, 76:6–15, 2016. ISSN 0735-1933. doi: <https://doi.org/10.1016/j.icheatmasstransfer.2016.05.009>. URL <https://www.sciencedirect.com/science/article/pii/S0735193316301476>.
- [43] E. Azad. Theoretical and experimental investigation of heat pipe solar collector. *Experimental Thermal and Fluid Science*, 32(8):1666 – 1672, 2008. ISSN 0894-1777.
- [44] Ahmet Çağlar and Cemil Yamalı. Performance analysis of a solar-assisted heat pump with an evacuated tubular collector for domestic heating. *Energy and Buildings*, 54:22 – 28, 2012. ISSN 0378-7788.
- [45] Giuseppe Emmi, Angelo Zarrella, Michele De Carli, and Antonio Galgaro. An analysis of solar assisted ground source heat pumps in cold climates. *Energy Conversion and Management*, 106:660 – 675, 2015. ISSN 0196-8904.
- [46] Mahmoud B. Elsheniti, Amr Kotb, and Osama Elsamni. Thermal performance of a heat-pipe evacuated-tube solar collector at high inlet temperatures. *Applied Thermal Engineering*, 154:315 – 325, 2019. ISSN 1359-4311.
- [47] Francesco Reda. Long term performance of different SAGSHP solutions for residential energy supply in finland. *Applied Energy*, 144:31 – 50, 2015. ISSN 0306-2619.
- [48] V. Pranesh, R. Velraj, S. Christopher, and V. Kumaresan. A 50 year review of basic and applied research in compound parabolic concentrating solar thermal collector for domestic and industrial applications. *Solar Energy*, 187:293 – 340, 2019. ISSN 0038-092X.
- [49] Abdellah Shafieian, Mehdi Khiadani, and Ataollah Nosrati. Theoretical modelling approaches of heat pipe solar collectors in solar systems: A comprehensive review. *Solar Energy*, 193:227 – 243, 2019. ISSN 0038-092X.
- [50] Tingting Sun, Lingyan Yang, Lu Jin, Zhiwen Luo, Yan Zhang, Yanzhu Liu, and Zhengru Wang. A novel solar-assisted ground-source heat pump (sagshp) with seasonal heat-storage and heat cascade utilization: Field test and performance analysis. *Solar Energy*, 201:362 – 372, 2020. ISSN 0038-092X.
- [51] Sassan Mohasseb and Alibakhsh Kasaeian. Comparing the performance of flat plate collector and evacuated tube collector for building and industrial usage in hot and cold climate in iran with trnsys software. 2014.
- [52] Georgios A. Florides and Soteris Kalogirou. Ground heat exchangers—a review of systems, models and applications. *Renewable Energy*, 32(15):2461 – 2478, 2007. ISSN 0960-1481.
- [53] Hossein Javadi, Seyed Soheil Mousavi Ajarostaghi, Marc A. Rosen, and Mohsen Pourfallah. Performance of ground heat exchangers: A comprehensive review of recent advances. *Energy*, 178:207–233, 2019. ISSN 0360-5442. doi: <https://doi.org/10.1016/j.energy.2019.04.094>. URL <https://www.sciencedirect.com/science/article/pii/S0360544219307273>.
- [54] M. Reuss. 6 - the use of borehole thermal energy storage (btes) systems. In Luisa F. Cabeza, editor, *Advances in Thermal Energy Storage Systems*, Woodhead Publishing Series in Energy, pages 117 – 147. Woodhead Publishing, 2015. ISBN 978-1-78242-088-0.
- [55] Daniel Adamovský, Pavel Neuberger, and Radomír Adamovský. Results of operational verification of vertical ground heat exchangers. *Energy and Buildings*, 152:185 – 193, 2017. ISSN 0378-7788.
- [56] Georgios A. Florides, Paul Christodoulides, and Panayiotis Pouloupatis. Single and double u-tube ground heat exchangers in multiple-layer substrates. *Applied Energy*, 102:364 – 373, 2013. ISSN 0306-2619. Special Issue on Advances in sustainable biofuel production and use - XIX International Symposium on Alcohol Fuels - ISAF.
- [57] Jun Gao, Xu Zhang, Jun Liu, Kui Shan Li, and Jie Yang. Thermal performance and ground temperature of vertical pile-foundation heat exchangers: A case study. *Applied Thermal Engineering*, 28(17):2295 – 2304, 2008. ISSN 1359-4311.
- [58] Jasmi Raymond, Serge Mercier, and Luc Nguyen. Designing coaxial ground heat exchangers with a thermally enhanced outer pipe. *Geothermal Energy*, 3, 2015.

- [59] Jin Luo, Haifeng Zhao, Shuqiang Gui, Wei Xiang, Joachim Rohn, and Philipp Blum. Thermo-economic analysis of four different types of ground heat exchangers in energy piles. *Applied Thermal Engineering*, 108:11 – 19, 2016. ISSN 1359-4311.
- [60] Jalaluddin and Akio Miyara. Thermal performance and pressure drop of spiral-tube ground heat exchangers for ground-source heat pump. *Applied Thermal Engineering*, 90:630 – 637, 2015. ISSN 1359-4311.
- [61] T. Sliwa and M.A. Rosen. Efficiency analysis of borehole heat exchangers as grout varies via thermal response test simulations. *Geothermics*, 69:132 – 138, 2017. ISSN 0375-6505.
- [62] Younes Noorollahi, Reza Saeidi, Mohammad Mohammadi, Ali Amiri, and Mehdi Hosseinzadeh. The effects of ground heat exchanger parameters changes on geothermal heat pump performance – a review. *Applied Thermal Engineering*, 129:1645 – 1658, 2018. ISSN 1359-4311.
- [63] Elisabeth Kjellsson, Göran Hellström, and Bengt Perers. Optimization of systems with the combination of ground-source heat pump and solar collectors in dwellings. *Energy*, 35(6):2667 – 2673, 2010. ISSN 0360-5442. 7th International Conference on Sustainable Energy Technologies.
- [64] Francesco Reda and Ari Laitinen. Different strategies for long term performance of sagshp to match residential energy requirements in a cold climate. *Energy and Buildings*, 86:557 – 572, 2015. ISSN 0378-7788.
- [65] Esa Dube Kerme and Alan S. Fung. Transient heat transfer simulation, analysis and thermal performance study of double u-tube borehole heat exchanger based on numerical heat transfer model. *Applied Thermal Engineering*, 173:115189, 2020. ISSN 1359-4311.
- [66] Esa Dube Kerme and Alan S. Fung. Heat transfer simulation, analysis and performance study of single u-tube borehole heat exchanger. *Renewable Energy*, 145:1430 – 1448, 2020. ISSN 0960-1481.
- [67] D. Bauer, W. Heidemann, Hans Müller-Steinhagen, and H.-J.G Diersch. Thermal resistance and capacity models for borehole heat exchanger. *International Journal of Energy Research*, 2010.
- [68] Weibo Yang, Mingheng Shi, Guangyuan Liu, and Zhenqian Chen. A two-region simulation model of vertical u-tube ground heat exchanger and its experimental verification. *Applied Energy*, 86(10):2005 – 2012, 2009. ISSN 0306-2619.
- [69] Benjamin Zühlsdorf, Jonas Kjær Jensen, and Brian Elmegaard. Heat pump working fluid selection—economic and thermodynamic comparison of criteria and boundary conditions. *International Journal of Refrigeration*, 98: 500 – 513, 2019. ISSN 0140-7007.
- [70] E. W. Lemmon, M. L. Huber, and M. O. McLinden. NIST standard reference database 23: Reference fluid thermo-dynamic and transport properties-REFPROP, Version 9.1. 2013.
- [71] Itho daalderop - w / w heat pump 5g - 4.5 kw individual source. <https://www.ithodaalderop.nl/nl-NL/professional/product/03-00354>.
- [72] Kaiser Ahmed, Petri Pylsy, and Jarek Kurnitski. Hourly consumption profiles of domestic hot water for different occupant groups in dwellings. *Solar Energy*, 137:516 – 530, 2016. ISSN 0038-092X. doi: <https://doi.org/10.1016/j.solener.2016.08.033>. URL <http://www.sciencedirect.com/science/article/pii/S0038092X16303711>.
- [73] Chapter 7 - high efficiency plants and building integrated renewable energy systems. In Francesco Asdrubali and Umberto Desideri, editors, *Handbook of Energy Efficiency in Buildings*, pages 441–595. Butterworth-Heinemann, 2019.
- [74] H.H.J. Vreuls. the netherlands: list of fuels and equivalent co2 emission factors.doc. <https://www.rvo.nl/sites/default/files/2013/10/Vreuls%202005%20NL%20Energiedragerlijst%20-%20Update.pdf>, 2014.